AD NUMBER

ADB002840

LIMITATION CHANGES

TO:

Approved for public release; distribution is unlimited.

FROM:

Distribution authorized to U.S. Gov't. agencies only; Test and Evaluation; 01 NOV 1974. Other requests shall be referred to Air Force Flight Dynamics Laboratory, Attn: FYS, Wright-Pattprson AFB, OH 45433.

AUTHORITY

AFFDL per DTIC form 55

GENERAL DECLASSIFICATION SCHEDULE

IN ACCORDANCE WITH
DOD 5200.1-R & EXECUTIVE ORDER 11652

THIS DOCUMENT IS:

CLASSIFIED BY_____

Subject to General Declassification Schedule of Executive Order 11652-Automatically Downgraded at 2 Years Intervals- DECLASSIFIED ON DECEMBER 31.

BY

Defense Documentation Center
Defense Supply Agency
Cameron Station
Alexandria Virginia 22314

AFFDL-TR-74-126

DEVELOPMENT OF ACTIVE FLUTTER SUPPRESSION WIND TUNNEL TESTING TECHNOLOGY

THE BOEING COMPANY
WICHITA DIVISION

TECHNICAL REPORT AFFDL—TR—74—126

JANUARY 1975

AIR FORCE FLIGHT DYNAMICS LABORATORY
AIR FORCE SYSTEMS COMMAND
WRIGHT—PATTERSON AIR FORCE BASE, OHIO 45433

NOTICE

When Government drawings, specifications, or other data are used for any purpose other than in connection with a definitely related Government procurement operation, the United States Government thereby incurs no responsibility nor any obligation whatsoever; and the fact that the Government may have formulated, furnished, or in any way supplied the said drawings, specifications, or other data, is not to be regarded by implication or otherwise as in any manner licensing the holder or any other person or corporation, or conveying any rights or permission to manufacture, use, or sell any patented invention that may in any way be related thereto.

AIR FORCE/56780/24 March 1975 — 150

DEVELOPMENT OF ACTIVE FLUTTER SUPPRESSION WIND TUNNEL TESTING TECHNOLOGY

Francis D. Sevart

The Boeing Company

Wichita, Kansas

FOREWORD

This report was prepared by The Boeing Company, Wichita Division, Wichita, Kansas, in fulfillment of Air Force Contract F33615-72-C-1913, Project 1370, "Dynamic Problems in Flight Vehicles," and Task No. 137001, "Aeroelastic Problems," for the Aerospace Dynamics Branch, Vehicle Dynamics Division, Air Force Flight Dynamics Laboratory, Air Force Systems Command, Wright-Patterson Air Force Base, Ohio. The work was administered by Mr. Thomas E. Noll, Project Engineer (prior to 31 August 1973) of the Vehicle Dynamics Division (AFFDL/FYS) and by Mr. Larry R. Felt, Project Engineer (after 31 August 1973) of the Vehicle Dynamics Division (AFFDL/FYS). This effort was made possible by the use of Laboratory Director's Funds.

The report presents results of a cooperative Air Force Flight Dynamics Laboratory-NASA Langley Research Center program, with Boeing participation funded under the above contract. Program managers were Dr. Gerald E. Bergmann, Group Engineer, Flight Controls Research and Development (prior to 19 February 1973) and Garold E. Hodges, Senior Specialist Engineer (after 19 February 1973). Francis D. Sevart, Specialist Engineer, was the principal investigator. Jean Gilman, Jr. and L. Tracy Redd, Aero-Space Engineers, Flutter Section, Aeroelasticity Branch, Structures and Dynamics Division, were the NASA Project Engineers. Gordon S. Shoup and Edward H. Williams, Structural Dynamics, and Suresh M. Patel, Flight Controls, were primary Boeing contributors. David L. Gray, Electro-Mechanical Instrumentation Branch, was a primary NASA contributor.

The authors express their appreciation to wind tunnel support personnel of the NASA Aeroelasticity Branch, and to Dynamic Engineering, Inc., Newport News, Virginia Division, for model modification support and ground vibration testing.

This report is identified internally within The Boeing Company, Wichita Division, as D3-9556.

The report covers work performed between June 1972 and August 1974.

This report was submitted by the authors on 30 August 1974.

This technical report has been reviewed and is approved for publication.

Walter J. Mykytow

WALTER J. MYKYTOW
Asst. for Research & Technology
Vehicle Dynamics Division

ABSTRACT

A research study was conducted to develop active flutter suppression wind tunnel testing technology. A one-thirtieth scale B-52 aeroelastic model was modified to represent the Control Configured Vehicles (CCV) B-52 flight test airplane with an active flutter mode control system (FMCS). The system was mechanized on the model using electromechanical actuation systems for the scaled CCV airplane outboard aileron and flaperon outboard segment control surfaces. The model was tested in the NASA-Langley Transonic Dynamics Tunnel to evaluate the unaugmented model flutter characteristics and performance of the flutter mode control system. Test results were compared with model analytical results and CCV program flight test results for equivalent weight and altitude conditions. The model flutter speed, in airplane scale, is 8.1 percent higher than the airplane flutter speed, less than 1.0 percent higher than the predicted difference. Flutter mode damping with the FMCS engaged is higher on the model than on the airplane, but the damping trends with increasing airspeed are similar. The good agreement attained between model and airplane test results demonstrates that dynamically scaled models can be used to verify analytical methods used to design active flutter mode control systems.

TABLE OF CONTENTS

LIST OF ILLUSTRATIONS

LIST OF ILLUSTRATIONS (CONT.)

LIST OF ILLUSTRATIONS (CONT.)

LIST OF TABLES

LIST OF ABBREVIATIONS AND SYMBOLS

Abbreviation	Definition
CCV	Control configured vehicles
Co-quad	Refers to coincident (in-phase) and quadrature (out-of-phase) components of steady-state sinusoidal frequency response
D.C.	Direct current
D.O.F.	Degree of freedom
FMC	Flutter mode control
FMCS	Flutter mode control system
KCAS	Knots calibrated airspeed
KTAS	Knots true airspeed
LAS	Lateral-directional augmented stability
WBL	Wing buttock line

Symbol	Definition	Unit
b	One-half of mean aerodynamic chord	feet
b_r	Reference semi-chord	inches
f	Frequency	Hertz
$f_{v=0}$	Frequency at zero velocity	Hertz
g	Damping coefficient (no structural damping assumed) (-2ζ)	-
$\tilde{g}$	Damping coefficient $(+2\zeta)$	-
H.M.	Hinge moment	in-lb or in-oz
j	Square root of -1 $(\sqrt{-1})$	-
K_A	FMCS aileron loop feedback gain	deg/g
K_F	FMCS flaperon loop feedback gain	deg/g
Q	Dynamic pressure	psf
S	Laplace transform variable	rad/sec

LIST OF ABBREVIATIONS AND SYMBOLS (CONT.)

Symbol	Definition	Units
U_o	Equilibrium forward airspeed	ft/sec
V	Airplane forward velocity or tunnel free-stream velocity	KTAS or ft/sec
V_f	Flutter speed	KTAS or ft/sec
V_g	Lateral gust velocity	ft/sec
W_g	Vertical gust velocity	ft/sec
X	Longitudinal displacement (positive aft)	inches
Y	Lateral displacement (positive left)	inches
Z	Vertical displacement (positive down)	inches
$\ddot{Z}_{WBL565}$	Vertical acceleration at WBL 565	g's
$\ddot{Z}_{WBL925}$	Vertical acceleration at WBL 925	g's
α_g	Angle of attack due to vertical gust	deg
δ_A	Aileron surface displacement	deg
δ_{A_c}	Aileron actuator command	deg
δ_C	Canard surface displacement	deg
δ_{C_c}	Canard actuator command	deg
δ_F	Flaperon surface displacement	deg
δ_{F_c}	Flaperon actuator command	deg
ζ	Damping ratio	-
θ_X	Roll rotation (positive right wing tip up)	rad
θ_Y	Pitch rotation (positive nose down)	rad
θ_Z	Yaw rotation (positive nose right)	rad
ρ	Test fluid mass density	$slug/ft^3$
ω	Frequency	rad/sec
ω_c	FMCS shaping filter cut-off frequency	rad/sec

1.0 INTRODUCTION

1.1 Background

In recent years airframe design trends have led to vehicles with increased flexibility, slenderness ratio, and maximum operating speeds, resulting in an increased likelihood of flutter within the desired aircraft operating envelope. Preliminary design trades performed by Boeing indicate that weight increases of as much as 2 to 4 percent of total structural weight may be required to provide flutter safety margins. Such weight increases are significant in modern aircraft from the standpoint of reducing performance. The flutter problem is further compounded on tactical aircraft with external stores, particularly when many combinations of stores are considered, and speed restrictions are frequently necessary to assure adequate flutter margins of safety.

Within the last ten years control systems that suppress low frequency structural modes have evolved from analytical feasibility studies to production hardware. An example is the B-52 ECP 1195 system which reduces structural fatigue damage rates and peak loads in the B-52G and H fleet. As a result of this new technology base, an active flutter suppression system is now feasible, offering the potential, in many instances, for solving flutter problems with significantly less weight and fewer performance penalties.

In July 1971, the Air Force initiated a program with The Boeing Company, Wichita Division, to conduct a Control Configured Vehicles study on a B-52E test airplane. This program was formulated to evaluate several advanced flight control concepts, including active flutter mode control, through analyses and flight tests.

Although analytical techniques are available for design of active flutter suppression systems, complementary aeroelastic model wind tunnel test data is needed to guide the airframe and system design and to supplement analytical techniques for establishing flight safety. Development of aeroelastic modeling technology with active controls is important in reducing technical risks in future aircraft applications and in ensuring full realization of the benefits of active flutter control.

The wind tunnel model used on the flutter suppression study reported herein was an aeroelastic model modified by Boeing-Wichita to represent the CCV program B-52E flight test aircraft with a flutter mode control system. This aeroelastic model was of a B-52E airplane and was provided under a research study in 1968 by the NASA Langley Research Center Aeroelasticity Branch to demonstrate active control of the model's symmetric gust response. The model is dynamically scaled over the frequency range of 0 to 25 Hz, which includes nine symmetric vibration modes. The model included active control systems for ailerons, elevator and horizontal stabilizer trim. In 1970, NASA-Langley conducted basic model gust response tests with the control system inoperative. Since 1970 Boeing-Wichita has provided technical support to the current NASA-Langley research program directed toward demonstration of active control systems on the B-52 model. The CCV horizontal canards and full three segment flaperons were added to the model for a full-fuselage ride control system to be tested under the NASA program.

1.2 Program Objectives

The NASA B-52 model provided a unique opportunity for a program to significantly advance wind tunnel testing technology by interfacing with the related Air Force and NASA programs. The objectives of this program were to determine compatible flutter configurations for the model and airplane, accomplish appropriate wind tunnel and flight testing to establish basic vehicle flutter characteristics and flutter mode control system performance, and compare test results to establish the degree of correlation between model and airplane, and analytical results. Thus, the program was formulated to develop and demonstrate wind tunnel model technology for active flutter suppression.

2.0 SUMMARY

Equivalent flutter conditions that could be tested on the B-52 aeroelastic model and the CCV program B-52 test airplane were determined through structural analyses. The flutter configuration used the CCV airplane ballasted external wing fuel tanks in a 375,000 pound gross weight, 21,000 feet altitude condition. The airplane without flutter mode control was predicted to flutter at 422.2 Knots True Airspeed (KTAS). The model, with outboard nacelle struts modified to better simulate the airplane struts, was predicted to flutter at 452.4 KTAS, in airplane scale, only 7.2 percent higher than the airplane predicted flutter speed.

A flutter mode control system (FMCS) was synthesized under the CCV program for flight tests at the three CCV fuel configurations (see Reference 2) to produce at least a 30 percent increase in flutter placard airspeed and satisfy ±6 db gain and ±60 degrees phase stability margins. This system was evaluated on model equations of motion to determine suitability of the system for the model wind tunnel tests. Results of the evaluation showed performance of the system on the model similar to that predicted for the system on the airplane.

The model was modified to the 375,000 pound configuration with outboard aileron and flaperon outboard segment surfaces mechanized with electromechanical actuation systems. Wind tunnel tests were conducted in the NASA-Langley Transonic Dynamics Tunnel to establish the unaugmented model flutter speed and FMCS performance for the nominal system and with FMCS gain and shaping filter variations. Results of the wind tunnel tests and CCV flight tests for comparable airplane gross weight and altitude conditions are summarized in the plots of flutter mode damping ($\tilde{g} = 2\zeta$) and frequency as functions of velocity shown in Figure 1.

The basic airplane flutter speed is 455.6 KTAS, about 7.9 percent higher than predicted, while the model flutter speed is 492.3 KTAS, in airplane scale, 8.8 percent higher than predicted. This shows the comparison of the model to its equations of motion is almost identical to the comparison of the airplane with its mathematical model. The basic model flutter mode damping is about twice the basic airplane flutter mode damping for airspeeds below 380 KTAS, which is consistent with its 8.1 percent higher flutter velocity.

Damping of the airplane flutter mode with the FMC system on is about .046 at the unaugmented airplane flutter speed. At the highest airspeed tested, 473.8 KTAS (353 KCAS), the flutter mode damping measured in the airplane flight tests was about .045. Damping of the model flutter mode with the FMCS engaged is about .080 at the unaugmented model flutter speed, and the higher speed conditions tested show damping increasing. Over the common range of equivalent airspeeds that the model and airplane were tested with the FMCS engaged, the model flutter mode damping is nearly 70 percent higher than the airplane flutter mode damping. But, the damping trends with increasing airspeed are similar.

The good agreement attained between the model and airplane test results demonstrates the validity of using dynamically scaled models to verify analytical methods used to design active flutter mode control systems. Thus, wind tunnel test models can be used in the development of CCV concepts to assure flight safety and more fully exploit the benefits of such active systems on advanced aircraft.

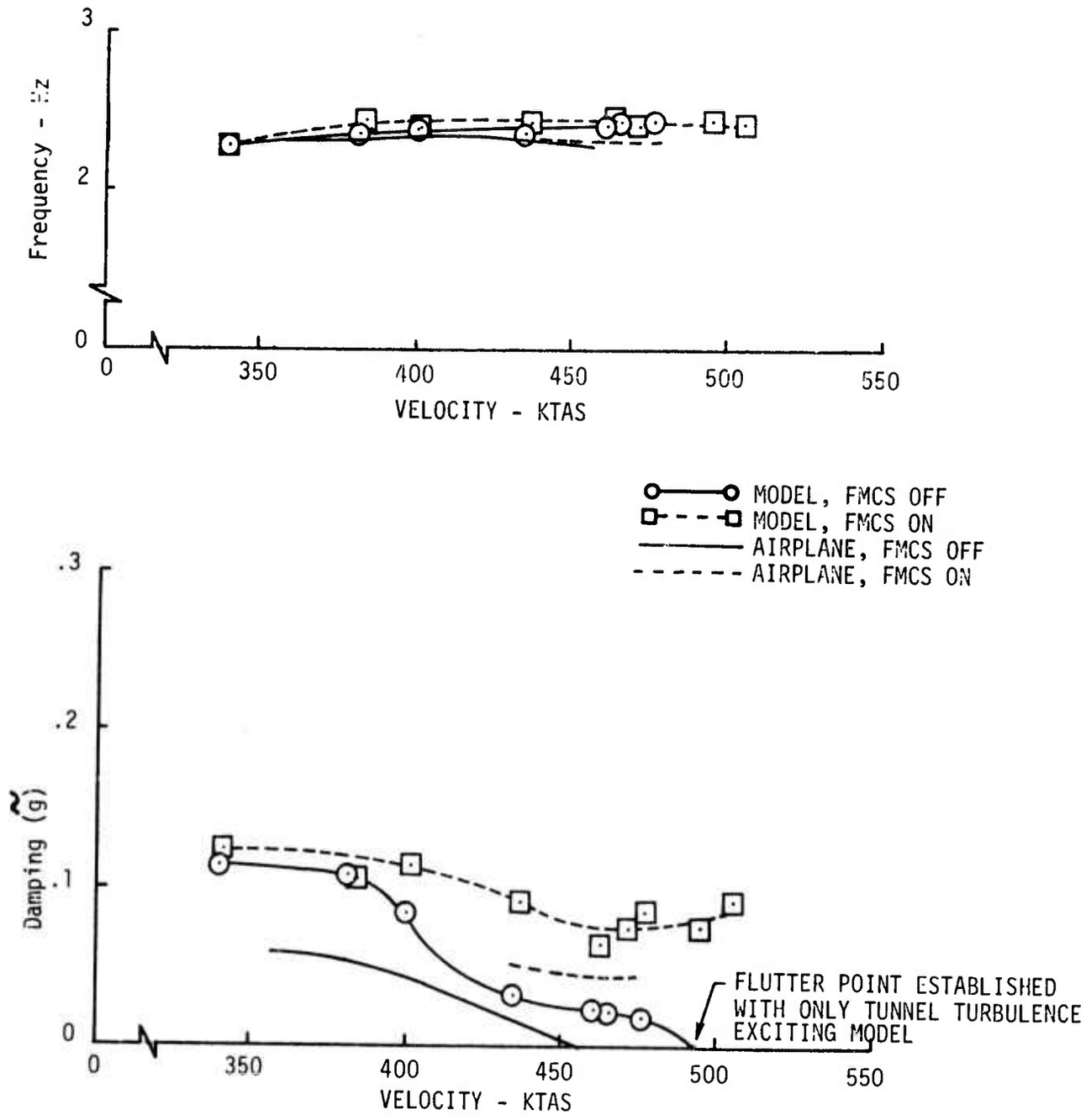

Figure 1. Flutter Mode Damping and Frequency-Model and Airplane Test Results Comparison

Extending results of this study to other CCV systems and other aircraft will require development of additional technology. For example, to more accurately model airplane control surface actuation system dynamic characteristics, electrohydraulic actuation systems will be required for the model control surfaces. This will require an on-board hydraulic power supply designed specifically for model use. New model mount systems need to be developed, or existing ones modified, to permit a more exact representation of airplane rigid body dynamic behavior, especially for testing CCV systems that control rigid body modes. Improvement is also needed in model testing techniques to provide more accurate means to estimate modal damping characteristics from the subcritical test responses required for correlation with analytical results.

3.0 MODEL CONFIGURATION

The NASA one-thirtieth scale B-52 aeroelastic model was designed to represent the B-52E airplane AF56-632 in a 419,000 pound equivalent gross weight condition. This test airplane was subsequently selected as the test vehicle to demonstrate new active control concepts under the Control Configured Vehicles (CCV) program. Thus, the NASA model was the logical choice for a test vehicle to develop CCV concept evaluation techniques through wind tunnel testing. A flutter configuration was defined for the model that was compatible with the CCV airplane at a higher gross weight condition than originally planned for the CCV program, but within the flight envelope of the airplane. The higher gross weight condition was necessary because of limitations in reducing model weight. The CCV contract was amended to add flight tests at this condition (Fuel Configuration 3) to obtain additional flight data for the CCV concepts, including flutter mode control, at off-design conditions, to demonstrate that the concepts were operationally practical.

The following sections discuss the development of the model and equivalent airplane test configurations. Included are discussions of the model characteristics, results of vibration and flutter analyses to establish the model and airplane structural compatibility, and model modifications performed to give the compatibility and to add the CCV airplane control surfaces required for the flutter mode control system (FMCS).

3.1 Model Background

The B-52 aeroelastic model was constructed in 1968 to Boeing specifications (Reference 3) to simulate the B-52E test airplane in a 5400 foot altitude condition for low speed gust response testing in the Langley Transonic Dynamics Tunnel. The model is dynamically scaled over the frequency range 0 to 25 Hz, which includes nine symmetric vibration modes.

Model scale laws were developed by choosing the one-thirtieth geometric scale factor and requiring model and airplane Froude numbers and mass ratios to be equal. Table I contains a listing of the model scale factors. The model density shown, .00499 slug/ft^3, is equivalent to a 21,000 foot airplane flight condition. The model has a wing span of 74 inches and weighed 63.2 pounds in the design condition. Model stiffness was provided by aluminum alloy fuselage and wing spars which were covered with flexible segmented pod fairings to provide the correct aerodynamic contour. The model was designed to use the NASA two-cable mount system, with the pulleys located on the tunnel walls, ceiling and floor. The forward cable lies in a vertical plane, and the aft cable in a horizontal plane. Both cables terminate at a mount block in the model fuselage near the center of gravity.

Electromechanical position servo systems were included in the model to drive scaled B-52E airplane midspan aileron and elevator control surfaces. Individual actuation systems were used for right and left hand ailerons to permit using differential ailerons for model roll trim control in the tunnel. Pitch trim control was provided by a d.c. gear reduction motor driving the horizontal stabilizer through a jack screw mechanism. Permanent magnent, brushless d.c. torque motors and d.c. servo potentiometers used in the aileron and elevator actuation systems were mounted in the model fuselage with torque

TABLE I: MODEL SCALE FACTORS

SCALE	SYMBOL	FORMULA	FACTOR
DIMENSION	$\frac{\ell_M}{\ell_A}$	SELECTED	$\frac{1}{30}$
DENSITY	$\frac{\rho_M}{\rho_A}$	$\frac{\text{TUNNEL} = .00499}{\text{AIRPLANE ALT.} = .0012249}$	4.07
FROUDE NO.	$\frac{FN_M}{FN_A}$		1.0
MASS RATIO	$\frac{\bar{M}_M}{\bar{M}_A}$	$\frac{W_M}{W_A} \cdot \left(\frac{\rho_A}{\rho_M}\right)\left(\frac{\ell_A}{\ell_M}\right)^3$	1.0
VELOCITY	$\frac{V_M}{V_A}$	$\left(\frac{\ell_M}{\ell_A}\right)^{\frac{1}{2}}$	.183
DYNAMIC PRESSURE	$\frac{q_M}{q_A}$	$\frac{\rho_M}{\rho_A} \cdot \left(\frac{V_M}{V_A}\right)^2$	.136
MACH NO.	$\frac{M_M}{M_A}$	$\frac{V_M}{V_A} \cdot \frac{a_A}{a_M}$	.375
FREQUENCY	$\frac{\omega_M}{\omega_A}$	$\frac{V_M}{V_A} \cdot \frac{\ell_A}{\ell_M}$	5.48
WEIGHT	$\frac{W_M}{W_A}$	$\frac{\rho_M}{\rho_A} \cdot \left(\frac{\ell_M}{\ell_A}\right)^3$	151×10^{-6}
MASS INERTIA	$\frac{I_M}{I_A}$	$\frac{\rho_M}{\rho_A} \cdot \left(\frac{\ell_M}{\ell_A}\right)^5$	$.168 \times 10^{-6}$
STIFFNESS	$\frac{E\bar{I}_M}{E\bar{I}_A} = \frac{GJ_M}{GJ_A}$	$\frac{\rho_M}{\rho_A} \cdot \left(\frac{\ell_M}{\ell_A}\right)^4 \cdot \left(\frac{V_M}{V_A}\right)^2$	$.168 \times 10^{-6}$
AREA INERTIA	$\frac{\bar{I}_M}{\bar{I}_A}$	$\left(\frac{\ell_M}{\ell_A}\right)^4$	1.23×10^{-6}
EXTERNAL LOADS	$\frac{F_M}{F_A}$	$\frac{q_M}{q_A} \cdot \left(\frac{\ell_M}{\ell_A}\right)^2$	151×10^{-6}
BENDING MOMENT	$\frac{BM_M}{BM_A}$	$\frac{F_M}{F_A} \cdot \frac{\ell_M}{\ell_A}$	5.03×10^{-6}
STRESS	$\frac{\sigma_M}{\sigma_A}$	$\frac{BM_M}{BM_A} \cdot \left(\frac{\ell_A}{\ell_M}\right)^3$	.136

transmitted to the surfaces through shafting and crank-pushrod linkages. Flexible bellows couplings were used in the aileron shaft runs to minimize changes in wing stiffness.

3.2 Vibration and Flutter Analyses

Structural analyses were conducted to define a model configuration representative of the CCV program B-52 test airplane such that the model and airplane would have similar symmetric flutter mode characteristics with the airplane flutter speed within the airplane flight envelope. All model analyses discussed in this section were accomplished in airplane scale for convenience in comparing with airplane analysis results. Model equations of motion were subsequently generated in model scale for evaluation of the CCV program flutter mode control system, discussed in Section 4. The analytical formulation of model and airplane equations of motion is discussed in Appendix I.

A 375,000 pound equivalent airplane gross weight configuration was selected for the model. The configuration was selected for evaluation because the mass distribution properties could be safely attained with the airplane and required minimum design changes to the model. The configuration required replacing the existing 94 percent full external tanks with empty tanks containing the equivalent to the 2000 pound nose ballast of the CCV airplane. The 375,000 pound model configuration was attained by removing approximately 12,000 pounds of fuel from forward body cell number 1 to maintain an acceptable center of gravity location for the airplane and the model. This configuration represents the maximum permissible inflight gross weight for the airplane and did not require revision of the model cable mount block to maintain model static stability.

3.2.1 Preliminary Analyses

Preliminary vibration and flutter analyses were conducted on the model and airplane in the 375,000 pound gross weight configuration at 21,000 feet altitude flight condition. The objective of these analyses was to verify acceptability of the symmetric flutter mode and to determine if any structural changes were required on the model to give the desired compatibility with the airplane.

Airplane mass and stiffness properties for the selected configuration were taken from the model design control specification, Reference 3, and updated to reflect known changes in the CCV airplane. A complete listing of component stiffness and structural and fuel mass properties used in the airplane analyses is included in Appendix A of Reference 4.

Preliminary lumped mass idealization of the model was developed using model design mass properties for the nacelles and empennage surfaces and measured mass properties for wing and fuselage adjusted to remove the 12,000 pound forward body weight. A complete listing of model measured mass and stiffness properties, and a comparison of actual and design stiffness values, are included in Appendix B of Reference 4. Design nacelle mass was used because it was known the model nacelles would be modified to correct mass errors. Due to reasonable agreement between actual and design stiffness properties, the design values were used in all analytical formulations.

Stiffness properties for the model cable mount system were generated from installation geometry and estimated cable tension and drag values supplied by NASA.

Free-free airplane and model, and restrained model vibration analysis results are summarized in Tables II and III. Table II shows frequencies of the first nine symmetric modes for airplane and preliminary model. The frequencies listed under Phase I and Phase II will be discussed in subsequent paragraphs. Frequencies for these modes plus the two cable modes are shown in Table III for the cable-mounted (restrained) model. Descriptions of the coupled modes are included in both tables. The cables have little effect on the mode frequencies, with all but the sixth and eighth elastic mode frequencies slightly lower than the free-free (unrestrained) model frequencies.

Results of the preliminary model and airplane flutter analysis are summarized in Figure 2. The V-g plot indicates the airplane flutter speed is well within the B-52E operational flight envelope for this gross weight/altitude condition. The model predicted flutter speed is about 20 percent higher than the airplane, assuming .015 structural damping for the airplane and .005 for the model. These damping values are based on past experience with the B-52 airplane and the B-52 .049 scale flutter model.

The cable mount system has little effect on the model flutter speed. The model results were obtained using design mass and stiffness values for the nacelles and nacelle struts. The airplane analysis was based on nacelle mode shapes and frequencies determined from airplane ground vibration testing.

A study was conducted to determine if better agreement between predicted model and airplane flutter velocities could be attained through redesign of the model nacelle struts. Results of using airplane nacelle mode shapes and frequencies in the model analysis show significantly better agreement, also shown in Figure 2. The model predicted flutter speed is only about 2 percent higher than the airplane for this case. The study results further showed that similar agreement could be attained if the vertical motion at the airplane outboard nacelle center of gravity were included in the model outboard nacelle side bending mode.

The original model nacelle struts were designed to geometric and stiffness requirements selected to match the node point of the pitch mode and node lines of the side bending and torsion modes. Final tuning of the nacelle struts was accomplished to obtain side bending and pitch mode frequencies within one percent (torsion mode frequency within ten percent) of those specified in Reference 3. Mode shapes at the nacelle center of gravity are shown in Tables IV, V and VI for the airplane and preliminary (original) model left wing nacelles. Right wing nacelle mode shapes are mirror images of the left wing nacelle mode shapes, with the fuselage X-Z plane as the plane of symmetry. The airplane nacelle mode shapes, determined from past uncoupled nacelle ground vibration testing, include significant coupling terms in the side bending mode (X, Z and θ_y motion) and vertical bending mode (Y, θ_x and θ_z). These coupling terms are not present in the original model nacelle modes because of design symmetry.

Vibration analyses of various strut configurations were accomplished to determine a strut design concept which would introduce the important coupling terms (primarily Z in the side bending mode) present in the airplane

TABLE II. AIRPLANE AND MODEL FREE-FREE VIBRATION ANALYSIS RESULTS COUPLED MODE FREQUENCIES

D.O.F.	MODE	PRELIMINARY ANALYSIS	PHASE I ANALYSIS	PHASE II ANALYSIS	AIRPLANE	MODE DESCRIPTION
1, 2, 3	R.B.-X, Z, θ_y	0	0	0	0	
4	EM-1	.784	.790	.789	.785	W-1V
5	EM-2	1.72	1.67	1.68	1.68	W-1V & 1T & 1C, ON-L
6	EM-3	1.98	1.98	1.99	2.00	IN-L, W-2V & 1C
7	EM-4	2.04	2.15	2.16	2.13	W-2V & 1T, ON-L
8	EM-5	2.19	2.21	2.21	2.22	W-1C & 1T, IN-L
9	EM-6	2.42	2.40	2.39	2.37	W-2V & 1T, B-1V
10	EM-7	2.81	2.82	2.77	2.78	B-1V, W-2T & 2V, ON-V, IN-V
11	EM-8	3.12	3.07	3.06	3.11	W-2V, IN-V, B-1V
12	EM-9	3.37	3.40	3.45	3.46	W-2V

NOTE: Flutter analyses of the free-free airplane and model were based on 30 modes. Table II includes all modes below 5 Hz (airplane scale).

SYMBOLS:
W - Wing
B - Body
IN - Inboard Nacelle
ON - Outboard Nacelle
C - Chordwise Bending
L - Lateral Bending
V - Vertical Bending
T - Torsion

TABLE III. RESTRAINED MODEL VIBRATION ANALYSIS RESULTS
COUPLED MODE FREQUENCIES

D.O.F.	MODE	PRELIMINARY ANALYSIS	PHASE I ANALYSIS	PHASE II ANALYSIS	FINAL ANALYSIS MODE DESCRIPTION
1	Cable-1	.074	.076	.075	RB-PITCH AND PLUNGE
2	Cable-2	.083	.085	.083	RB-PLUNGE AND PITCH
3	EM-1	.783	.789	.787	W-1V
4	EM-2	1.66	1.63	1.63	W-1V & 1T & 1C, ON-L
5	EM-3	1.93	1.93	1.94	W-2V & 1C & 1T, IN-L, ON-V
6	EM-4	2.04	2.08	2.09	IN-L, W-1C & 2V & 1T
7	EM-5	2.08	2.15	2.16	W-2V & 1T, ON-L
8	EM-6	2.42	2.40	2.39	W-2V & 1T, B-1V
9	EM-7	2.80	2.82	2.77	B-1V, W-2T & 2V, IN-V, ON-V
10	EM-8	3.12	3.07	3.06	IN-V, W-2V, B-1V
11	EM-9	3.37	3.40	3.45	W-2V

NOTES:
1. Flutter analyses of the restrained model were based on 27 modes. Table III includes all modes below 5 Hz (airplane scale).
2. Mode descriptions for the Phase I analysis also apply to all modes except elastic modes 4 and 5 of the preliminary and Phase II analyses. In the latter analyses, elastic mode 4 is ON-L, W-2V & 1C, whereas elastic mode 5 is IN-L, W-1C & 2V & 1T.

SYMBOLS:
W - Wing
B - Body
IN - Inboard Nacelle
ON - Outboard Nacelle
C - Chordwise Bending
L - Lateral Bending
V - Vertical Bending
T - Torsion

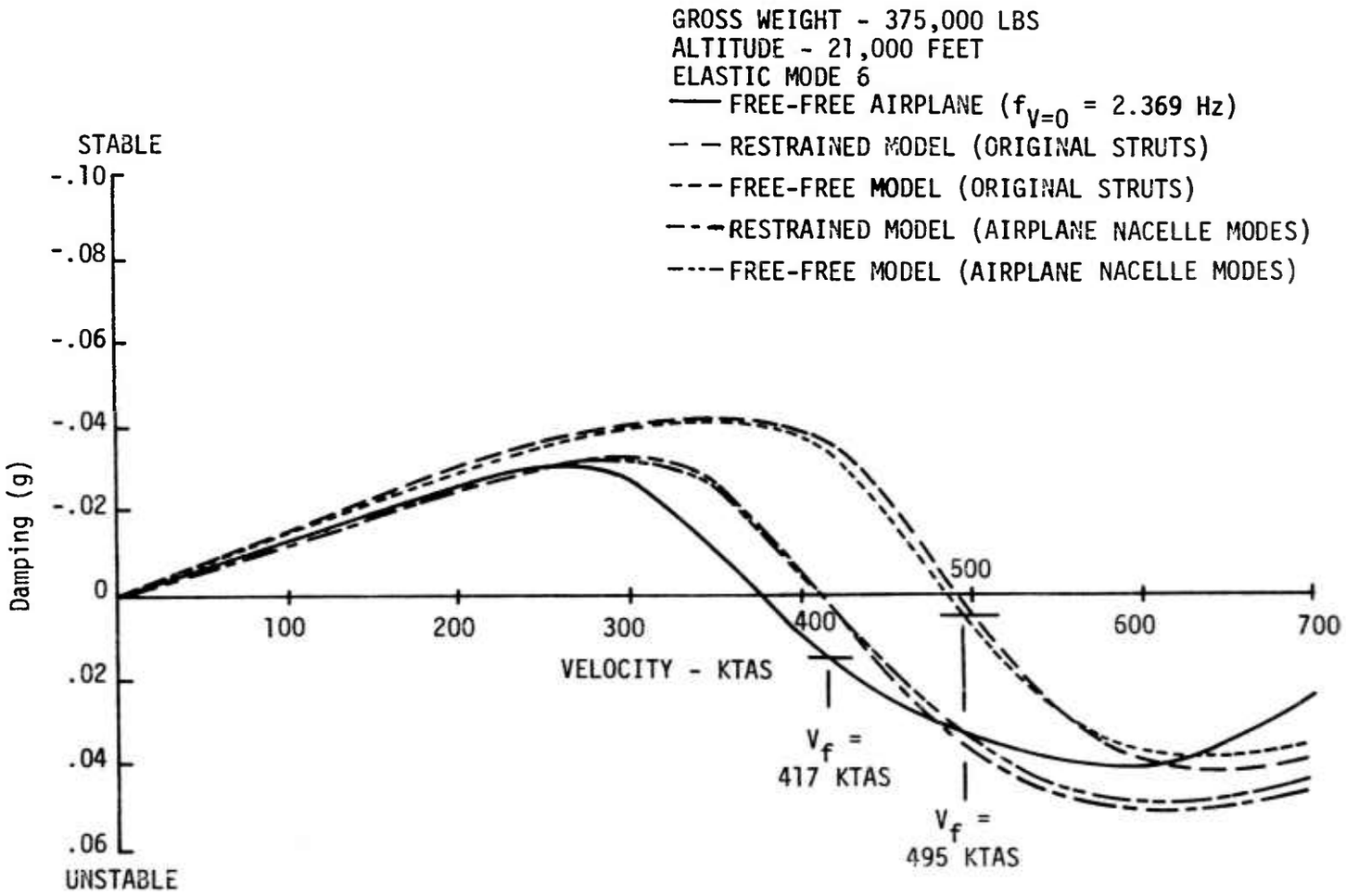

Figure 2. Airplane and Preliminary Model Symmetric Flutter Analysis Results

TABLE IV. NACELLE MODE 1 - SIDE BENDING

LEFT WING
INBOARD NACELLE:

	AIRPLANE	PRELIMINARY MODEL	FINAL MODEL
FREQ. - HZ	2.04	2.04	2.04
X/br	.0535	0	0
Y/br	- .3578	- .3578	- .3578
Z/br	- .0528	0	0
θ_x - RAD	1.0	.1795	.1490
θ_y - RAD	.1384	0	0
θ_z - RAD	.3525	.3726	.3884

LEFT WING
OUTBOARD NACELLE:

	AIRPLANE	PRELIMINARY MODEL	FINAL MODEL
FREQ. - HZ	2.10	2.10	2.12
X/br	.1569	0	.0636
Y/br	- .6495	- .6495	- .6495
Z/br	.1614	0	.1691
θ_x - RAD	.8895	.3367	.3056
θ_y - RAD	.1618	0	.2315
θ_z - RAD	1.0	.7595	.7739

NOTE: Mode data are expressed in airplane scale where br = 130 inches.

TABLE V. NACELLE MODE 2 - VERTICAL BENDING

LEFT WING
INBOARD NACELLE:

	AIRPLANE	PRELIMINARY MODEL	FINAL MODEL
FREQ. - HZ	4.07	4.07	3.915
X/br	.2824	.3063	.3071
Y/br	- .0227	0	0
Z/br	.7874	.7874	.7874
θ_x - RAD	.4311	0	0
θ_y - RAD	1.0	.9772	.9827
θ_z - RAD	- .3173	0	0

LEFT WING
OUTBOARD NACELLE:

	AIRPLANE	PRELIMINARY MODEL	FINAL MODEL
FREQ. - HZ	4.02	4.02	3.95
X/br	.2192	.2591	.2598
Y/br	.1879	0	.2094
Z/br	.6892	.6892	.6892
θ_x - RAD	.1308	0	- .2779
θ_y - RAD	1.0	.9427	.9471
θ_z - RAD	- .3543	0	- .1701

NOTE: Mode data are expressed in airplane scale where b_r = 130 inches.

TABLE VI. NACELLE MODE 3 - STRUT TORSION

LEFT WING
INBOARD NACELLE:

	AIRPLANE	PRELIMINARY MODEL	FINAL MODEL
FREQ. - HZ	6.01	6.01	7.280
X/br	- .0866	0	0
Y/br	.0437	- .0474	- .0788
Z/br	- .0093	0	0
θ_x - RAD	1.0	1.0	1.0
θ_y - RAD	- .0465	0	0
θ_z - RAD	- .4847	- .5199	- .5768

LEFT WING
OUTBOARD NACELLE:

	AIRPLANE	PRELIMINARY MODEL	FINAL MODEL
FREQ. - HZ	5.94	5.94	6.36
X/br	- .0803	0	.0007
Y/br	- .0573	- .0521	- .0598
Z/br	.0087	0	.0203
θ_x - RAD	1.0	1.0	1.0
θ_y - RAD	- .0492	0	- .0208
θ_z - RAD	- .4863	- .4923	- .5132

NOTE: Mode data are expressed in airplane scale where b_r = 130 inches

nacelle modes. The analyses revealed that nacelle mass unbalance in the Y direction (center of gravity not on centerline) could not be responsible for the magnitude of the coupling terms. It was concluded that the airplane nacelle mode coupling terms must be associated with local deformations at the front spar of the airplane wing.

A simple nacelle/strut design concept was found which provided adequate agreement between model and airplane nacelle mode shapes. The concept required rotating the principal axes of the outboard nacelle strut flexure segment through a 16 degree roll angle (clockwise when viewed from front of the model for right hand wing, and counterclockwise for left hand wing). Position of the nacelles and the streamwise orientation of the strut fairings were unchanged. Nacelle mode shapes based on measured nacelle mass and design stiffness values (including the outboard nacelle strut revision) are shown in Tables IV, V and VI, labeled "final model."

3.2.2 Final Analyses

The B-52 aeroelastic model was modified to represent the CCV program flight test airplane in the 375,000 pound condition. New outboard nacelle struts, as described above, were incorporated into the model. Model modifications are discussed in more detail in paragraph 3.3. After completion of the modifications, model mass properties were remeasured to update the analytical vibration and flutter analyses.

Vibration analysis results for the model as tested in the Phase I wind tunnel tests are shown in Table II for free-free coupled mode frequencies and Table III for the restrained model coupled mode frequencies. The analysis was based on measured mass properties and design stiffness values. The nacelle representations included measured frequencies, averaged mass properties, and the analytical mode shapes of Tables IV, V and VI. Also shown in Tables II and III are vibration analysis results for the model as tested in the second entry (Phase II). Between the two series of wind tunnel tests, the model was modified to bring wing tip mass closer to the design specification and to have the model elevator operative. The latter modification added a small amount of mass to the aft body.

Flutter analysis results for the first nine symmetric modes are shown in Figures 3 through 11 for the model as tested in the two wind tunnel entries. Free-free airplane analysis results are included for reference. The V-g plots show little difference in the model as tested in the two entries, except for lower damping in the seventh mode for the model as tested in Phase II. Figure 8 shows the predicted flutter speeds to be very nearly identical. Differences in damping levels between airplane and model modes 2, 3 and 4 are due primarily to the effects of the cable mount system (the relatively stiff fore and aft cable restraint and the strong coupling with chordwise wing deflections).

Antisymmetric flutter analyses were conducted for the airplane and the model as tested during Phase I. The results show the airplane and model to be free of antisymmetric flutter up to about 600 KTAS (about 85 psf model dynamic pressure), well above the planned test velocities. V-g plots for these conditions are shown in Reference 4. An antisymmetric flutter analysis of the model as tested in the second entry was not conducted because it was

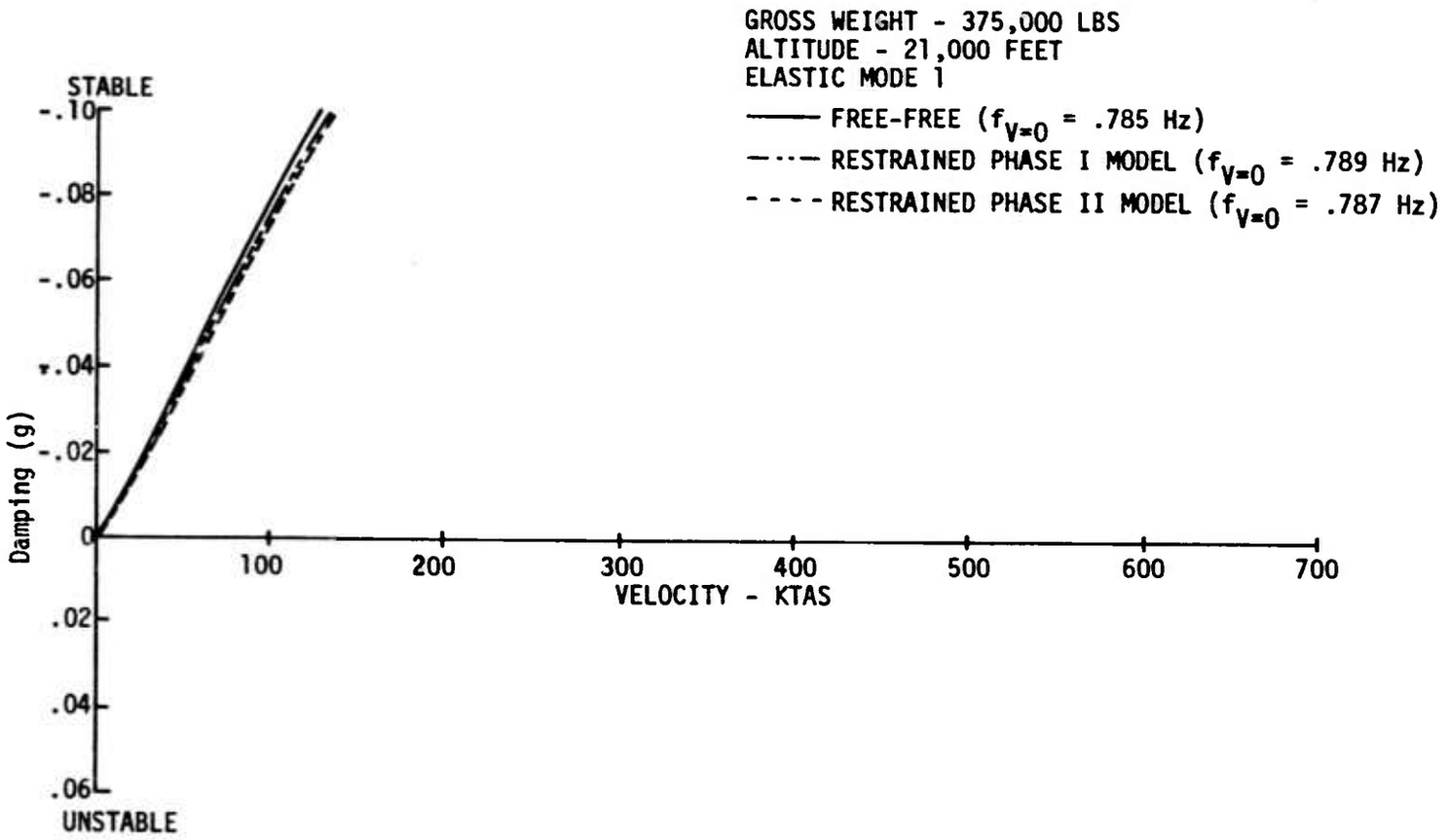

Figure 3. Airplane and Model Symmetric Flutter Analysis Results - Mode 1

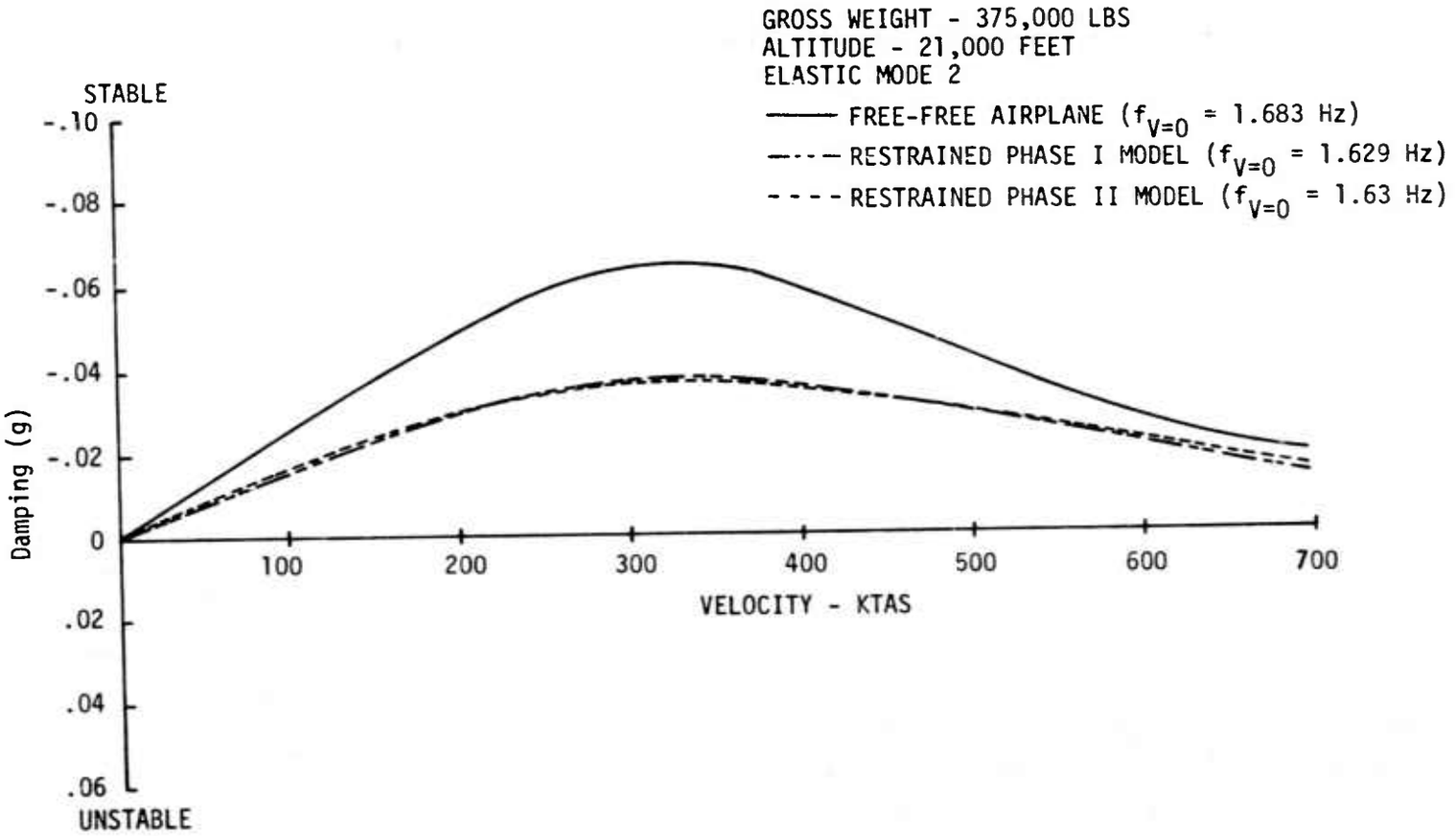

Figure 4. Airplane and Model Symmetric Flutter Analysis Results - Mode 2

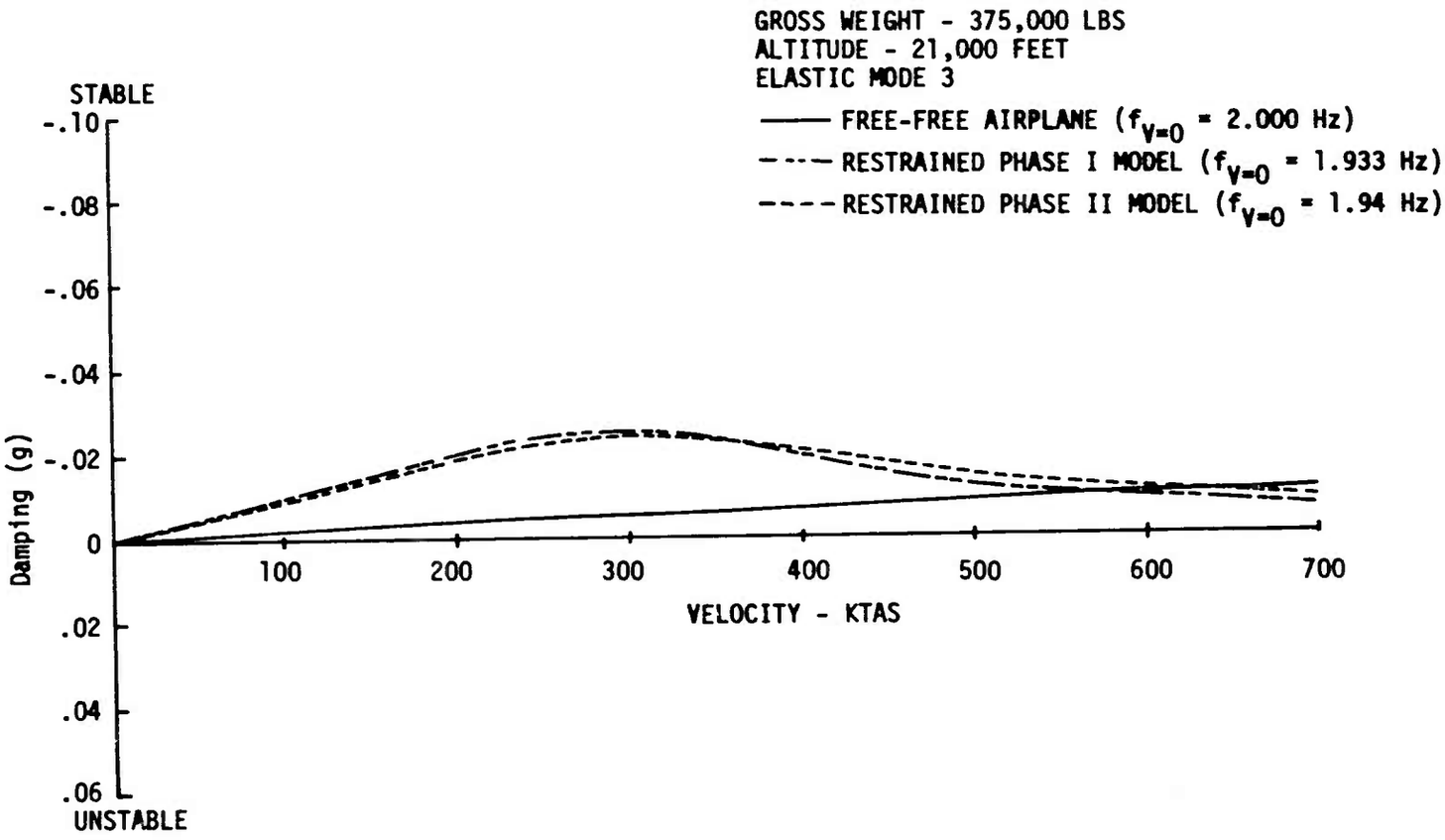

Figure 5. Airplane and Model Symmetric Flutter Analysis Results - Mode 3

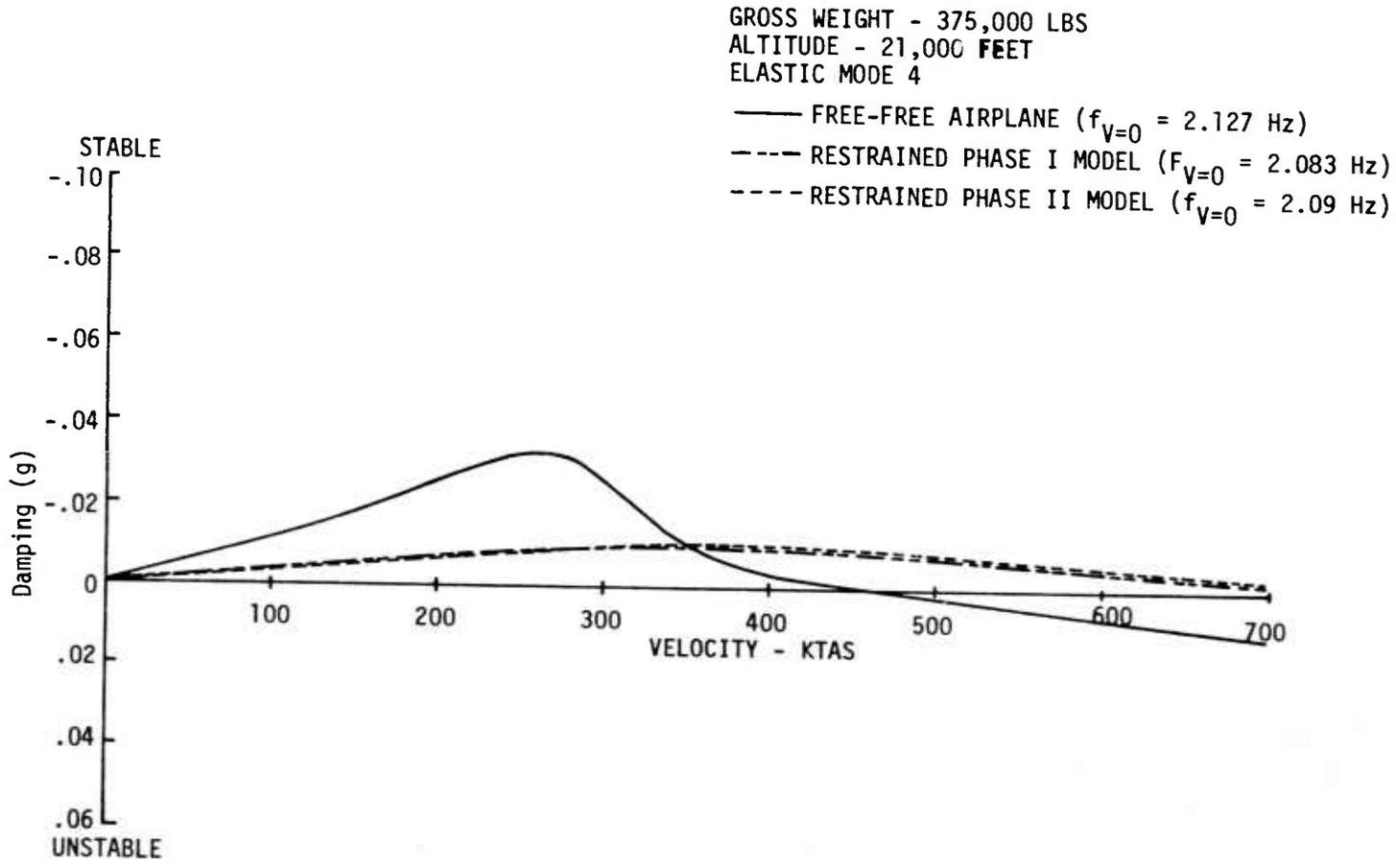

Figure 6. Airplane and Model Symmetric Flutter Analysis Results - Mode 4

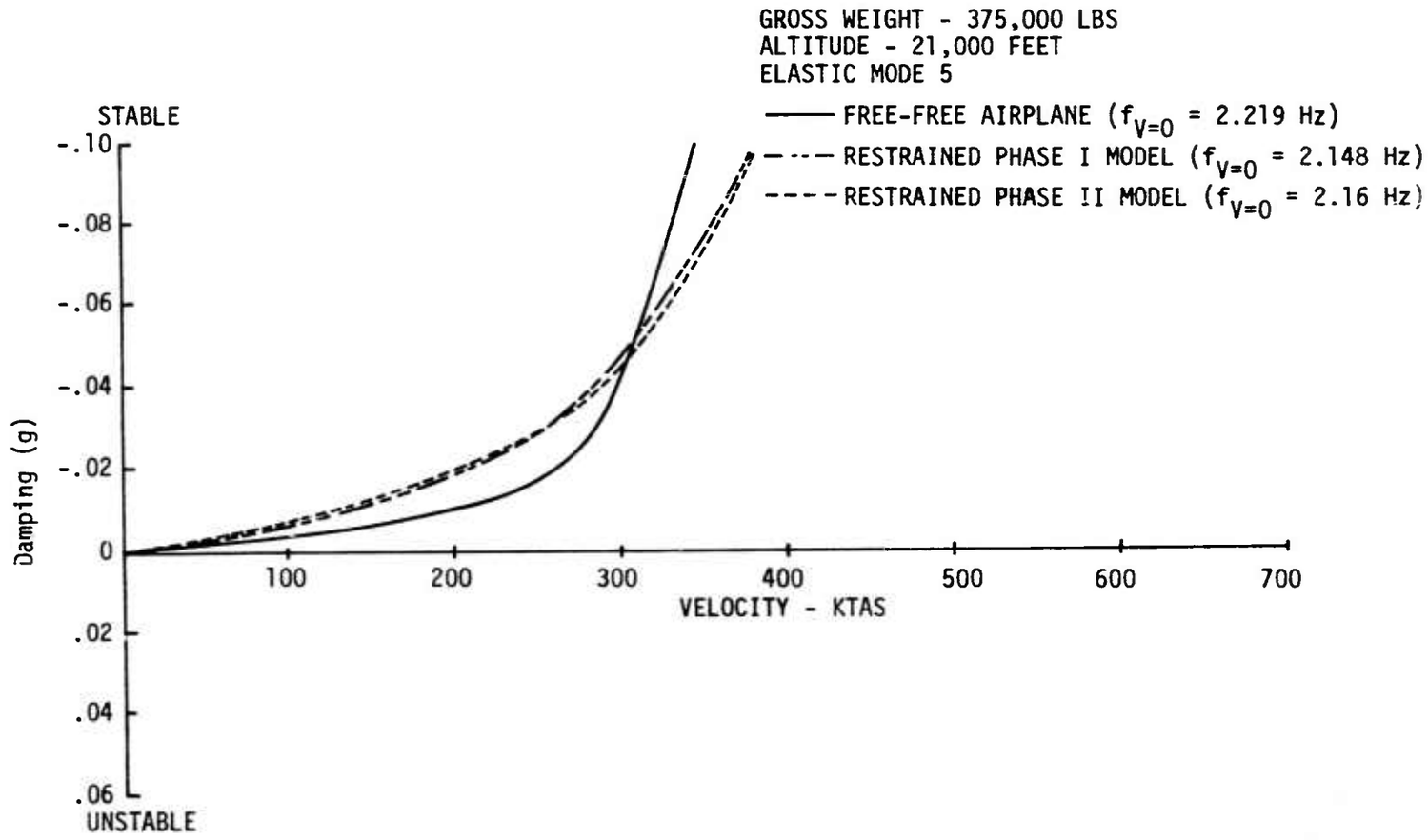

Figure 7. Airplane and Model Symmetric Flutter Analysis Results - Mode 5

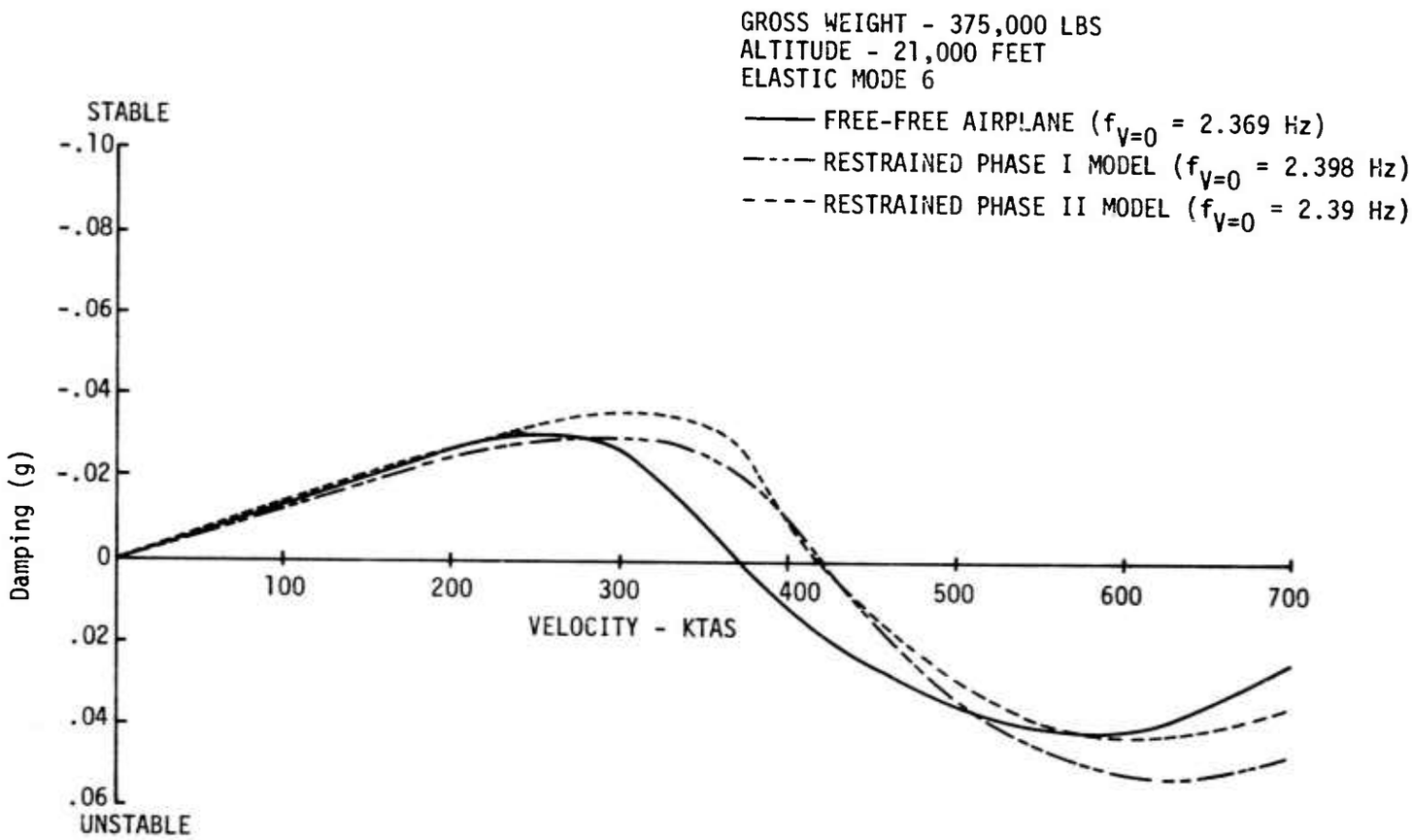

Figure 8. Airplane and Model Symmetric Flutter Analysis Results - Mode 6

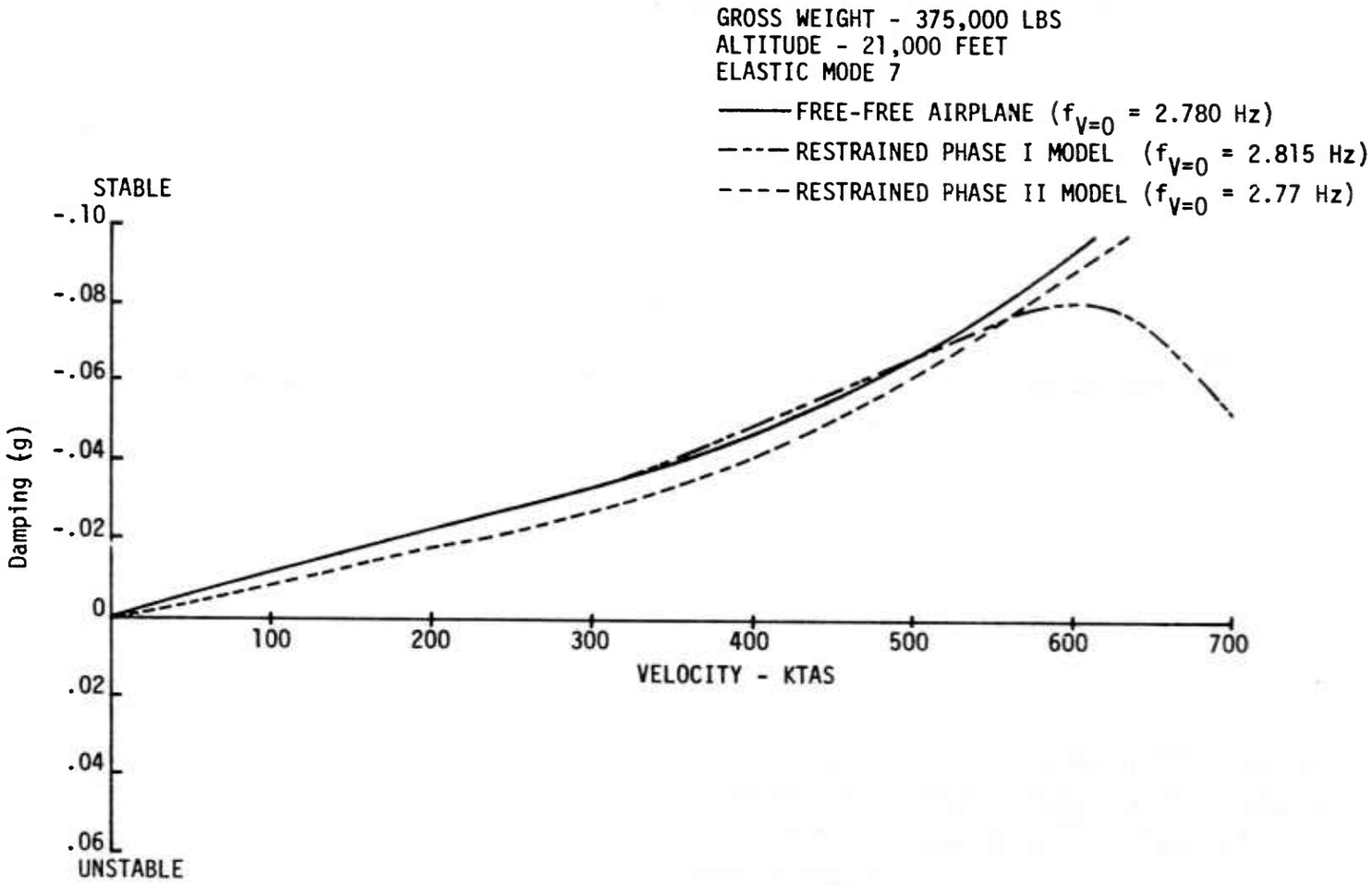

Figure 9. Airplane and Model Symmetric Flutter Analysis Results - Mode 7

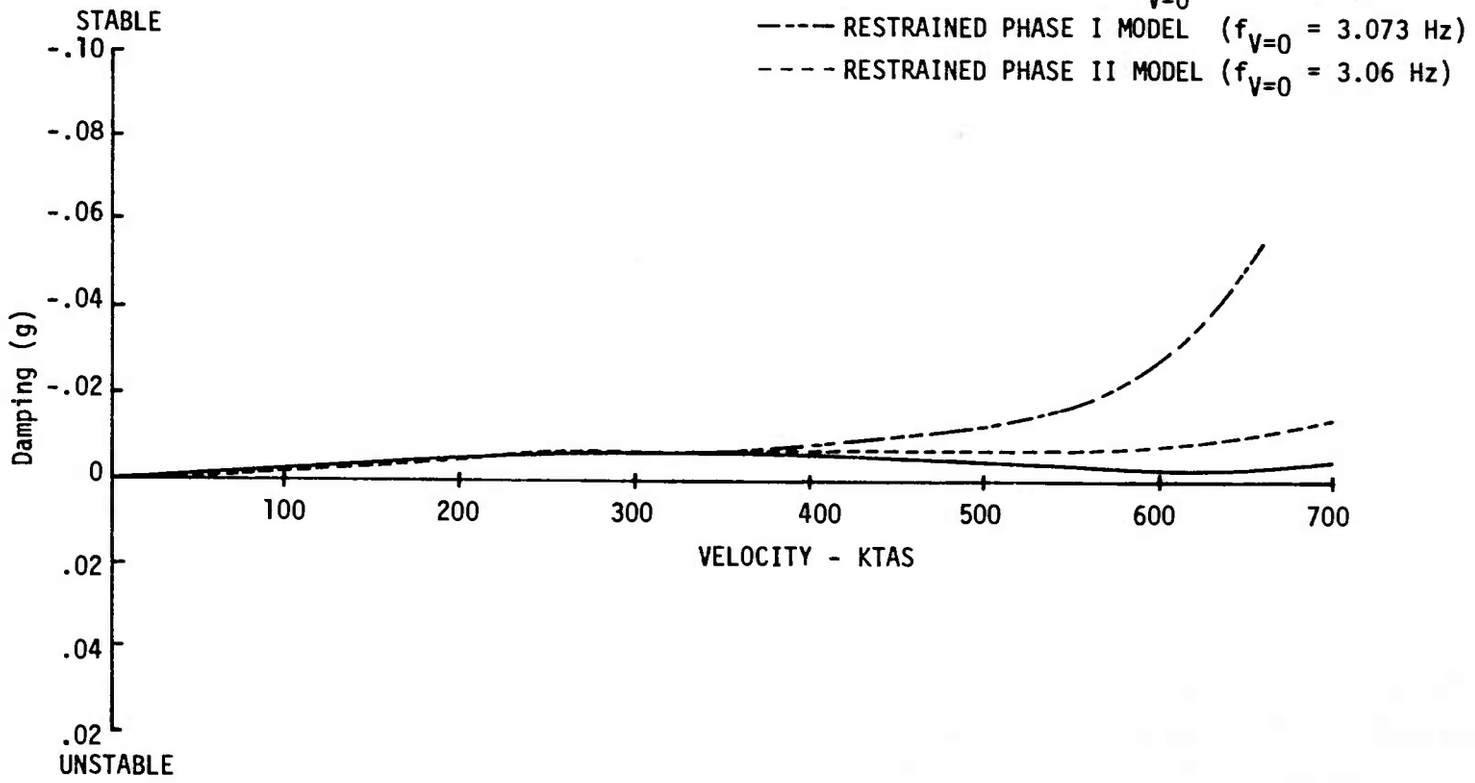

Figure 10. Airplane and Model Symmetric Flutter Analysis Results - Mode 8

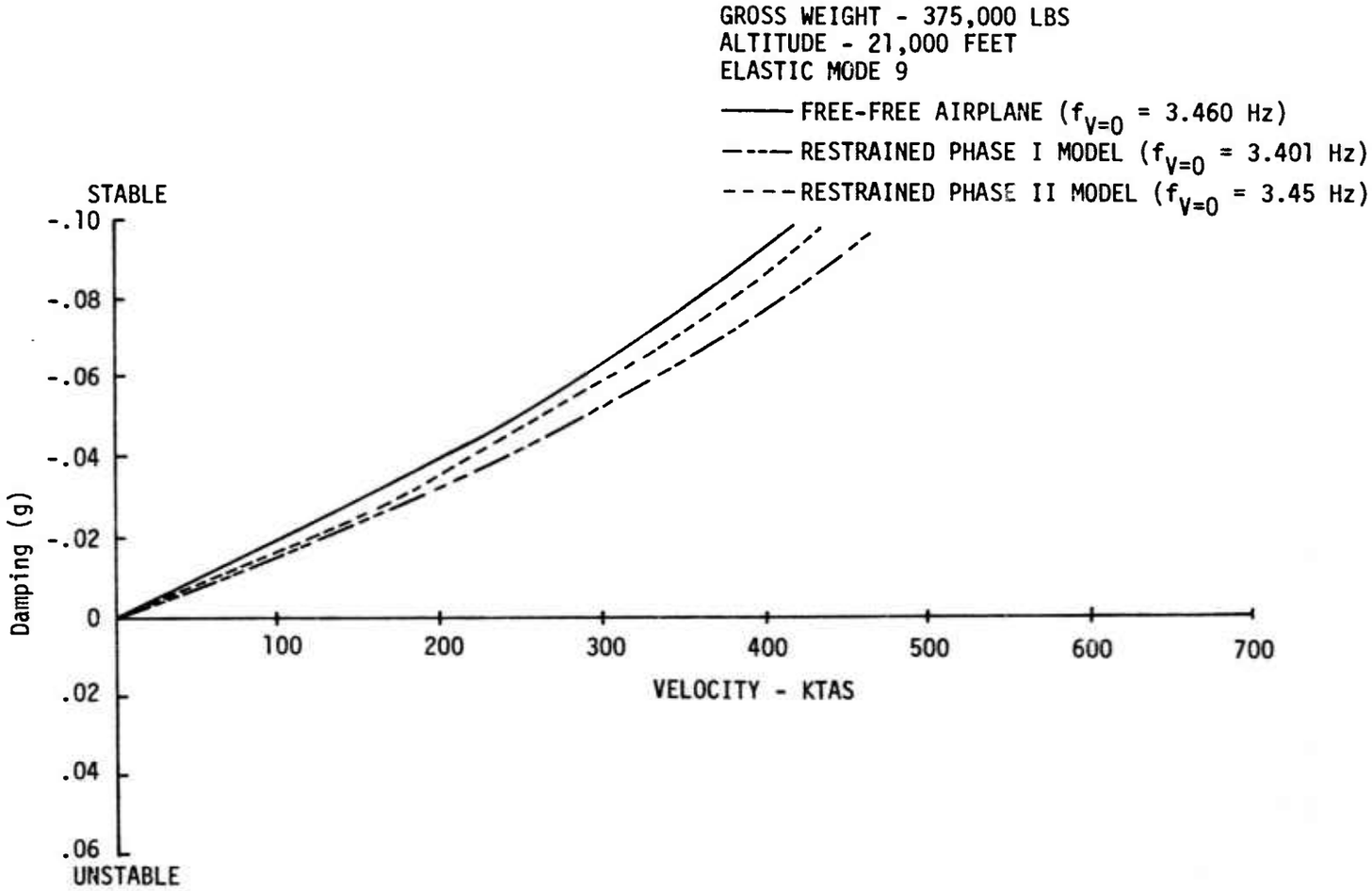

Figure 11. Airplane and Model Symmetric Flutter Analysis Results - Mode 9

felt the model modifications would not affect the previous antisymmetric flutter analysis results.

3.3 Model Modifications

The NASA B-52 aeroelastic model was modified to convert from the 419,000 pound design condition to the 375,000 pound CCV Fuel Configuration 3 condition. The modifications included installation of new ballasted tip tanks, new outboard nacelle struts, and outboard aileron and outboard flaperon segment control surfaces. Model ballast was removed in the center wing section to simulate the 12,000 pound reduced forward body tank fuel.

3.3.1 Control Surface Mechanization

The model was constructed with electromechanical position servo systems for mid-span aileron and elevator control surfaces. The model was subsequently modified by Boeing under a NASA contract to add forward body horizontal canards and the full three-segment CCV airplane flaperons (as one surface on each wing) for wind tunnel demonstration of a full-fuselage ride control system (see Reference 5). The flaperon surfaces are driven by the two torque motors originally installed to drive the left and right hand mid-span ailerons. New wing segments were constructed to omit the original aileron surfaces. Permanent magnet, d.c. tachometers were added to provide rate feedback for the torque motors so the bandpass required for the wind tunnel testing could be attained. The d.c. torque motor, potentiometer and d.c. tachometer for the canards are mounted in the forward fuselage near the surfaces. A sketch of the outboard aileron and flaperon outboard segment installation is shown in Figure 12.

The full three-segment flaperon installation was modified to actuate the outboard segment only for the CCV flutter mode control system. This was accomplished by fabricating new surfaces and installing a balsawood filler where the two inboard segments were omitted, as shown in Figure 13. This photograph shows the details of the left hand flaperon installation. The aft torque motor drives this surface through a crank-pushrod linkage, with a flexible bellows coupling used in the shaft run to accomplish the 29 degree change of direction between the wing and fuselage. The next motor forward drives the right hand flaperon through a similar linkage/shaft arrangement. Stainless steel, precision ball bearings are used at all shaft supports to minimize friction. The control surface size and location are scaled from the CCV airplane.

Between the two wind tunnel entries, a strain gaged flexible torsional link was installed in the one-eighth inch precision shaft just inboard of the right hand surface. This link was installed within the balsawood filler that represented the two inboard flaperon segments in the zero angular displacement position. The strain gages were subsequently calibrated to measure total hinge moment on the flaperon surface.

Components of the outboard aileron actuation system are identical to the components used for the flaperon and elevator systems. These components were purchased for the aileron system to maintain commonality of components to minimize spares requirements. The aileron torque motor, potentiometer and

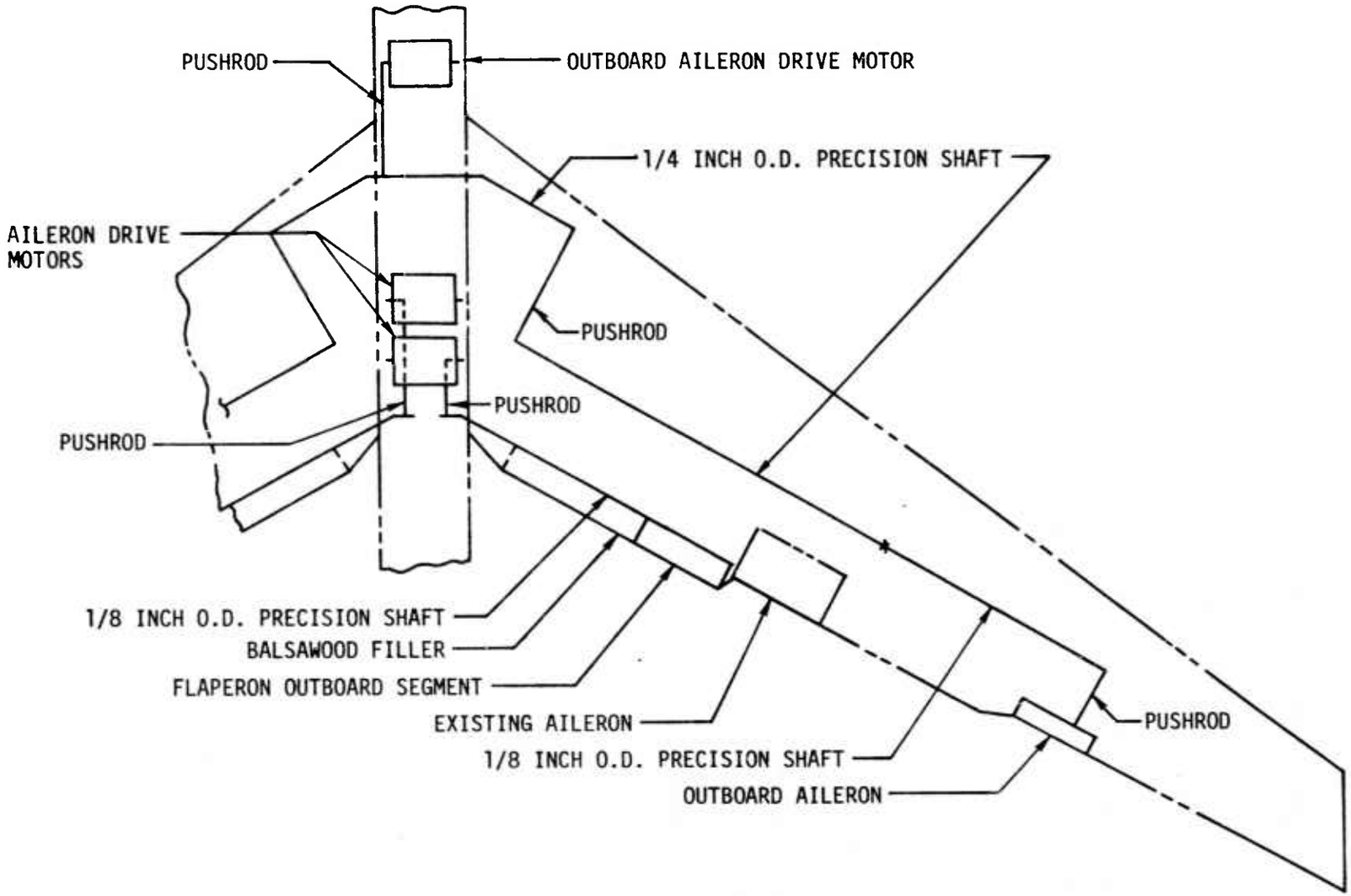

Figure 12. Sketch of Outboard Aileron and Flaperon Installation

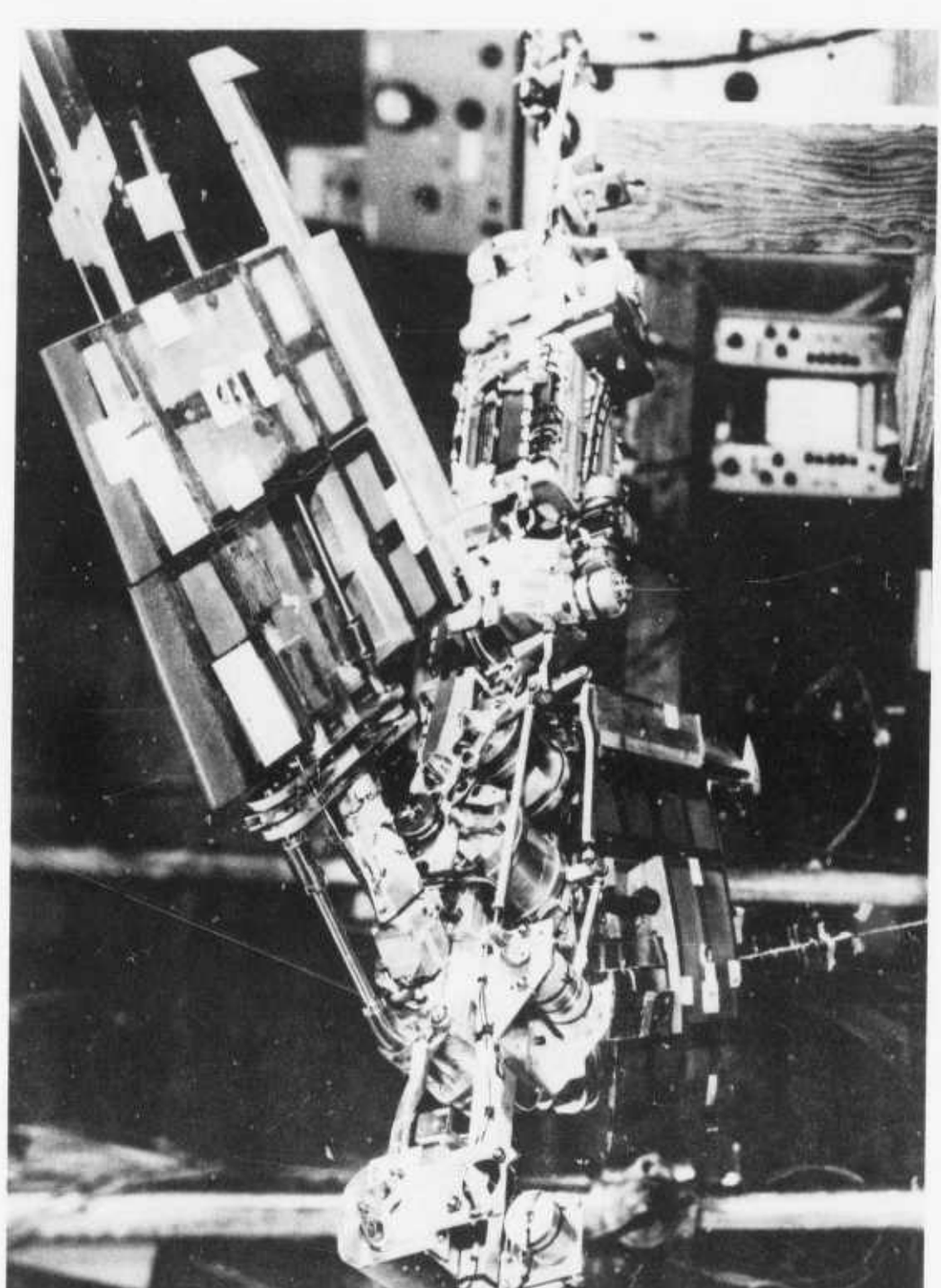

Figure 13. Flaperon and Outboard Aileron Actuation System Installations

tachometer are mounted in the model fuselage, just forward of the wing attachment point (see Figure 13). Torque is transmitted aft through a crank-pushrod linkage and then out the inboard wing leading edge. Another crank-pushrod linkage transmits torque aft to the original aileron shaft run. This shaft run was extended, with one-eighth inch stainless steel precision shafting, out to the aileron surfaces. Torque was then transmitted aft through another crank-pushrod linkage to the surface, as shown in Figure 14. This pushrod protrudes below the wing surface and is covered by a fairing. Flexible bellows couplings are used in the shaft run through the wing to minimize wing stiffness changes. Note that both surfaces are driven by one torque motor. Careful alignment of the precision ball bearing supports was required to minimize friction and resulting hysteresis.

Each torque motor is driven by a d.c. power amplifier. The amplifiers were rack mounted and located in the tunnel control room during the wind tunnel tests. Feedback loops around each torque motor were mechanized on a general purpose analog computer, also located in the control room during testing.

3.3.2 Modifications for Model/Airplane Compatibility

Additional modifications were accomplished on the model to represent the CCV test airplane Fuel Configuration 3 and to improve the model representation of the airplane. The original 94 percent full external wing tip tanks were replaced with empty tanks with nose ballast equivalent to the CCV airplane 2,000 pound ballasted tank configuration. The tanks were fabricated with a honeycomb shell and covered with fiberglass. Accelerometers were subsequently installed inside each tank to provide voltage proportional to vertical acceleration required by the FMC system at the equivalent to Wing Buttock Line (WBL) 925.

New struts for the outboard nacelles were designed and fabricated by NASA to Boeing specifications to provide the required coupling motions in the nacelle vertical and lateral vibration modes. Damping material was added to the new struts, and to the original inboard nacelle struts, by sandwiching epoxy plasticizer between two thin aluminum strips along the struts. This was done to give nacelle mode damping values more nearly representative of the airplane.

Other modifications were performed to improve the model representation of the airplane. Ballast was removed from the equivalent forward body fuel tank to reduce the gross weight and keep the desired center of gravity location. Ballast in other locations in the model was revised as necessary to produce desired mass/inertia properties. All parts added for the control surface mechanizations were lightened as much as possible.

Installation of instrumentation and wiring harness, and fabrication of umbilical cables, were accomplished by NASA. The umbilicals were fabricated with instrumentation signals separated from power signals and with proper shielding and grounding to minimize interference.

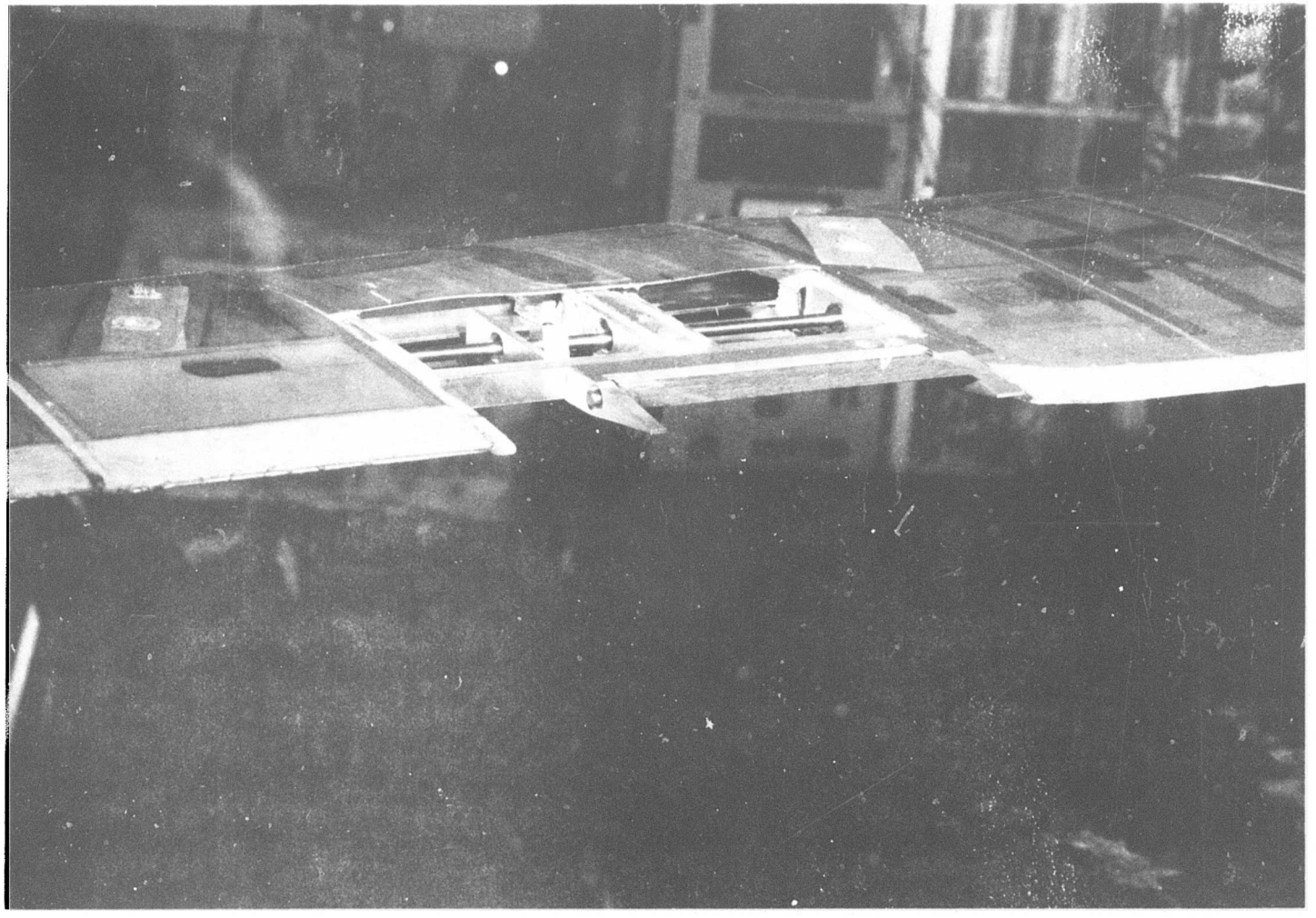

Figure 14. Outboard Aileron Installation

3.4 Model Ground Vibration Tests

Ground vibration tests were conducted by NASA before each of the two wind tunnel entries. In each case, the ground vibration tests were conducted twice, one with soft spring support outside the tunnel, and the other on the model cable mount system in the tunnel test section. Results of the GVT's conducted in the tunnel are discussed in Section 5.

Results of the soft spring complete model ground vibration tests are summarized in Table VII. This table shows the measured frequencies of the first nine symmetric modes, with the free-free vibration analysis frequencies shown for reference. The predicted frequencies are the free-free mode frequencies shown in Table II in airplane scale.

The first, second, fifth, eighth and ninth modes were identified through comparison of predicted and measured mode shapes. For these modes, the vibration characteristics were similar in nature to the characteristics predicted by the vibration analysis, but vibration frequencies do not agree exactly. The mode frequencies shown were obtained with the force shaker applied to the fuselage vertically near the model center of gravity. Frequencies of the modes change some for other shaker locations.

Frequency of the second mode is 6 to 7 percent higher than predicted. A wing antisymmetric mode was found at about 8.5 Hz, which made identity of the second mode difficult. The second antisymmetric mode had been predicted at 8.18 Hz, with the third mode at 10.08 Hz. Thus, it appears the second antisymmetric mode is also higher in frequency than predicted.

Frequency of the ninth mode is also higher than predicted, but the first, fifth and eighth are lower. For these five modes, even though the mode frequencies do not agree exactly, the vibratory motion for each was similar to the predicted characteristics.

Neither mode between the second and fifth can be identified definitely as the third or fourth elastic mode predicted in the vibration analysis. The third mode was predicted to show more inboard than outboard nacelle lateral motion, with motion of the two nacelles out-of-phase. The fourth mode was predicted to be the opposite, with more outboard nacelle lateral motion and the two nacelles in-phase. The measured mode tentatively identified as mode four (based on frequency) shows both inboard and outboard nacelle lateral motion with the nacelles out-of-phase.

The sixth and seventh modes are the most difficult to identify from the GVT data. The ground vibration test conducted before the first tunnel entry shows three symmetric modes between the fifth and eighth modes. The mode frequencies were 13.29, 13.50 and 13.64 Hz. Mode shapes for all three modes are similar to the predicted sixth mode. The GVT conducted in the tunnel during the first entry shows only two modes in this frequency range, at 12.9 and 13.5 Hz (see Section 5). Thus, the 13.29 and 13.50 Hz modes were tentatively identified as the sixth and seventh modes, respectively, for the Phase I model, although the 13.5 Hz mode shape does not agree with the predicted seventh mode shape. The sixth mode was predicted analytically to be the flutter mode for the model and airplane.

Both ground vibration tests conducted before the second series of

TABLE VII. MODEL SYMMETRIC GROUND VIBRATION TEST RESULTS-COUPLED MODE FREQUENCIES

	PHASE I MODEL		PHASE II MODEL	
MODE	PREDICTED (HZ)	ACTUAL (HZ)	PREDICTED (HZ)	ACTUAL (HZ)
EM-1	4.33	4.30	4.32	4.25
EM-2	9.15	9.80	9.21	9.78
EM-3	10.85	10.93	10.91	10.74
EM-4	11.78	11.00	11.84	11.10
EM-5	12.11	12.00	12.11	12.00
EM-6	13.15	13.29	13.10	13.28
EM-7	15.45	13.50	15.18	13.62
EM-8	16.82	16.25	16.77	16.15
EM-9	18.63	19.07	18.91	19.60

Note: Model supported by soft spring during the ground vibration tests.

wind tunnel tests showed only two symmetric modes between the fifth and eighth elastic modes. The mode shape of the 13.28 Hz mode is almost identical to the mode shape of the 13.5 Hz mode found before the first entry. Mode shape of the 13.62 Hz mode is not available. The model was modified between the two entries to correct wing tip mass properties, to install all elevator components so the elevator could be used to excite the model, and to correct alignment of the aft fuselage main spar. Therefore, some difference would be expected in the mode frequencies, primarily the seventh mode which shows strong body first vertical bending motion.

Another possibility is that the seventh mode was "masked" during the ground vibration tests by a strong 15.5 Hz antisymmetric mode, but this mode was not excited appreciably by the fuselage shaker oriented vertically. The "actual" vibration mode frequencies shown in Table VII were obtained by the author from the limited ground vibration test data available.

4.0 FLUTTER MODE CONTROL SYSTEM EVALUATION

Under the CCV program, a flutter mode control system was synthesized for the flight test airplane for Fuel Configuration 1 (260,700 pounds) and 2 (298,500 pounds) at 21,000 foot altitude conditions. The FMC system designed for these conditions met the performance goal, increasing the flutter placard airspeed by 30 percent with ±6 db gain and ±60 degree phase stability margins. But, the system required modification to provide a common FMCS configuration that would meet the performance requirements for the 375,000 pound Fuel Configuration 3. The modification, consisting of changes in the shaping filter and sensor alignment for the outboard aileron, was necessary because the off-design condition was specified subsequent to the original FMCS synthesis. The final airplane FMC system, shown in the block diagram of Figure 15, met the performance requirements at all three CCV fuel configurations. A more detailed discussion of the FMC system analysis and synthesis is contained in Reference 2.

The final airplane system was evaluated on model equations of motion. The following sections discuss this evaluation and the results of a hybrid computer simulation study conducted to evaluate FMC system nonlinearity effects. Preparation of wind tunnel test plans is discussed in Section 4.3.

4.1 FMC System Evaluation

The airplane system was scaled to model frequencies for evaluation on 18 degree-of-freedom model equations of motion that included vertical displacement and pitch degrees of freedom to represent cable mount dynamics. Mach 0.24 aerodynamic parameters were used in the equations, with tunnel test fluid density and free-stream velocity as explicit parameters so model analyses could be conducted in the same manner as airplane analyses. The nominal density, .00499 slug/ft^3, is equivalent to the airplane 21,000 foot altitude density and was attained in the tunnel using 95 percent freon and 5 percent air as the test fluid.

Model analyses were conducted on three different model configuration equations of motion. The first equations used were based on original model mass and design stiffness data, with scaled airplane nacelle/nacelle strut characteristics, discussed in paragraph 3.2.1. The airplane FMCS was also evaluated on equations based on measured mass and design stiffness properties, with the original nacelle struts. The following paragraphs discuss only the last analyses, which were conducted on equations of motion based on measured mass and design stiffness properties with measured revised nacelle frequencies, damping and mass properties, but with analytical nacelle mode shapes (see paragraph 3.2.2). This configuration represents the model as tested in the first entry. The model equations assumed .005 structural damping for all modes but the nacelle modes (see paragraph 3.2.1).

A block diagram of the nominal FMC system is shown in Figure 16 in model scale. This block diagram differs from that shown in Figure 15 only in that the shaping filters are expressed in model frequency scale and the actuator transfer function represents the model electromechanical actuation systems. Actuation system feedback gains were adjusted with the model in the tunnel to match the transfer functions shown. Actuator performance equivalent to the

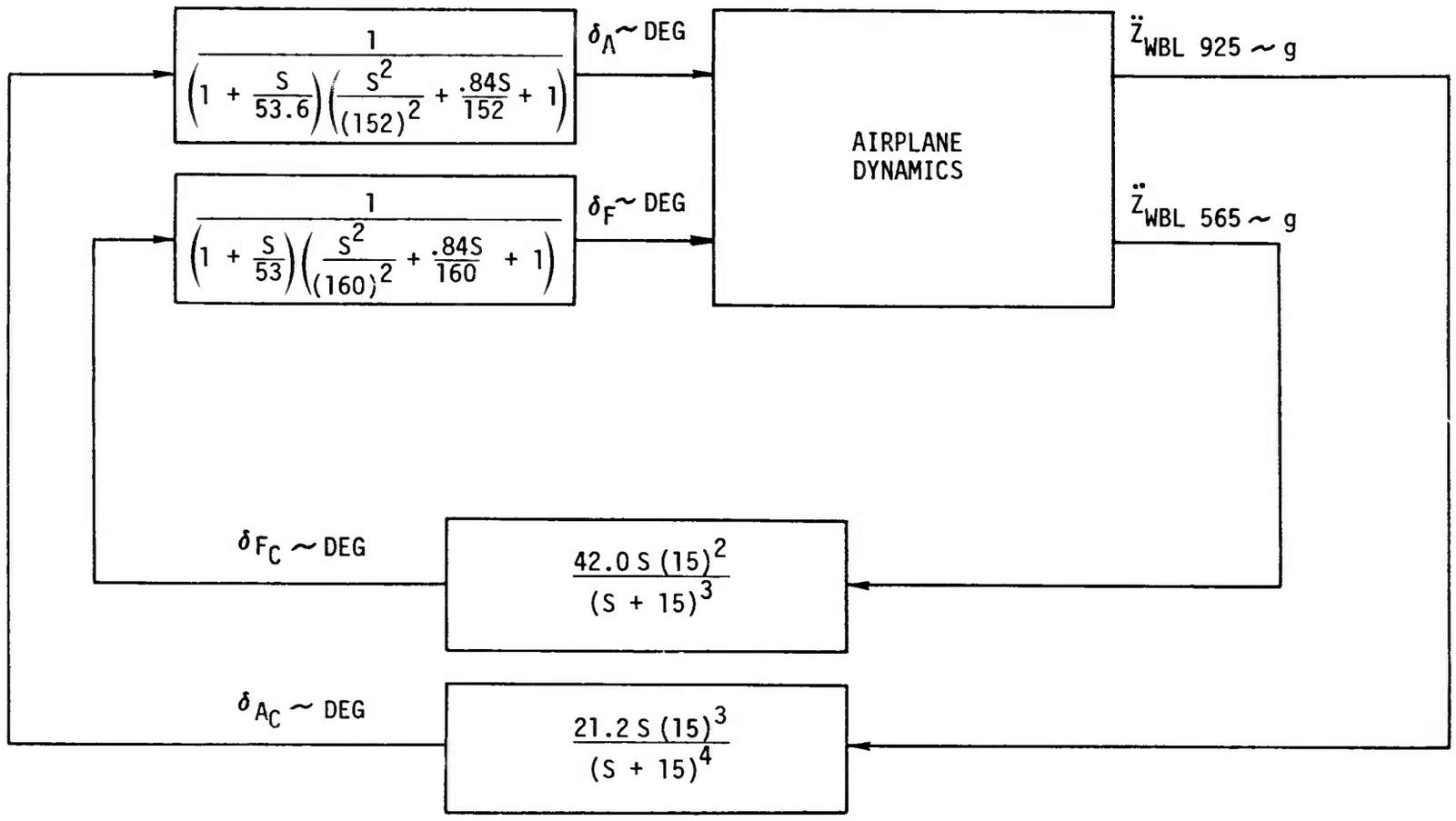

Figure 15. Airplane FMCS Block Diagram

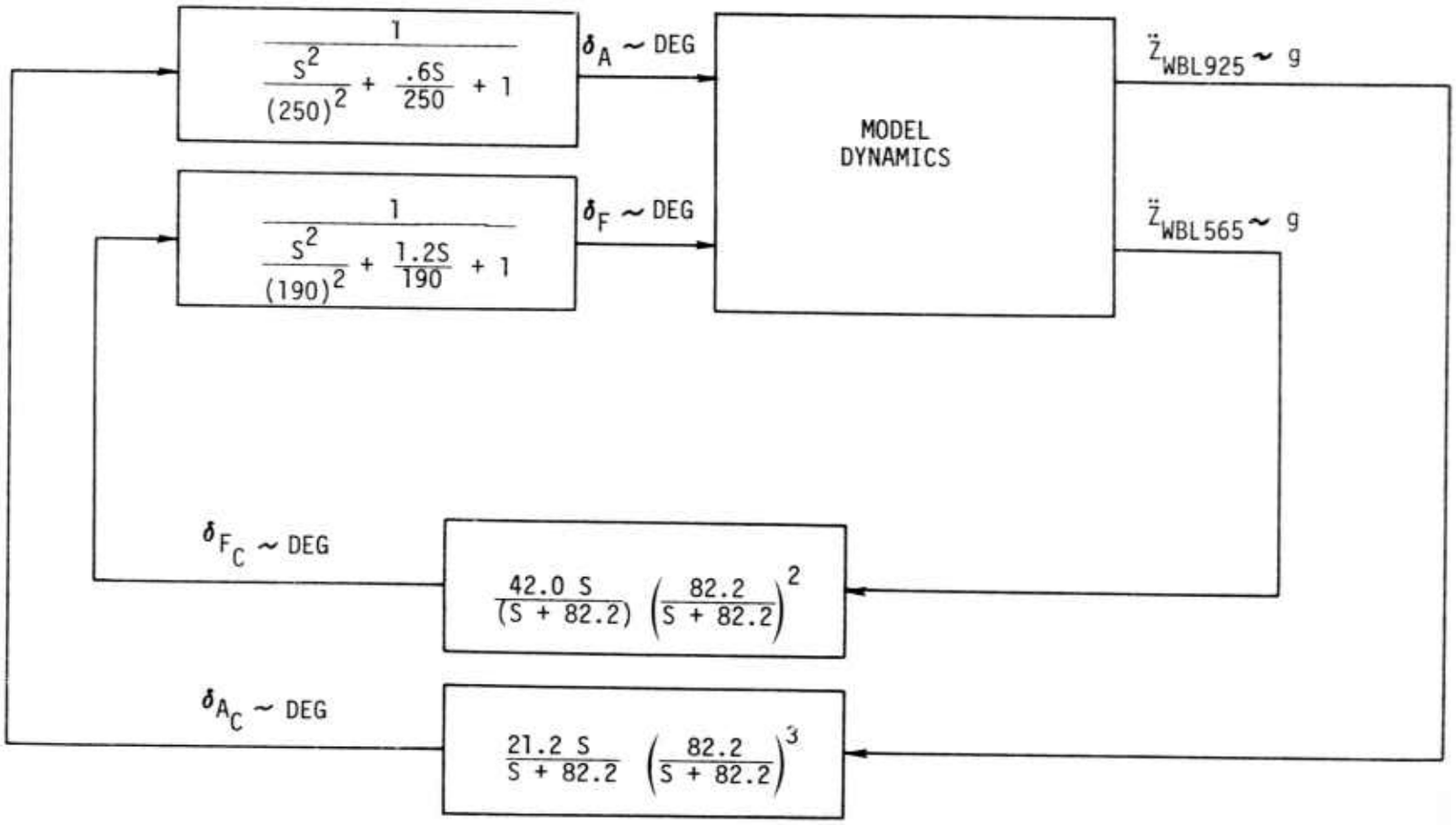

Figure 16. Model FMCS Block Diagram

airplane actuators in model scale was not possible with the model actuation system components. However, in the frequency range that includes the flutter mode, the model actuators closely represent the airplane actuators. The model accelerometers were located to the scaled airplane locations and the same control surfaces are used. Model fuselage and wing buttock line designations discussed in this section are in airplane scale for clarity, but all data are in model scale.

The two model modes with lowest damping are shown in the Q-ζ plot of Figure 17. The model predicted flutter dynamic pressure is 45.6 psf for this model configuration (which represents the model as tested in the Phase I wind tunnel tests discussed in paragraph 5.2.1). The flutter point is equivalent to about 325 KCAS in airplane scale, about 13 KCAS higher than the airplane flutter speed. Figure 17 also shows performance of the FMC system. The predicted flutter mode damping is similar to that predicted for airplane Fuel Configuration 3.

A gain/phase root locus analysis was conducted at 45 psf dynamic pressure for the aileron loop with the flaperon loop at nominal gain, and for the flaperon loop with the aileron loop at nominal gain. The analysis results showed that the design criteria of ±6 db gain and ±60 degrees phase stability margins were satisfied. The airplane FMC system could then be simulated on the model with similar performance predicted.

Figure 18 shows the effects of FMCS gain variations on the flutter mode damping. This figure shows the flaperon loop at nominal gain to be more effective than the aileron system at twice nominal gain. But, either loop operating individually adds damping to the flutter mode, providing a margin of safety for the wind tunnel tests. A similar trend was noted for the airplane.

The effects on system performance of filter cutoff frequency variations in both channels simultaneously can be seen in Figure 19. The frequency variations analyzed are 0.75 and 1.25 times the nominal 82.2 rad/sec frequency. The lower frequency, 61.65 rad/sec, introduces phase lag and decreases gain at the flutter mode frequency, relative to the nominal system, which degrades the FMC system performance. Phase lead and increased gain introduced by the higher cutoff frequency increases the effectiveness of the system above about 40 psf dynamic pressure.

The Phase I wind tunnel test results, discussed in paragraph 5.2.1, showed the system with nominal gains to be less effective than predicted in controlling the flutter mode. The system feedback gains were subsequently increased for the Phase II tests to produce the performance predicted for the nominal gains. The gains used in the Phase II wind tunnel tests were the same as used in the final airplane flight tests, twice nominal in the aileron channel and 1.25 times nominal in the flaperon channel. The model was modified between the two tunnel entries to correct wing tip mass properties and to install all elevator actuation system components so the elevator could be used to excite the model as was planned for airplane flight tests. Predicted performance for the higher gains on the revised model is discussed in Section 6, where it is compared to wind tunnel test results. Analytical subcritical model responses were generated for comparison with test data. Reference 6 contains a complete set of these plots, which includes frequency response and co-quad plots for outboard wing vertical acceleration (WBL 925) and inboard wing vertical acceleration (WBL 565) due to aileron, flaperon and horizontal canard control surfaces. The plots were generated with FMCS off and on at

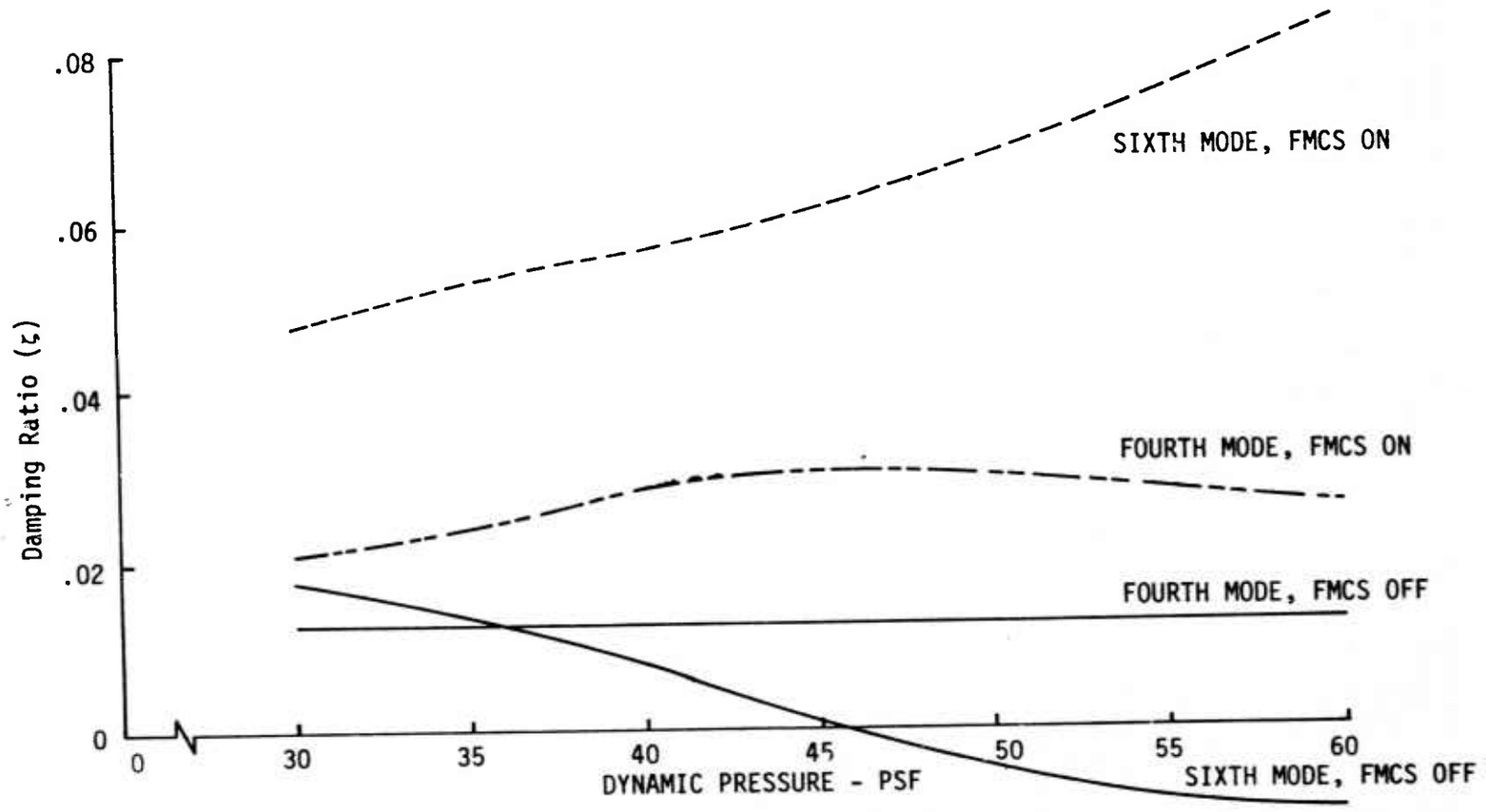

Figure 17. Model FMCS Performance (Analytical)

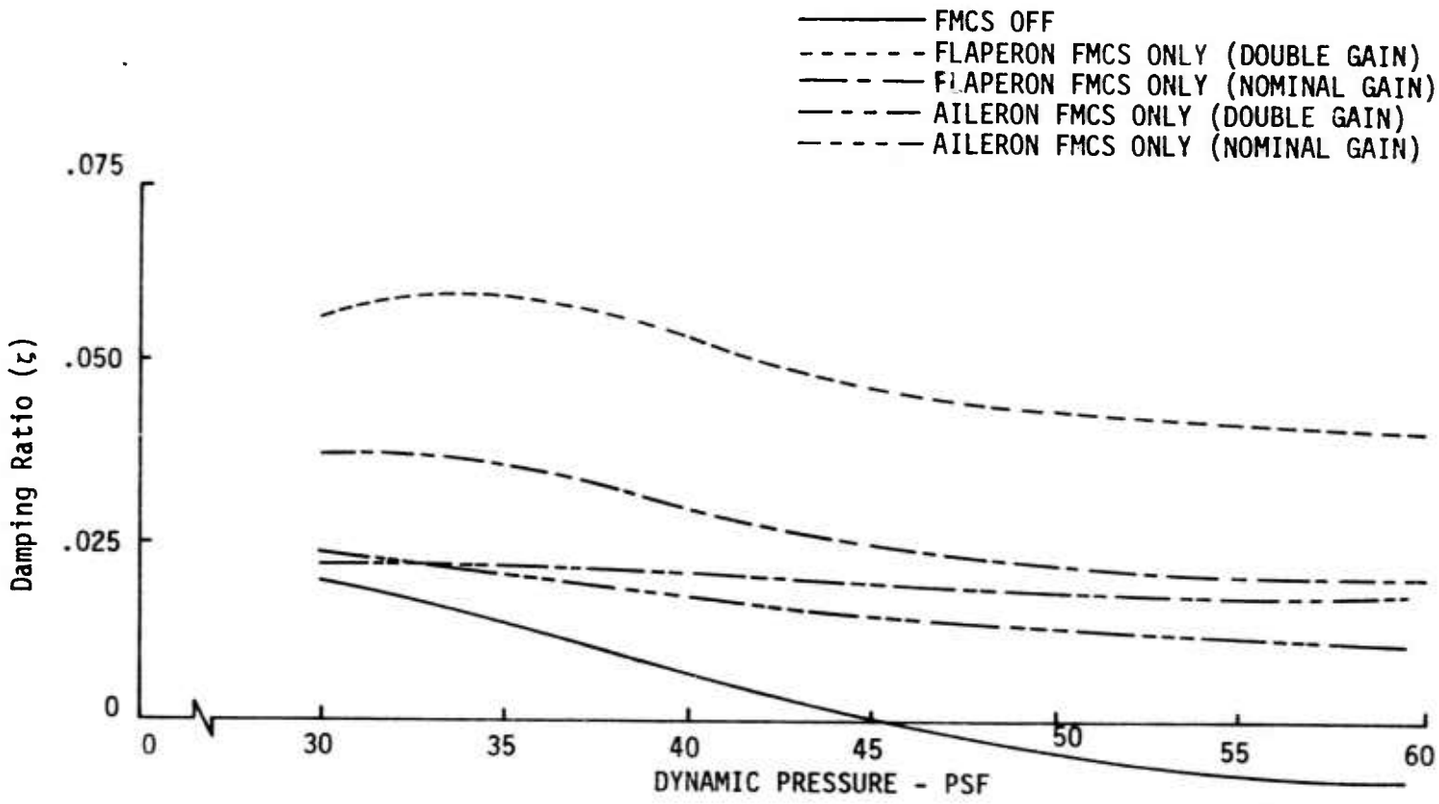

Figure 18. Effects of FMCS Gain Variations on Model Flutter Mode Damping (Analytical)

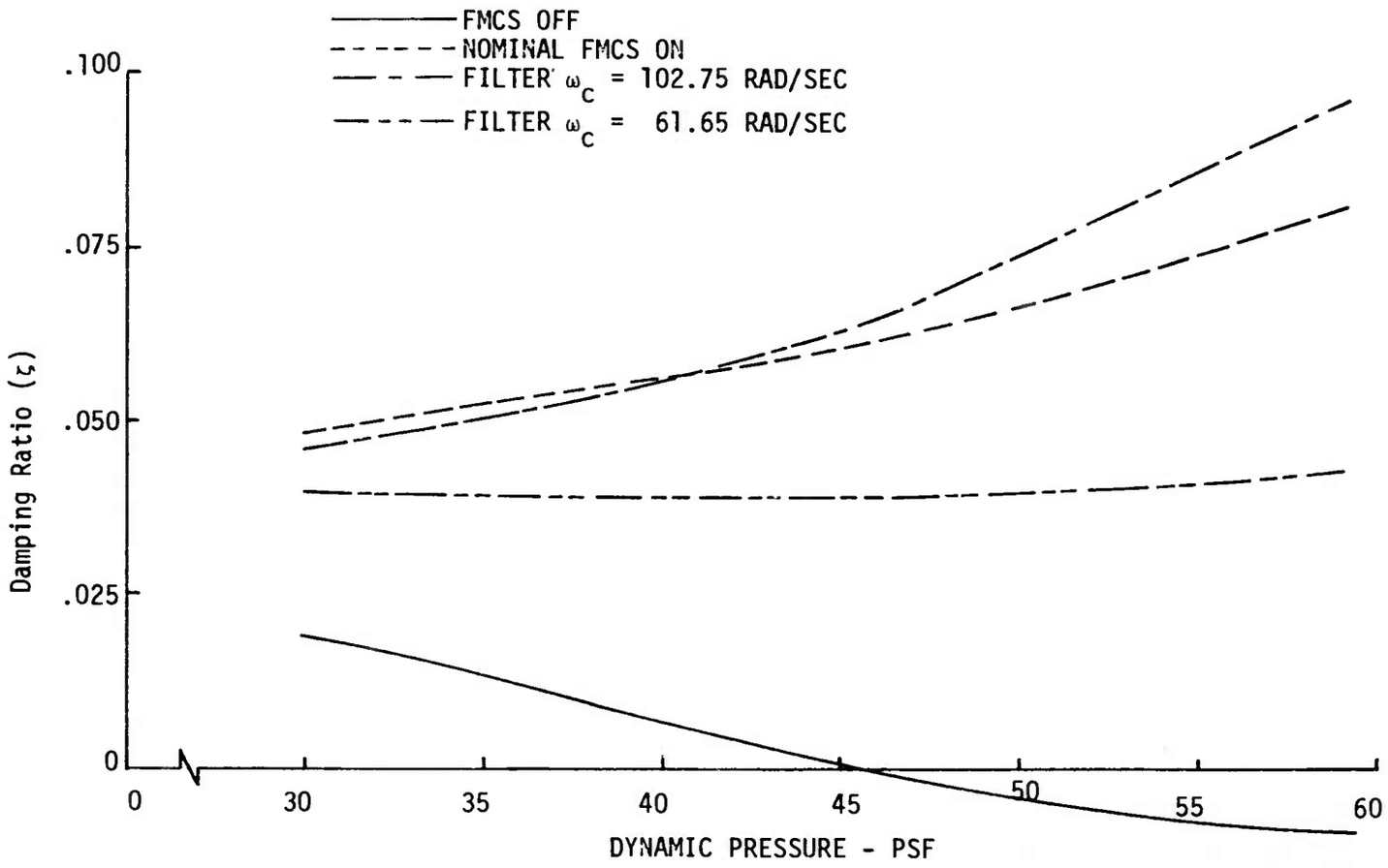

Figure 19. Effects of Filter Cutoff Frequency Variations on Model Flutter Mode Damping (Analytical)

27.75, 35.00, 38.12, 45.00 and 50.00 psf dynamic pressure. The first three conditions correspond to three airplane Fuel Configuration 3 flight test airspeeds (250, 280 and 295 KCAS). Reference 6 also contains copies of airplane responses at these conditions as well as model wind tunnel data for these and other conditions.

4.2 Hybrid Computer Simulation Studies

Simplified model equations of motion were simulated on a hybrid computer primarily to evaluate actuator and FMCS nonlinearities. Tests were also conducted to evaluate using the horizontal canards for excitation during model dynamic response flutter testing.

Two separate simulation studies were conducted. The first used model equations of motion based on existing nacelle struts and was conducted before the Phase I wind tunnel tests. The second study was accomplished with new nacelle strut representation, for the model as tested in the Phase I tests. The two studies evaluated similar nonlinearities with similar results.

In both studies, two cable and six symmetric elastic modes were simulated. The first study considered two conditions, one marginally stable and the other unstable, but only an unstable condition was simulated in the second study. The unstable conditions were simulated to detect limit cycle tendencies with hysteresis in the actuation system dynamic representations. The first study equations of motion were simplified by using only a first order lift growth representation for all eight degrees of freedom. Four lift growth terms for cable constraint modes and one term for elastic modes were used in the second study. These simplifications were included to facilitate simulating all eight degrees of freedom without losing accuracy for the nonlinear simulation test results.

The simulation test results showed that actuator rate limits would cause a large amplitude limit cycle in the flutter mode frequency when rate commands from the FMC system exceeded the limit. The time histories shown in Figure 20 were obtained with ±25 degrees rate limits imposed on the aileron and flaperon. The responses with .95 ft/sec vertical gust amplitude are approaching a limit cycle with amplitude larger than the responses with FMCS off. Actuator position limits, imposed on the command from the FMCS, did not cause a limit cycle, but did degrade the system performance depending upon the amplitude of sensed motion being fed to the FMC system. This latter condition was set up identically to the saturation testing to be conducted in Phase II wind tunnel tests, except sinusoidal vertical gust was used in the simulation, and sinusoidal aileron frequency sweeps were to be used in the wind tunnel for model safety.

Tests conducted with control surface actuation system hysteresis similar to that measured on the model systems indicated some FMCS degradation, and a limit cycle was found at conditions where the unaugmented model was unstable, as shown in Figure 21. The hysteresis simulated was ±0.4 degrees on the aileron and ±0.2 degrees on the flaperon. The Phase I wind tunnel tests were conducted with similar hysteresis values, but only testing below the open loop flutter point was accomplished. The hysteresis was lowered for Phase II, as discussed in paragraph 5.1, and no limit cycle during supercritical testing was noted. Model actuator hysteresis represents one of the major difficulties

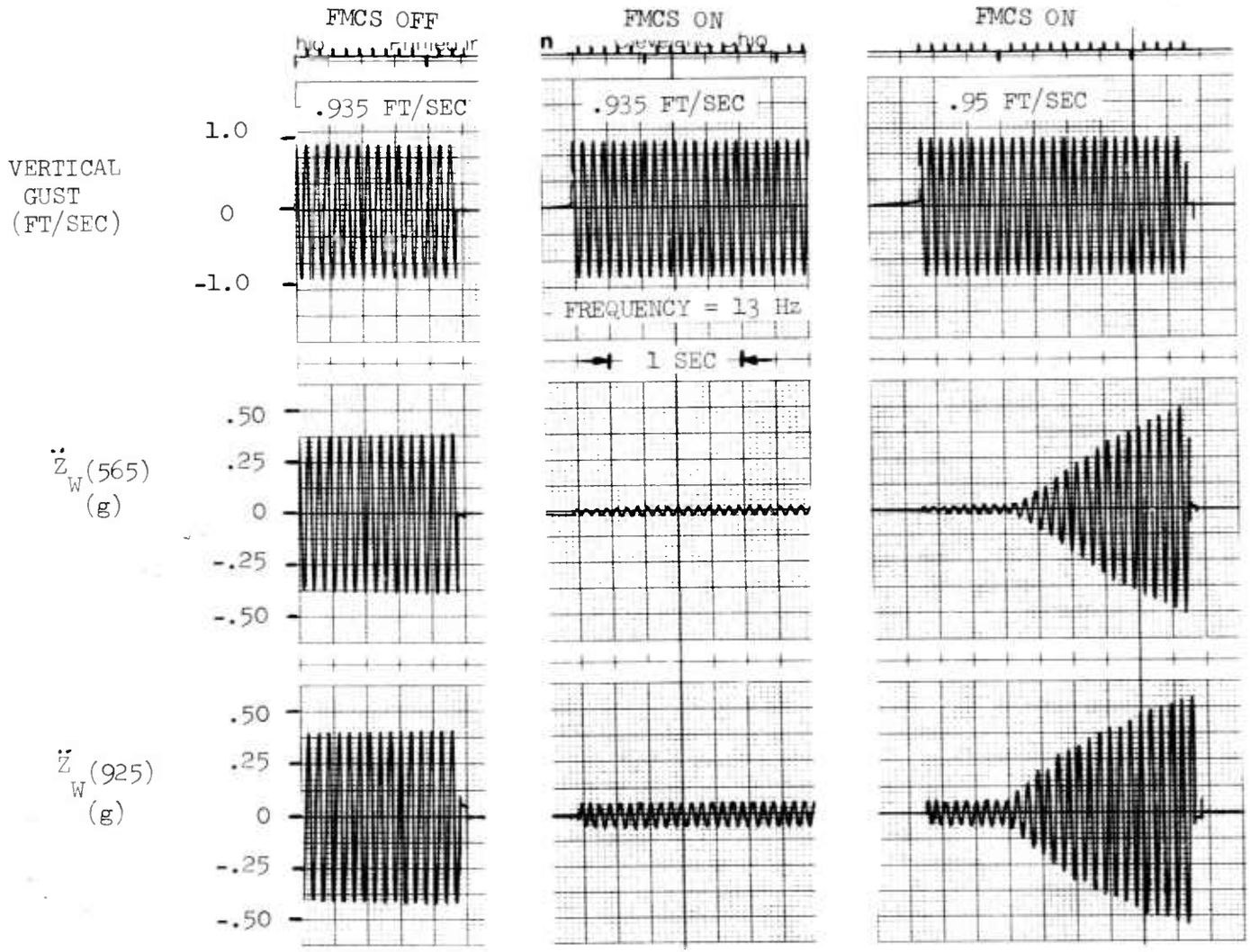

Figure 20. Effect of ±25 Deg/Sec Aileron and Flaperon Actuation System Rate Limits on FMCS Performance

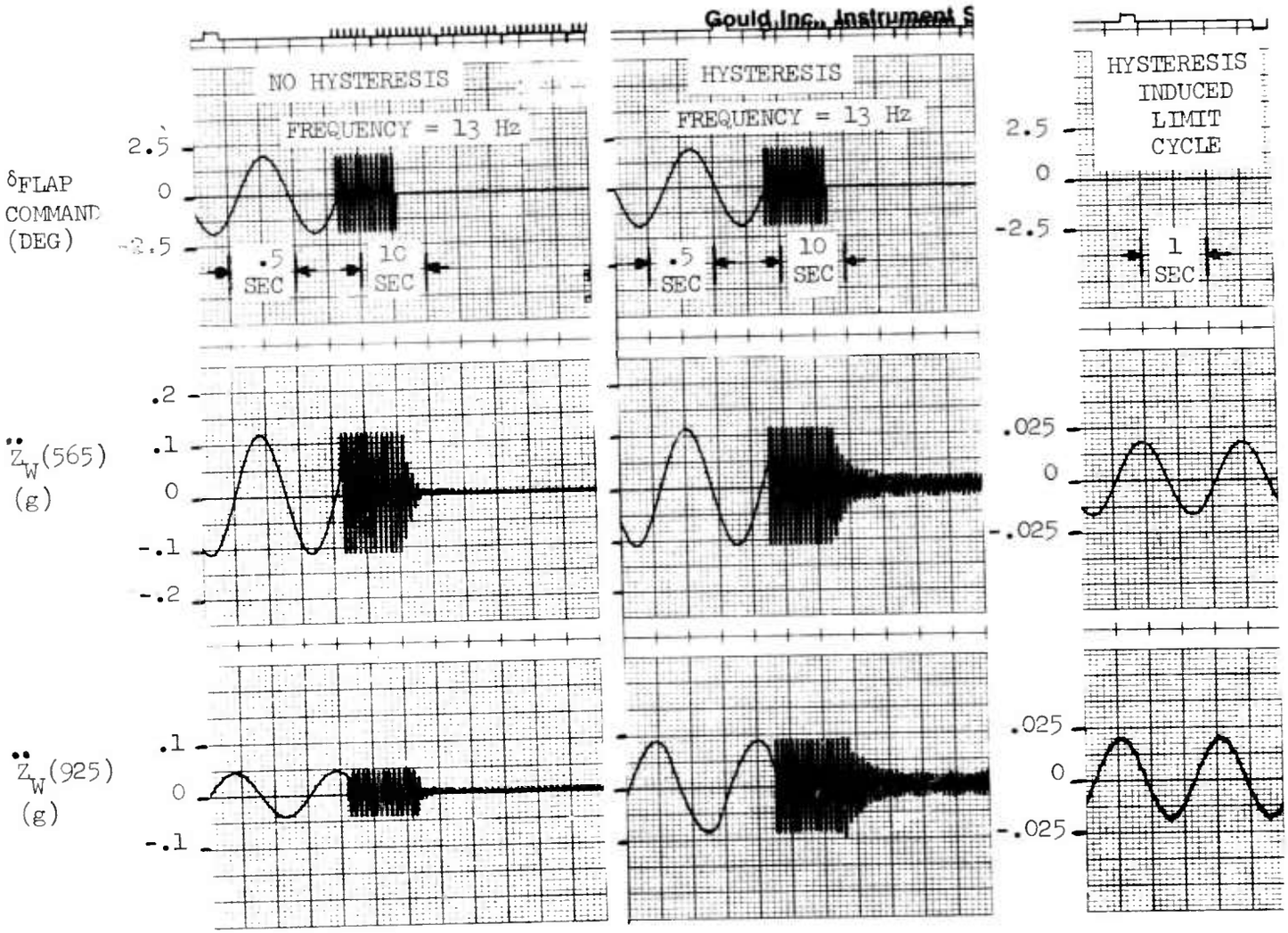

Figure 21. Effect of ±0.20 Degree Flaperon Hysteresis and ±0.40 Degree Aileron Hysteresis on FMCS Performance

to be overcome in successfully testing a system such as flutter mode control in the wind tunnel.

Results of the simulation studies showed that without tunnel turbulence, aileron dwell and clamp (at flutter mode frequency) and one cycle sine wave pulse excitation should produce good wing vertical acceleration decay time histories. This result was indicated in the Phase I wind tunnel tests, but the tunnel turbulence excited the flutter mode after the sine wave command was removed so that damping estimates could not be made. The simulation study showed the flaperon was more effective in exciting the flutter mode than the canards. The outboard aileron was found to excite the flutter mode about as well as the flaperons. But, the ailerons excited more modes in the frequency sweeps, so they were chosen for the model wind tunnel tests.

4.3 Wind Tunnel Test Plans

Detailed test plans were prepared for both wind tunnel entries. The Phase I test plan was prepared to include sufficient wind tunnel tests to verify the model flutter characteristics and the FMC system performance and to evaluate dynamic response flutter testing techniques. The Phase I tests described in paragraph 5.2.1 were conducted according to this plan, but with some deviations as the tests results indicated were desirable.

The test plans were prepared assuming a NASA engineer would serve as test director, with support provided by two Boeing engineers familiar with the structural analyses, FMC system analyses and model actuation system hardware, including the analog computer.

The Phase II wind tunnel test plan is shown in Appendix II. This plan includes all conditions and tests required for correlation with flight test results. The model test conditions were selected to provide three conditions that were equivalent to conditions at which airplane Fuel Configuration 3 dynamic response testing was to be conducted. The control surfaces and types of inputs shown in Table XII for model excitation correspond to that used during the airplane flight tests.

The Phase I wind tunnel test results showed the transient response methods did not give data for reliable flutter mode damping estimates due to tunnel turbulence. The elevator actuation system was operative in the Phase II entry, and the test plan included one-cycle sine wave elevator pulses to simulate the pilot command used in flight tests.

The tunnel test procedure in Table XIII was prepared to minimize tunnel condition changes. The first series of tests was planned to determine the basic model flutter condition and to demonstrate the FMCS performance. This testing was assigned the highest priority. The remaining tests were planned to be accomplished at one tunnel condition at a time until all tests were completed.

The general philosophy followed in preparing the test plan was to assign highest priority to the minimum items that would fulfill the test objectives. These tests were then to be conducted so as not to jeopardize the model. Before testing was to be done with FMCS on above the basic model flutter point, the fact that the system was functioning properly had to be

demonstrated. This includes all hardware items comprising the feedback system, from sensors to the aileron and flaperon control surface actuation systems.

The remaining items were to be conducted as time permitted, and again, each item was assigned priority according to its importance. The plan was prepared from an optimistic point of view such that all testing could be accomplished in the allotted tunnel time if no major difficulties were encountered.

5.0 MODEL TESTING

The B-52 aeroelastic model was tested in the NASA Langley Research Center Transonic Dynamics Tunnel during two entries. The first series of tests (Phase I) were conducted in June and July 1973, primarily to establish the degree of correlation of the model with the CCV program flight test airplane through comparison of wind tunnel test data with model and airplane analytical results. The Phase I test results showed no additional modification of the model was required to provide the desired correlation.

All of the data required for comparison with airplane flight test results was obtained in the second tunnel entry, conducted in December 1973 and January 1974.

The following sections discuss preparation of the model for the wind tunnel test, the test plans, and the wind tunnel testing conducted. A more complete discussion of the Phase I testing is given in Reference 4.

5.1 Model Preparation

Before the model was installed in the tunnel for the first series of tests, it was completely assembled and set up for final evaluation of the flaperon and aileron actuation systems. Feedback loops for the systems were mechanized on a general purpose analog computer that was also used to mechanize the FMC system. Wiring between the model and the computer included the umbilical cables that were to be used in the tunnel. Only the wiring between the control room and the tunnel test section was not included during this testing.

Position and rate feedback gains were determined for the outboard aileron and two outboard segment flaperon actuation systems to provide the desired performance. This was done by experimentally determining the gains required to match the system frequency responses to the desired transfer functions discussed in paragraph 4.1. The dynamic testing conducted showed two shaft modes between 60 and 80 Hz on the outboard aileron system, and no shaft modes below 100 Hz on either flaperon system. Hysteresis of the outboard aileron surface relative to a 0.1 Hz triangular wave command measured about ±0.44 degrees. Hysteresis of the flaperon actuation systems measured ±0.28 and ±0.16 degrees for the left and right hand systems, respectively, in terms of motor shaft displacement relative to displacement command. Hysteresis of both flaperon surfaces relative to the motor shafts was estimated to be less than ±0.05 degrees. Hysteresis was reduced before the Phase II wind tunnel tests by careful alignment of all shafting and bearings to ±0.26 degrees for the aileron and ±0.13 degrees for the right hand flaperon, for motor shaft displacement relative to commanded displacement.

Figure 22 is a photograph of the model installed on the cable mount system in the tunnel. The photograph shows the flying cables, snubber cables and the umbilical cable routing. Power signals going into the model were carried by the umbilicals attached to the snubber cables, and instrumentation signals were carried by the umbilical seen coming out of the model fuselage aft to the tunnel sting. Power and instrumentation voltages were routed separately to minimize interference difficulty.

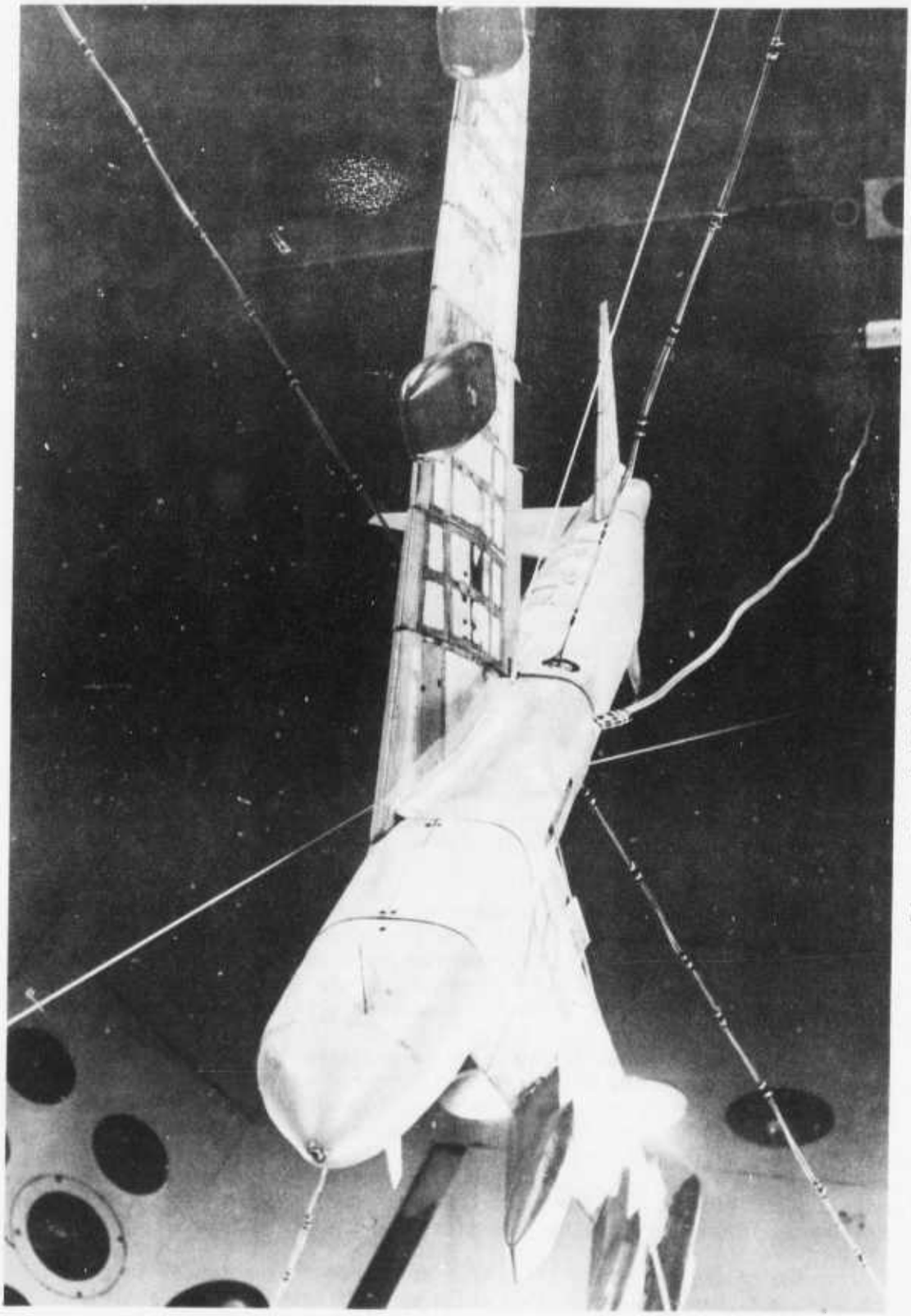

Figure 22. B-52 Model Installed in Wind Tunnel

With the model installed in the tunnel, functional checks of the FMC system, from sensors to control surfaces, were conducted. Feedback gains in the surface actuation systems had to be readjusted to give the desired performance due to the additional wiring resistance in series with the torque motor coils picked up in the wiring between the control room and test section. Signals from the model sensors required for the FMCS, wing inboard and outboard accelerometers and actuation system motor shaft servopotentiometers and tachometers, came out to a signal conditioning electronics rack in the tunnel control room. These signals were then passed to the analog computer through the computer trunk system. Actuation system feedback signals and FMCS and external commands to the actuation systems passed from the computer to the rack mounted power amplifiers and then through internal wiring and umbilical cables to the actuation system torque motors.

Each day before testing began, dynamic checks were conducted on the actuation systems and the FMCS mechanization on the analog computer. This was done to detect any malfunction in the electromechanical and electronic components. Use of an analog computer for the actuation system feedback and FMCS mechanization requires an experienced computer operator who can detect malfunctions before disastrous results occur during testing.

Before the start of wind-on testing in both Phase I and Phase II, a brief GVT was conducted with the model mounted on the flying cables in the tunnel test section. The snubber cables were relaxed and a soft spring was employed to hold the model vertically on the tunnel centerline. Figure 23 shows the results obtained during the second tunnel entry. The co-quad plot is for right hand outboard wing vertical acceleration due to a force shaker applied to the model fuselage near the center of gravity. The first elastic mode has been omitted from this plot because of its large amplitude. Frequency of the sinusoidal force was swept from 4 to 24 Hz logarithmically in 30 minutes.

The co-quad plot shows some antisymmetric as well as symmetric modes, but it is not apparent which modes are symmetric. Identity of the modes was established by visual observation of the model and by comparing this plot with similar plots obtained during soft spring ground vibration tests conducted previously outside the tunnel. Results of the previous tests are discussed in paragraph 3.4.

Symmetric coupled mode frequencies measured before the Phase I and Phase II tests are shown in Table VIII. The predicted mode frequencies are shown for reference. The predicted frequencies were taken from Table III and converted to model frequency scale. The measured mode frequencies were taken from the out-of-phase component of the co-quad plot obtained during each test.

The actual frequencies compared to predicted frequencies show the same trend noted in comparing GVT results with free-free vibration analysis results discussed in paragraph 3.4. The second and ninth modes are significantly higher in frequency and the seventh is apparently significantly lower. Identities of the sixth and seventh modes, shown in Table VIII, are tentative and were established from the limited ground vibration test data available. The model was modified slightly between the two tunnel entries, so the predicted and actual mode frequencies are not identical for the two entries.

The ground vibration tests were conducted in the tunnel to ensure the model had not changed structurally while being transported and installed

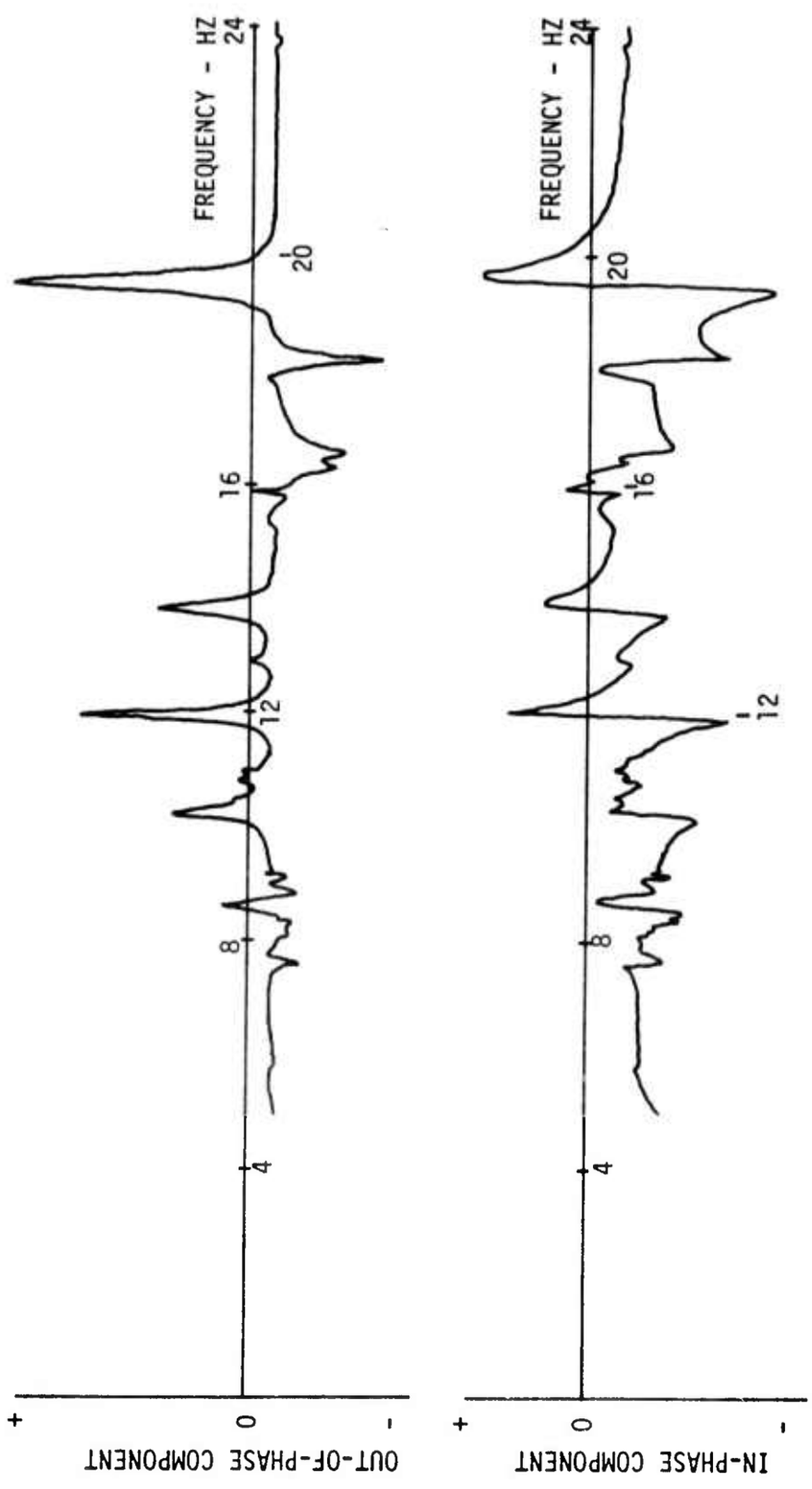

Figure 23. Outboard Wing Vertical Acceleration Due to Shaker Force Co-Quad Plot Pre-Test GVT in Tunnel on Cables and Soft Spring

TABLE VIII. RESTRAINED MODEL SYMMETRIC GROUND VIBRATION TEST RESULTS-COUPLED MODE FREQUENCIES

	PHASE I MODEL		PHASE II MODEL	
MODE	PREDICTED (HZ)	ACTUAL (HZ)	PREDICTED (HZ)	ACTUAL (HZ)
EM-1	4.32	4.20	4.31	4.37
EM-2	8.93	10.10	8.93	10.25
EM-3	10.57	10.80	10.63	10.80
EM-4	11.39	11.20	11.45	11.00
EM-5	11.78	11.80	11.84	11.95
EM-6	13.15	12.90	13.10	12.95
EM-7	15.45	13.50	15.18	13.85
EM-8	16.82	15.90	16.77	16.60
EM-9	18.63	19.00	18.91	19.55

Note: Model supported by soft spring and restrained by mount system cables in tunnel test section during the ground vibration test.

in the tunnel. It should be noted that some of the differences between the Phase I and Phase II measured frequencies can be attributed to higher cable tension in the second entry. The Phase II tests were conducted with about 95 pounds nominal cable tension, about 10 pounds more than used in the first entry. This change in cable tension was not incorporated into the Phase II vibration and flutter analyses. The cable tension was increased for the Phase II tests to provide better model rigid body lateral stability at the higher dynamic pressure conditions to be tested.

5.2 Wind Tunnel Tests

The Phase I and Phase II wind tunel tests were conducted using 95 percent freon, 5 percent air, as the test fluid. The Phase I tests were conducted to verify validity of the model in representing the airplane flutter characteristics. All data required for final correlation with model analytical and airplane flight test results were obtained in the Phase II testing.

5.2.1 Phase I Wind Tunnel Tests

In addition to the model verification, testing was conducted during the first entry to verify the FMCS performance and to evaluate possible subcritical testing techniques. A summary of the testing conducted is presented in Table IX. The testing accomplished was equivalent to that planned for the airplane flight tests, except for the randomdec method. The model elevator was not operative during this entry, so model responses to elevator could not be obtained as was planned for the Fuel Configuration 3 flight tests.

The Q-$\tilde{g}$ and Q-f plots shown in Figure 24 summarize the model flutter testing accomplished during this tunnel entry. The model flutter point was extrapolated out to about 55 psf dynamic pressure, about 10 psf higher than the 45.6 psf predicted analytically. The flutter mode is obviously better damped with the FMCS on, but not as well damped as predicted above 40 psf. The FMCS aileron and flaperon channel feedback gains were doubled, and the resulting flutter mode damping was significantly higher than predicted for the nominal FMCS gains. The flutter mode frequencies agree well with predicted values, probably within the accuracy of the co-quad method.

The difference between actual and predicted flutter points was attributed primarily to using .005 structural damping for all but nacelle modes in the analysis. Damping of the modes, estimated during ground vibration test, ranged from .012 to .094, with damping of the sixth (flutter) mode estimated at .023. Because a complete set of mode damping values was not obtained and some estimated values appeared too high based on previous experience, damping in the equations of motion was not changed. The lower than predicted performance obtained with the nominal FMCS gains was attributed to phasing differences at the flutter mode frequency caused by the mode frequencies and damping being different than predicted. Hysteresis known to be present in the outboard aileron and flaperon actuation system also would cause degradation in system performance. The aileron and flaperon surface effectiveness may have been lower than used in the analyses. Flight test results for Fuel Configuration 3 (equivalent to the model) showed similar trends for the basic airplane flutter speed and FMCS performance with the same gains.

TABLE IX. SUMMARY OF PHASE I WIND TUNNEL TESTING

TUNNEL CONDITION		OUTBOARD AILERON INPUTS			FLAPERON INPUTS		CANARD FREQUENCY SWEEP
DYNAMIC PRESSURE	MACH NUMBER	FREQUENCY SWEEP	SINE WAVE PULSE	DWELL AND CLAMP	FREQUENCY SWEEP	DWELL AND CLAMP	
30.0 PSF	.215	8 MINUTE 4-24 HZ	X	X			
35.0 PSF	.232	8 MINUTE 4-24 HZ	X	X	8 MINUTE 4-24 HZ FMCS OFF		
40.0 PSF	.248	20 SECOND 8 MINUTE 4-24 HZ	X	X	8 MINUTE 4-24 HZ FMCS OFF		
42.5 PSF	.256	↑	X				
45.0 PSF	.263		X	X	8 MINUTE 4-24 HZ FMCS OFF	FMCS OFF	8 MINUTE 4-24 HZ
47.5 PSF	.270		X	X			
50.0 PSF	.277	↓	X	X	8 MINUTE 4-24 HZ FMCS OFF		
52.5 PSF	.284	20 SECOND 8 MINUTE 4-24 HZ					
53.9 PSF	.287	RANDOMDEC RECORD ONLY AT THIS CONDITION					

NOTE: All testing conducted with FMCS Off and On, except as noted.

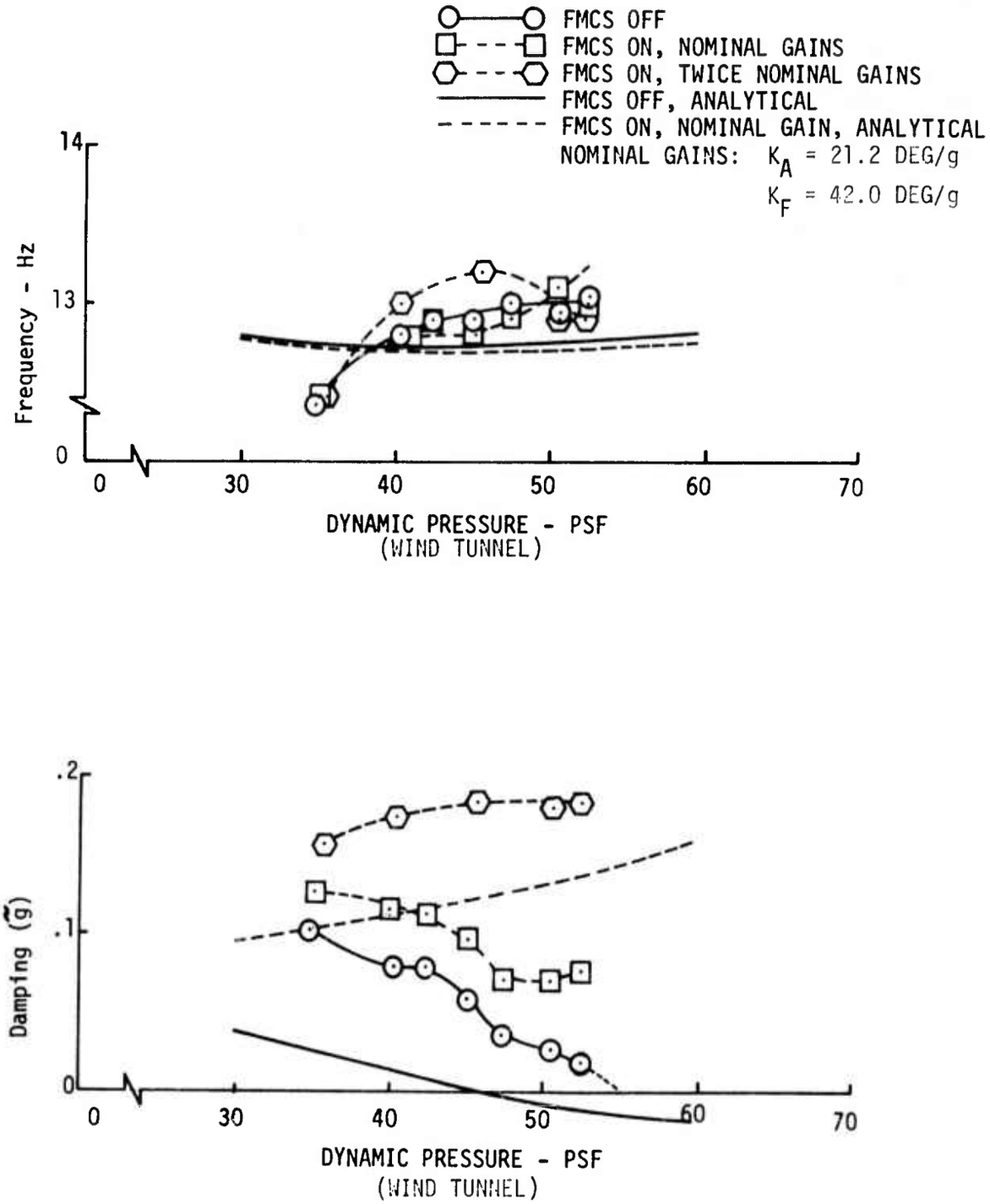

Figure 24. Flutter Mode Damping and Frequency - Phase I Wind Tunnel Test Results

Results of evaluation of model subcritical flutter testing methods showed the co-quad method using either outboard aileron or flaperon control surfaces to excite the modes provided the best results. The transient methods, tuned frequency dwell and clamp and one-cycle sine wave pulses, did not produce strip chart time history data that could be used to estimate damping because tunnel turbulence masked any decay caused by the input. The randomdec method worked well near flutter because it could give good damping estimates (at low damping) with only the tunnel turbulence exciting the model.

Outboard flaperon segment total hinge moments were measured during this entry by measuring current to the torque motor. The results were not satisfactory due to sensitivity being too low for the low torque values to be measured.

5.2.2 Phase II Wind Tunnel Tests

The data required for correlation with airplane flight test results was obtained during the second wind tunnel entry. A detailed test plan (see Appendix II) was prepared to obtain model data using testing methods similar to the methods used in flight flutter testing. The test plan was prepared from an optimistic point of view so the full period scheduled for testing this model could be utilized in obtaining data meeting the objectives of the overall study. Although no major problems arose during the wind tunnel testing, not all of the items shown in the test plan were completed due to lack of time or because the quality of the data did not warrant spending the time to accomplish the testing. In other words, each item of testing was assigned a priority, with the highest priority including the minimum testing required to meet the objectives. The test plan was followed, in general, but with some flexibility at the discretion of the NASA test director.

A summary of the testing accomplished is presented in Table X. The table also indicates the data obtained. The co-quad and randomdec data was obtained on-line during the wind tunnel testing to provide a continuous estimate of the flutter mode damping. Because only one sensor output could be monitored, some of the co-quad data was plotted from recorded data tapes after the testing was completed. The frequency response (amplitude and phase versus frequency) plots were also obtained after completion of the tests. Copies of some of the test co-quad plots are shown in Section 6. Reference 6 contains a copy of all data plots used to form results and conclusions discussed in this report. This data document also contains a complete listing of wind tunnel test conditions (dynamic pressure, Mach number, mass density, temperature, etc.).

The inboard and outboard wing accelerometers required for the FMCS were rewired between the two wind tunnel entries to bring right and left wing vertical accelerometer signals out of the model separately. This was done to detect any antisymmetric motion picked up in the accelerometers. The signals were averaged on the analog computer as required for the FMC system, with the outboard accelerometers feeding the aileron channel and inboard accelerometers feeding the flaperon channel. Only minor differences were noted between right and left hand accelerometer outputs for a given test condition. The wind tunnel data discussed in Section 6 is all for right wing sensors.

Before the second wind tunnel entry, a strain gaged torsional link was installed in the right hand flaperon linkage just inboard of the control

TABLE X. SUMMARY OF PHASE II WIND TUNNEL TESTING

ITEM NO.	MODEL EXCITATION	FMCS				NOMINAL DYNAMIC PRESSURE (PSF)										DATA OBTAINED				COMMENTS
		STATUS	K_A	K_F	ω_c	27.59	35	37.91	45	50	52.5	55	57.5	60	63	CD-QUAD	FREQ. RESP.	RANDOM-DEC	TIME HISTORY	
1	TUNNEL TURBULENCE	OFF	-	-	-	X	X	X	X	X	X	X	X	-	-			✓		
		ON	NOM	NOM	NOM	X	X	X	X	X	X	X	X	X	62			✓		
2	AILERON SWEEP (8-MIN)	OFF	-	-	-	X	X	X	X	X	X	X	X	-	-	$\ddot{z}_{565}/\delta_{A_C}$ & $\ddot{z}_{925}/\delta_{A_C}$	$\ddot{z}_{925}/\delta_{A_C}$ See Note 1		Q ≥ 55, AT PEAK FREQUENCIES	
		ON	NOM	NOM	NOM	X	X	X	X	X	X	X	X	X	-					
3	ELEVATOR SINUSOIDAL PULSE	OFF	-	-	-	-	X	X	X	X	X	X	-	-	-			✓	SAMPLE AT EACH CONDITION	
		ON	NOM	NOM	NOM	-	X	X	X	X	X	X	X	X	X			✓		
4	CANARD SWEEP (8-MIN)	OFF	-	-	-	-	-	X	X	X	X	-	-	-	-	$\ddot{z}_{565}/\delta_{C_C}$ & $\ddot{z}_{925}/\delta_{C_C}$			ALL Q, AT PEAK FREQUENCIES	
		ON	NOM	NOM	NOM	-	-	X	X	X	X	-	-	-	-					
5	FLAPERON SWEEP (8-MIN)	OFF	-	-	-	X	X	X	X	X	-	-	-	-	-	H.M./δ_F, $\ddot{z}_{565}/\delta_{F_C}$, $\ddot{z}_{925}/\delta_{F_C}$	H.M./δ_F			
		ON	NOM	NOM	NOM	-	-	-	-	-	-	-	-	-	-					
6	FLAPERON SWELL	OFF	-	-	-	-	-	X	-	-	-	-	-	-	-	H.M./δ_{F_C}			AT 7.1, 10.95, 11.7, 13.12, 15.4 HZ	
		ON	NOM	NOM	NOM	-	-	-	-	-	-	-	-	-	-					
7	AILERON SWEEP (20-SEC)	OFF	-	-	-	X	X	X	-	-	-	-	-	-	-		$\ddot{z}_{925}/\delta_{A_C}$			
		ON	NOM	NOM	NOM	X	X	X	-	-	-	-	-	-	-					
8	AILERON SWEEP (40-SEC)	OFF	-	-	-	-	-	X	-	-	-	-	-	-	-		$\ddot{z}_{925}/\delta_{A_C}$			
		ON	NOM	NOM	NOM	-	-	X	-	-	-	-	-	-	-					
9	AILERON SWEEP (20-SEC UP, 20-SEC DOWN)	OFF	-	-	-	-	-	X	-	-	-	-	-	-	-		$\ddot{z}_{925}/\delta_{A_C}$			
		ON	NOM	NOM	NOM	-	-	X	-	-	-	-	-	-	-					
10	GUST VANE SWEEP	OFF	-	-	-	-	-	-	X	X	-	-	-	-	-	$\ddot{z}_{565}/\alpha_g$ & $\ddot{z}_{925}/\alpha_g$	$\ddot{z}_{565}/\alpha_g$ & $\ddot{z}_{925}/\alpha_g$			
		ON	NOM	NOM	NOM	-	-	-	X	X	-	-	-	-	-					
11	AILERON SWEEP (8-MIN)	ON	NOM	NOM	NOM	-	-	X	X	X	X	-	-	-	-	$\ddot{z}_{925}/\delta_{A_C}$				±1.0 DEG LIMITS
		ON	NOM	NOM	51.65	-	-	X	X	X	X	-	-	-	-					
		ON	NOM	NOM	100.	-	-	X	X	X	X	-	-	-	-					
		ON	0	NOM	NOM	-	-	-	X	X	X	-	-	-	-					
		ON	NOM	0	NOM	-	-	-	X	X	X	-	-	-	-					
		ON	21.2	42.0	NOM	-	-	-	X	X	X	-	-	-	-					
		ON	63.6	126.	NOM	-	-	X	X	X	X	-	-	-	-					
12	TUNNEL TURBULENCE	OFF	-	-	-	48.00	54.89	63.75	-	-	-	-	-	-	-			✓		ρ=.0073 SLUG/FT^3
		ON	NOM	NOM	NOM	48.00	54.89	63.75	-	-	-	-	-	-	-			✓		
13	AILERON SWEEP (8-MIN)	OFF	-	-	-	48.00	54.89	63.75	-	-	-	-	-	-	-	$\ddot{z}_{925}/\delta_{A_C}$				ρ=.0073 SLUG/FT^3
		ON	NOM	NOM	NOM	48.00	54.89	63.75	-	-	-	-	-	-	-					

Note 1. FMCS OFF: Q = 27.59, 37.91 and 50.00 psf;
FMCS ON: Q = 27.59, 37.91, 50.00 and 60.00 psf.

surface. The strain gages were calibrated to read hinge moment on the surface. The hinge moment data is discussed in paragraph 6.2.3.

Items 1, 2 and 3 shown in Table X provided the flutter data required for correlation with the airplane. The 8-minute logarithmic outboard aileron sweeps provided the best flutter data. As the flutter condition (with FMCS off) was approached, the randomdec method, described in Section 6, gave good damping estimates. The highest dynamic pressure condition tested with the FMCS on was 62.6 psf, about 4.2 psf above the FMCS off flutter point. This condition was roughly equivalent to the 10 KCAS above basic airplane flutter point flown during the Fuel Configuration 3 flight tests. Aileron frequency sweep tests were conducted up to about 60 psf. The flutter mode damping was increasing with increasing dynamic pressure and higher conditions could have been tested. The elevator one-cycle sine wave pulse data was masked by the tunnel turbulence as was similar aileron pulse data during Phase I testing. The data was processed with the randomdec method using 6 to 8 degree elevator pulse commands every four seconds for about 40 seconds. However, the damping estimates obtained were no better above about .05 structural damping than obtained from the randomdec using only tunnel turbulence to excite the model.

Flutter mode damping estimates were made from canard and flaperon sweep co-quad plots, but the flaperon sweeps were conducted primarily to obtain right hand flaperon total hinge moment measurement. The flaperon dwell testing at tuned frequencies provided data to check validity of the hinge moment data obtained from continuous sweeps.

The short duration aileron sweeps, Items 7, 8 and 9, were conducted to simulate the 0.5 to 5.0 Hz, 2 minute sweeps conducted in the airplane flight tests. Little model response was observed during the short duration sweeps, even at the flutter mode frequency. NASA processed the data using a digital computer program. The 40 second sweep data was usable, but the 20 second sweep data was distorted so that frequency and damping estimates could not be made. None of the resulting data plots are available for inclusion in this report.

Model responses to vertical gust, generated by the tunnel gust vanes, were obtained with the FMCS off and on to demonstrate the capability of the system to function in a gust environment.

The FMC system was tested with variations in flaperon and aileron channel gains and filter time constants and ±1.0 degree limits on surface commands in both channels. This testing was accomplished to determine sensitivity of the system to gain and phase variations and to system saturation.

All of the testing listed in Items 1 through 11 were conducted at .00499 slug/ft^3 nominal tunnel fluid mass density, which is equivalent to the airplane Fuel Configuration 3, 21,000 foot altitude, flight test condition. The system was evaluated at about .0073 slug/ft^3 density to demonstrate performance of the system at lower altitude (about 9300 feet). This testing was planned to be accomplished at 5400 feet equivalent altitude, but due to a limited freon supply at the time of the testing, the .008 slug/ft^3 density could not be reached.

A detailed discussion of the Phase II test results is presented in Section 6, where wind tunnel data is compared to model analytical and airplane flight test results.

6.0 DATA REDUCTION AND CORRELATION

The primary objective of this program was to obtain wind tunnel test data on an aeroelastic model of the CCV flight test airplane equipped with an active flutter mode control system (FMCS) to permit comparison of model results with model analytical and airplane flight test results. This correlation of data is discussed in the following paragraphs. The comparisons include flutter behavior of the test vehicles with the FMCS off as well as performance of the system on both vehicles.

To provide data for the correlation, model testing was conducted using the same testing techniques that were employed during the flight flutter testing. Transient and steady state dynamic response methods were used during both the wind tunnel and flight testing. But, due to turbulence in the tunnel airstream, the model transient responses were masked to the point modal damping estimates could not be made with consistent accuracy. Steady state sinusoidal responses to the outboard aileron control surface 8-minute logarithmic 4 to 24 Hz frequency sweeps, plotted in the in-phase and out-of-phase component form, provided the best model subcritical flutter data. These tests were conducted up to near the model flutter condition with the FMCS off, and above this flutter condition with the system on.

Steady-state dynamic response testing on the airplane could be conducted only at speeds less than 87 percent of the basic airplane flutter speed due to safety requirements. Thus, the airplane transient response data is more complete and flutter mode damping estimates were made using logarithmic decrement techniques applied to strip chart recordings of the transient responses.

Model testing was also conducted with variations in the FMCS and tunnel density. The results of this testing, and model responses to sinusoidal gust vanes, are discussed in paragraph 6.3.

6.1 Model Test and Analytical Data Comparison

The objective of correlating model test results with analytical results is to determine how well the analytical equations of motion describe the model dynamic characteristics. This correlation is accomplished through comparison of damping and frequencies of the dominant modes estimated from Phase II wind tunnel test results with predicted values.

6.1.1 Dominant Mode Comparisons

Figure 25 shows the flutter mode damping and frequency as a function of model dynamic pressure for the wind tunnel test results and analytical results obtained from roots of the characteristic equation. The basic model flutter dynamic pressure is about 10 psf higher than the equations of motion predicted. The test data plot shows the slope of the Q-$\tilde{g}$ curve increases around 45 psf and decreases again about 52 psf to the 58.4 psf flutter point. Damping at all points except the flutter point was estimated from plots of the in-phase (coincident) and out-of-phase (quadrature) components (co-quad plots) of wing vertical acceleration due to outboard aileron frequency sweeps. The flutter point was established with only the tunnel turbulence exciting the model. The test data shows better damping than predicted at low dynamic

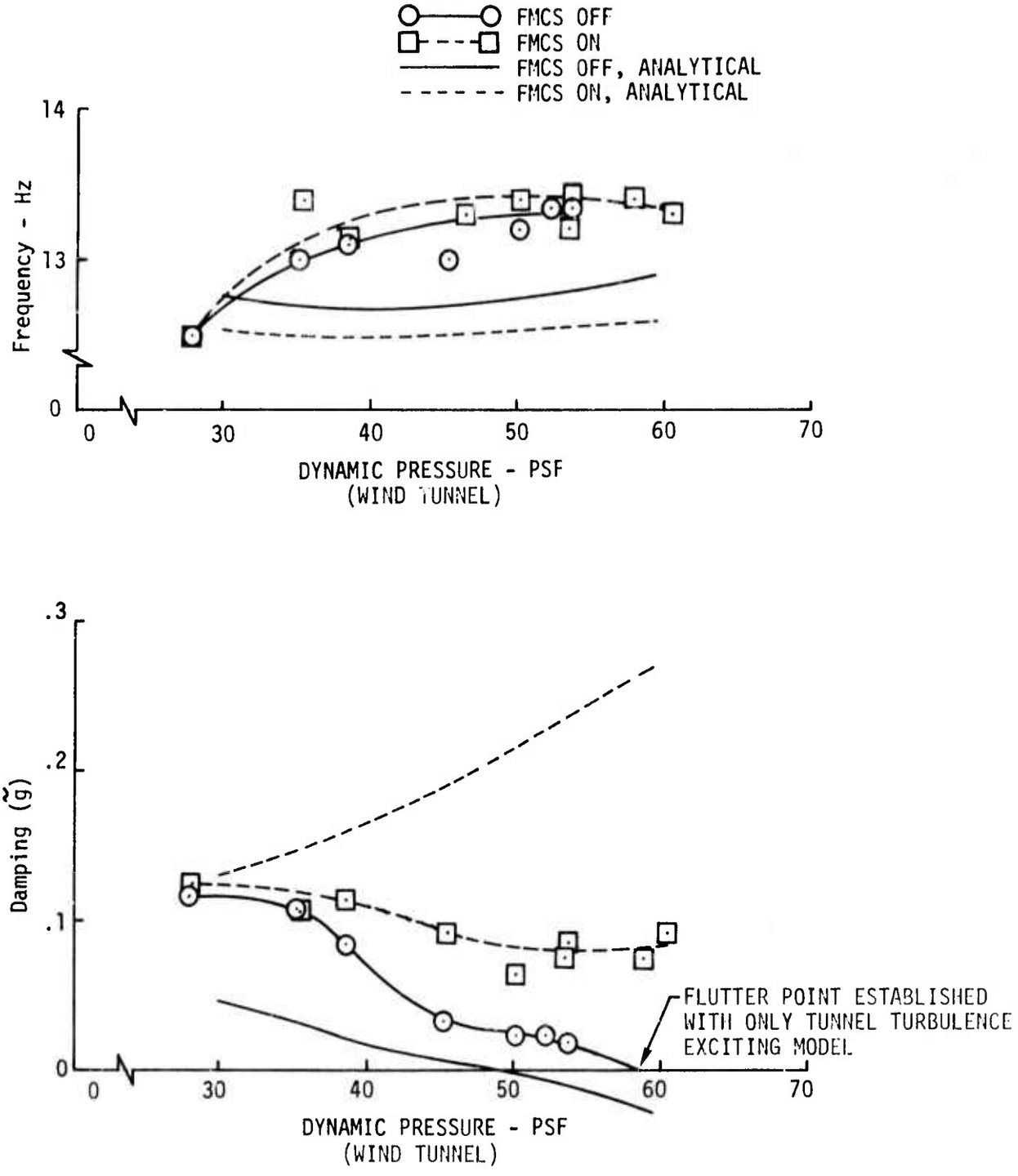

Figure 25. Flutter Mode Damping and Frequency - Phase II Wind Tunnel Test Results

pressure, which is consistent with the higher flutter point. The measured frequency values were estimated from the co-quad plots, which could explain some of the difference in frequencies, as discussed below.

The flutter mode control system increases the flutter mode damping, especially above 40 psf dynamic pressure as the basic model damping starts decreasing dramatically. But, the damping values measured in the tunnel are significantly lower than predicted for the same FMCS feedback gains. The lower damping appears to be due to phasing different than predicted due to mode frequencies and damping being different and because of aileron and flaperon hysteresis.

The measured flutter mode frequency is slightly higher with the FMCS on, instead of lower than with FMCS off as predicted. This could be due in part to the method used to estimate modal frequencies on a co-quad plot. The co-quad plots shown in Figures 26 and 27, with the FMCS off and on, respectively, can be used to show the difficulty in estimating frequency and damping from a co-quad plot. The method used was developed for a single degree of freedom system, as discussed in Reference 7.

Using Figure 26 as an example, the flutter mode damping can be estimated using the equation

$$\tilde{g} = \left[\left(\frac{f_A}{f_B}\right)^2 - 1\right] \Big/ \left[\left(\frac{f_A}{f_B}\right)^2 + 1\right] = 2\zeta ,$$

where f_A is the frequency in Hertz of the first relative maximum or minimum point on the in-phase component plot higher in frequency than the flutter mode and f_B is the frequency at the relative minimum or maximum below the flutter mode. The flutter mode undamped natural frequency is at the relative maximum or minimum amplitude of the out-of-phase component that occurs between f_A and f_B. By examining the in-phase component, a relative maximum occurs at about 12.2 Hz and a relative minimum at 13.6 Hz. From the analysis results, it is known the flutter mode should have about 12.7 Hz natural frequency. Thus f_A = 13.6 Hz and f_B = 12.2 Hz. The actual mode frequency is at the relative minimum that occurs in the out-of-phase component between f_A and f_B. This frequency is estimated to be 13.0 Hz. The mode damping is calculated as .108, using the above equation. For Figure 27, with the FMCS on, the damping of the flutter mode is estimated (calculated) as .106 with f_A = 13.9 Hz and f_B = 12.5 Hz, and the flutter mode frequency is 13.4 Hz. Note that the accuracy of this method increases as the response approaches that of a single second order system; i.e., when the mode damping becomes small and/or the residue of all other modes makes them insignificant.

Analytical co-quad plots for this nominal condition are shown in Figure 28 for FMCS off and Figure 29 with FMCS on, for the same system feedback gains. Comparing Figures 26 and 28, both the in-phase and out-of-phase components indicate the flutter mode is better damped than predicted. Note that both components for the model test data are similar to the analytical plots, with the major difference, besides the flutter mode damping, of two additional modes below the flutter mode apparent on the analytical plots. These are the second and third (or fourth) elastic modes. The fifth elastic mode is well damped and cannot be seen in either the test or analytical data. The flutter mode for the model configuration is the sixth elastic mode.

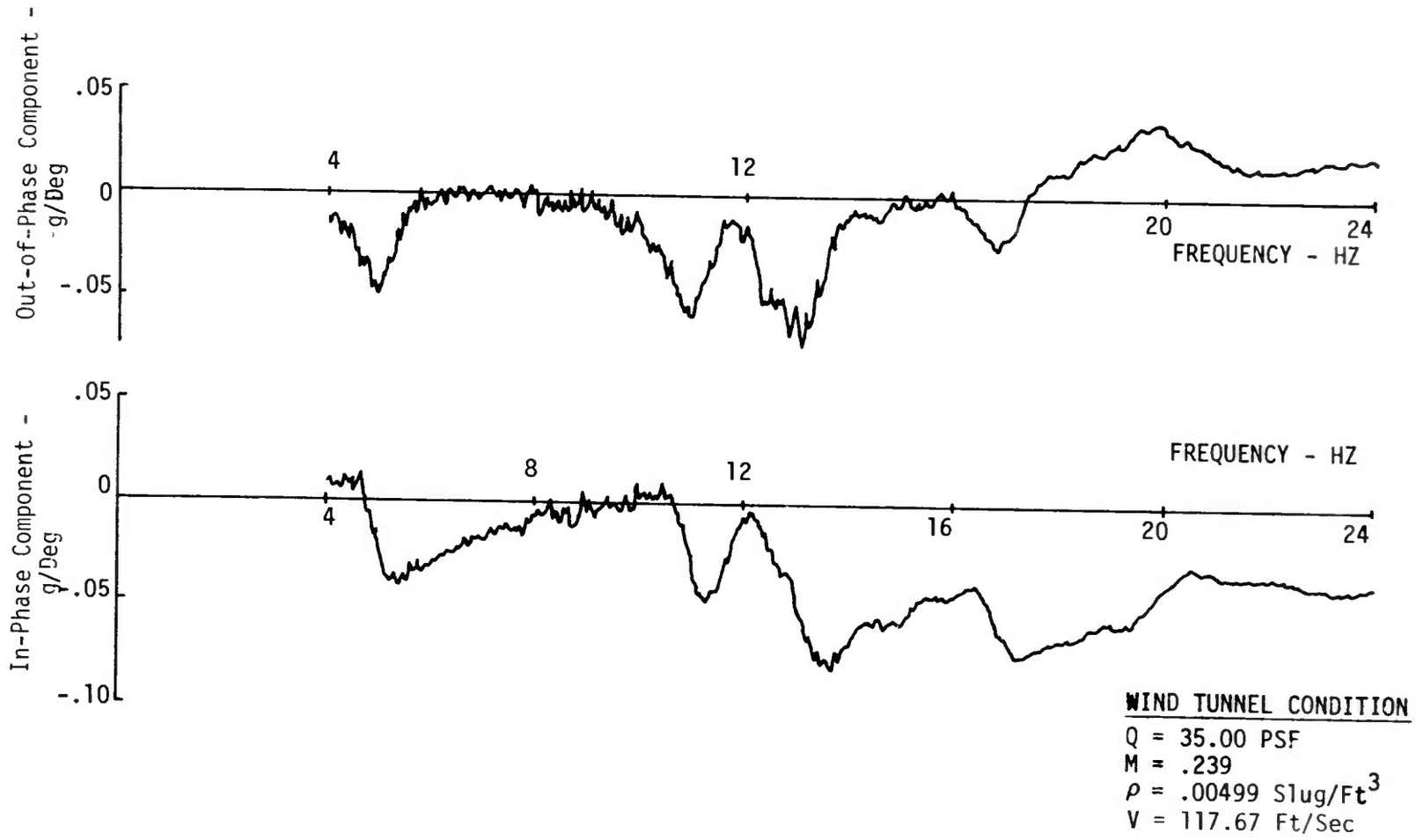

Figure 26. Outboard Wing Vertical Acceleration Due to Aileron Command Co-Quad Plot - FMCS Off

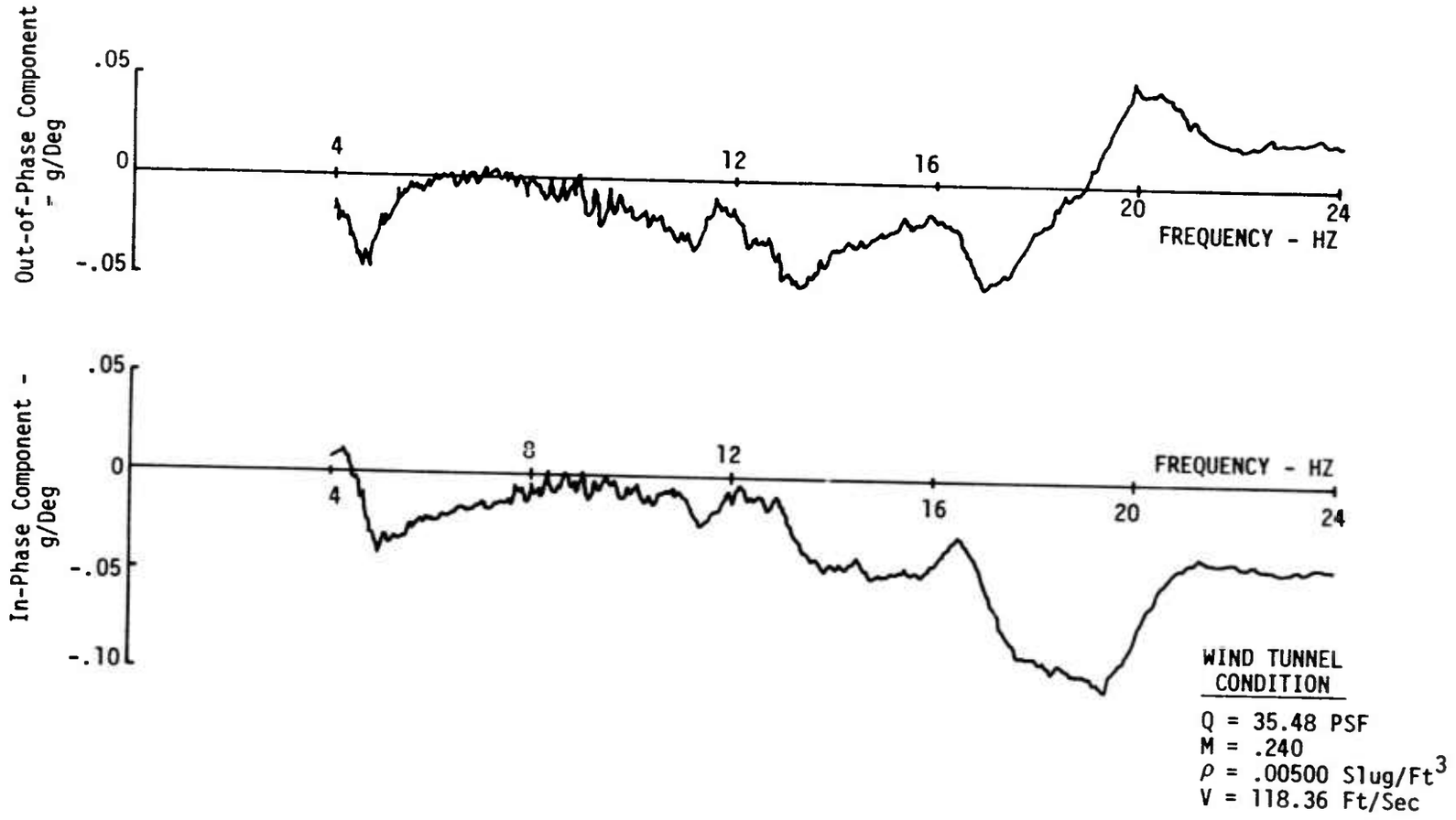

Figure 27. Outboard Wing Vertical Acceleration Due to Aileron Command Co-Quad Plot - FMCS On

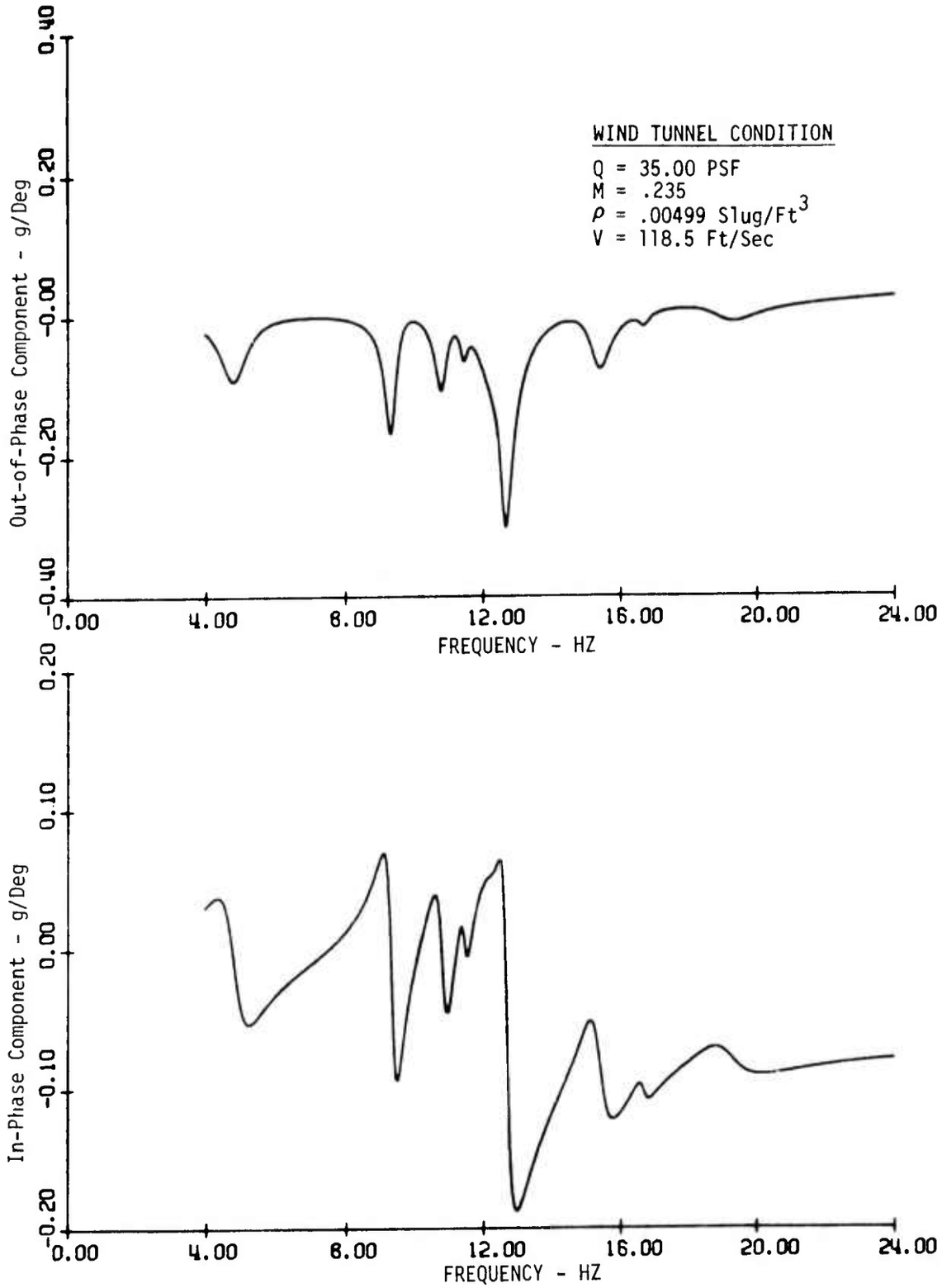

Figure 28. Analytical Outboard Wing Vertical Acceleration Due to Aileron Command Co-Quad Plot - FMCS Off

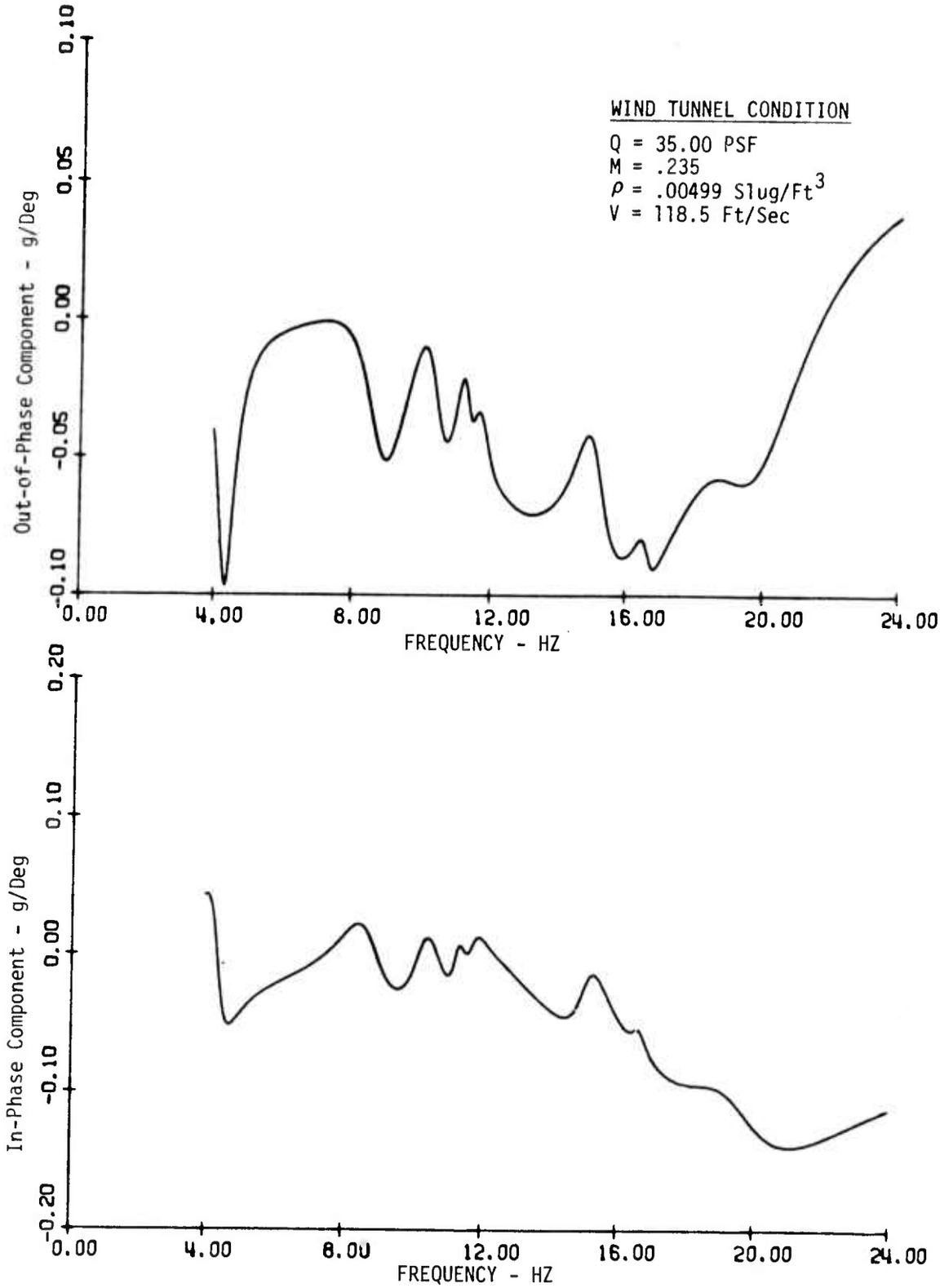

Figure 29. Analytical Outboard Wing Vertical Acceleration Due to Aileron Command Co-Quad Plot - FMCS On

Figure 30 shows Q-$\tilde{g}$ and Q-f plots for the mode just lower in frequency than the flutter mode that can be seen in the test data. The FMCS off frequencies agree well with frequencies predicted for the third elastic mode, Figure 31. But, the FMCS on frequencies agree with those predicted for the fourth mode, shown in Figure 32. The analytical Q-$\tilde{g}$ and Q-f plots for the second elastic mode are shown in Figure 33, but this mode was not observable in the test data. GVT results discussed previously showed this mode higher in frequency than predicted.

The mode lowest in frequency shown in the test data of Figures 26 and 27 is the first elastic mode (first wing vertical bending). Figures 34 and 35 show Q-$\tilde{g}$ and Q-f plots for this mode for test and analytical data, respectively. Mode frequencies with the FMCS off and on show good agreement, and the damping values are reasonably close considering the high damping levels measured from the test co-quad plots.

The seventh elastic mode also cannot be seen in the test co-quad plots shown in Figures 26 and 27. As noted above in the discussion of GVT results, this mode appears to be about two Hz lower in frequency than predicted and its mode shape is different. The mode at 16.85 Hz in Figure 26 is the eighth elastic mode. Q-$\tilde{g}$ and Q-f plots for this mode are shown in Figure 36 for test data and Figure 37 for analytical results. The frequencies measured with the FMCS off agree very well with predicted values, but the FMCS on values are higher and increase dramatically above about 50 psf. Both the FMCS off and on damping values are higher than predicted. This mode exhibits strong inboard nacelle vertical motion which could be readily observed visually during the wind tunnel tests.

Results of comparing the model test and analytical results follow the trend noted in paragraphs 3.4 and 5.1 in discussing the ground vibration test results. The actual flutter point was about 10 psf higher in dynamic pressure than predicted, in both series of wind tunnel tests. The flutter mode control system was able to increase the flutter mode damping, but not as effectively as predicted.

In general, good agreement was attained for the first, third (FMCS off), sixth and eighth elastic modes as found in comparing the test and analytical co-quad plots. The fifth elastic mode cannot be seen in either response. The second, fourth and seventh elastic modes cannot be seen in the test response while all three are apparent in the analytical responses. Regardless of these differences, the equations of motion possessed sufficient accuracy to predict a model configuration that would flutter and permitted synthesis of a closed loop system to control the flutter mode.

6.1.2 Phase I and Phase II Test Results Comparison

A comparison of Figure 25 with the results of the Phase I tests shown in Figure 24 shows some obvious differences between the basic model and the FMCS performance attained in the two entries. The basic model flutter point was predicted at 45.6 psf dynamic pressure for the model as tested in Phase I, and 48.5 psf for Phase II. The actual Phase II flutter point was at 58.4 psf and the Phase I point was estimated to be about 55 psf. Thus, the higher basic model flutter point between the two entries agrees with the predicted trend.

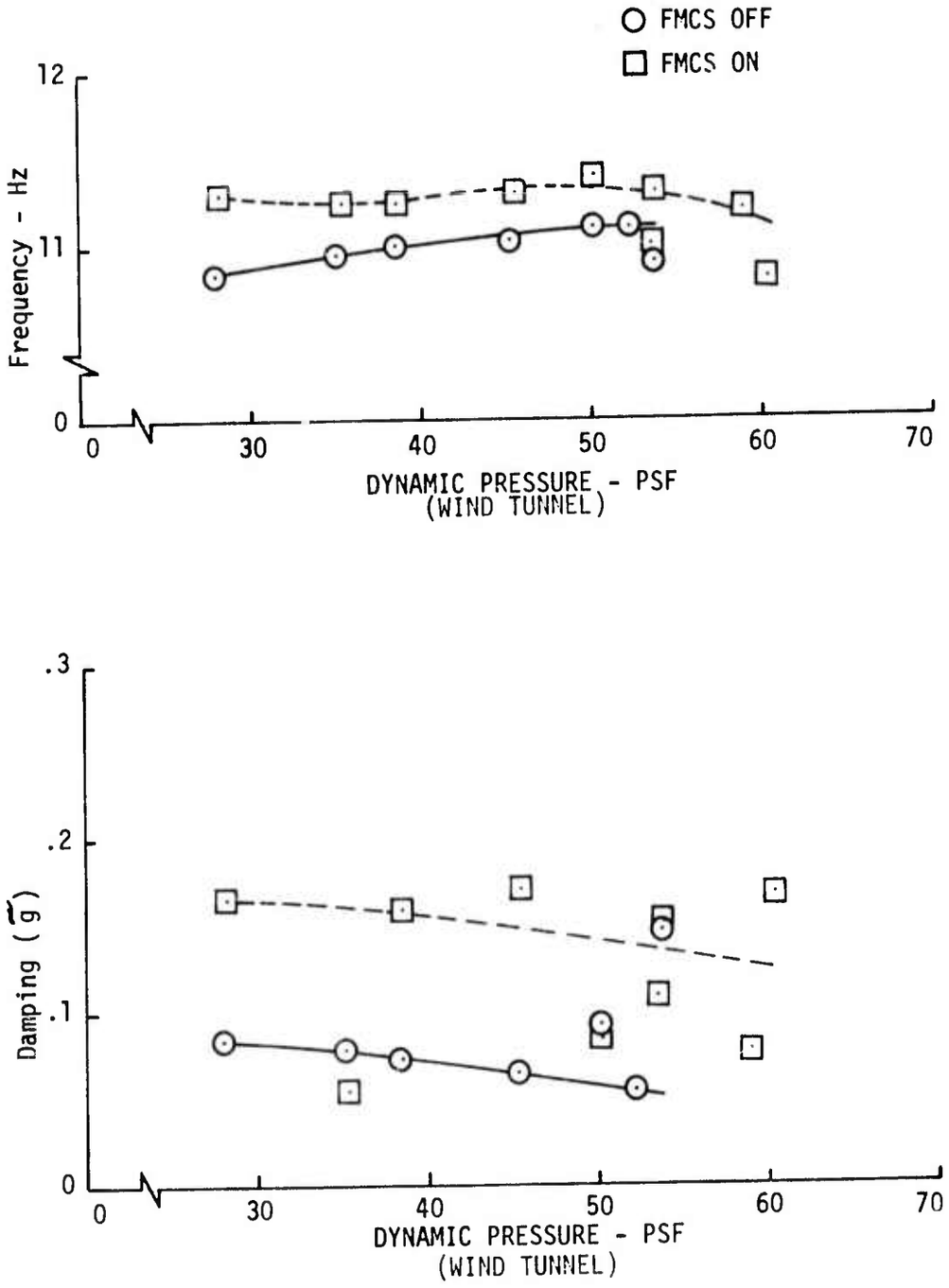

Figure 30. Second Observable Elastic Mode Damping and Frequency - Wind Tunnel Test Data

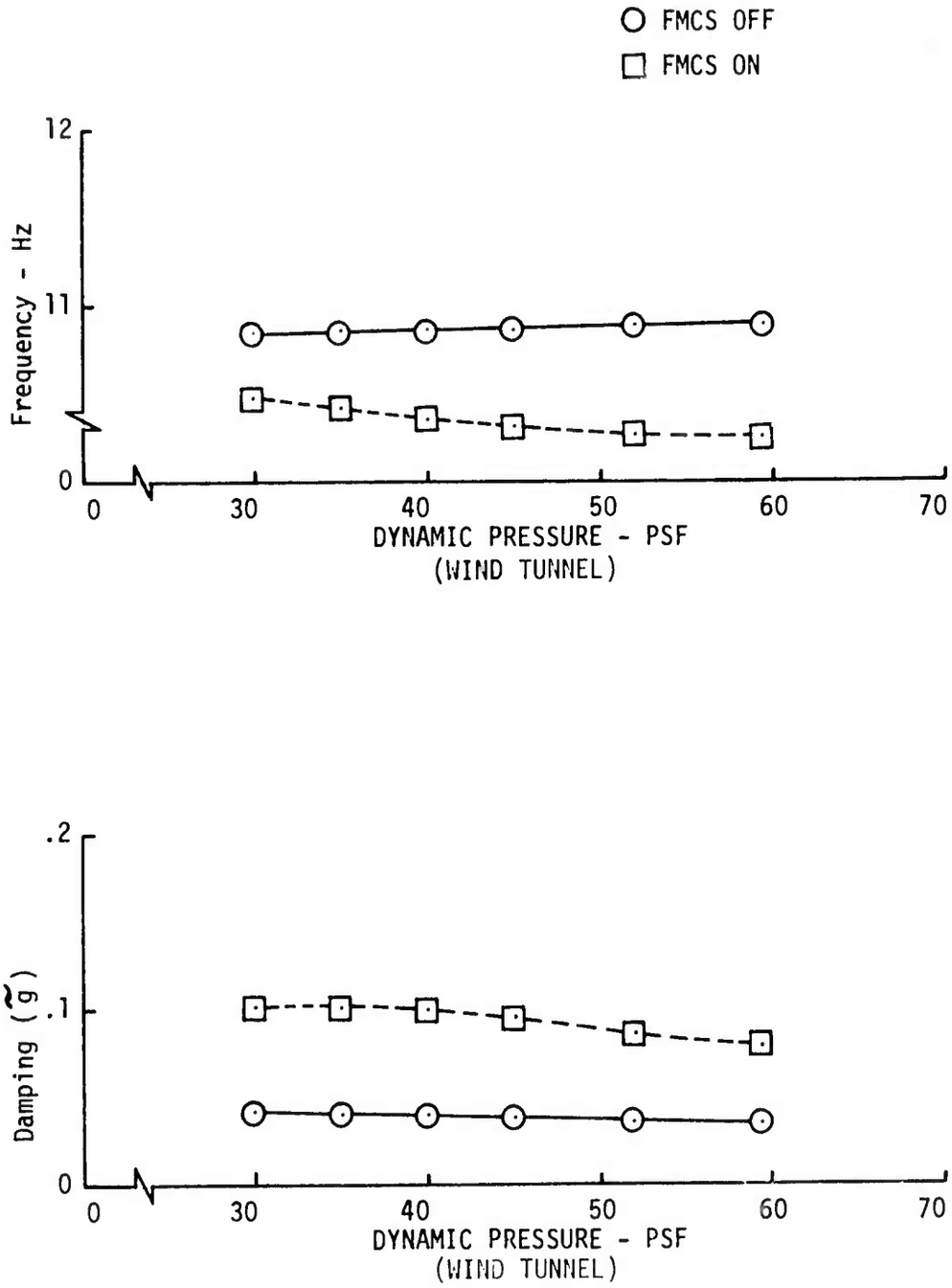

Figure 31. Third Elastic Mode Damping and Frequency – Theoretical Characteristic Equation Roots

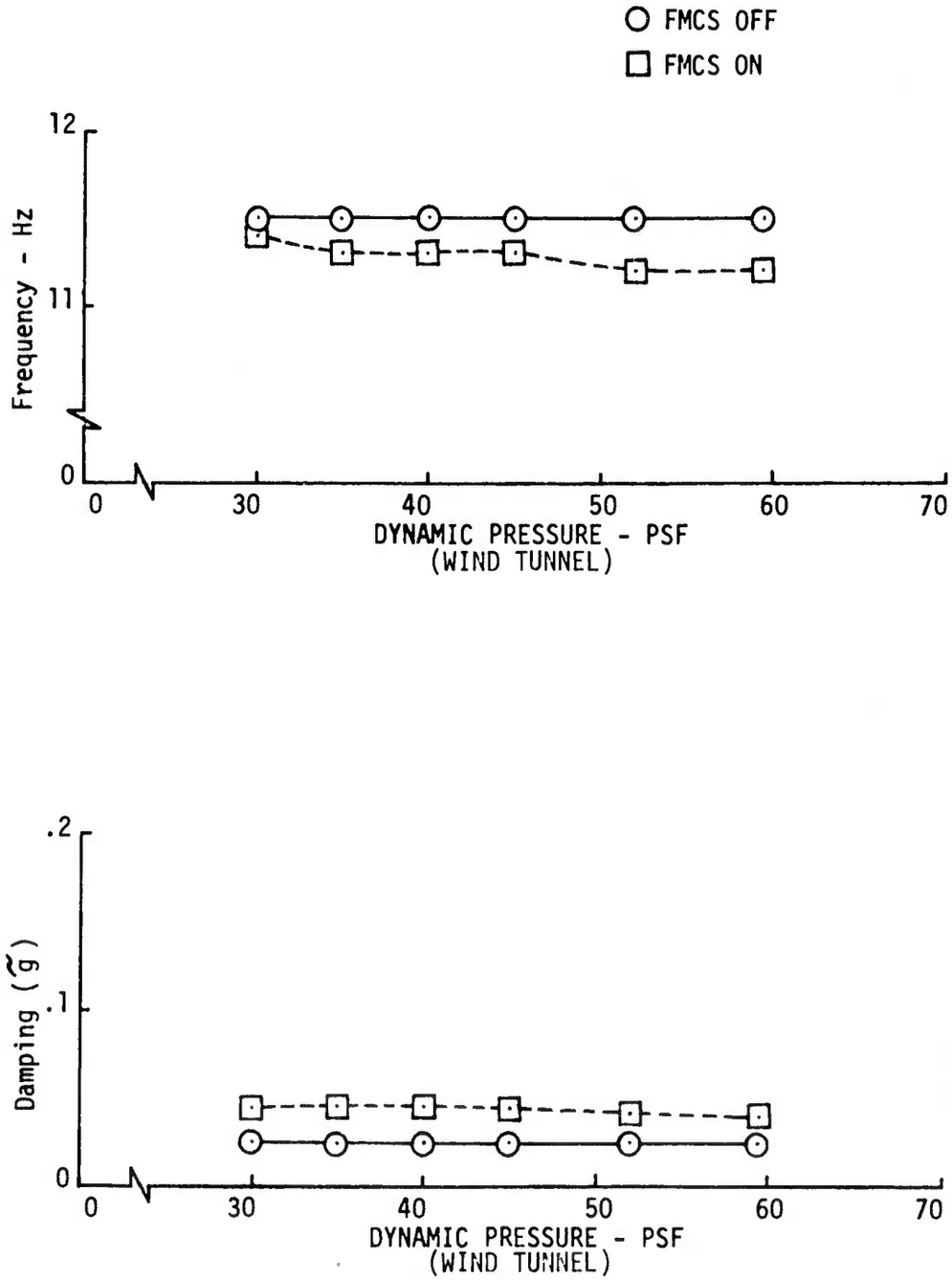

Figure 32. Fourth Elastic Mode Damping and Frequency - Theoretical Characteristic Equation Roots

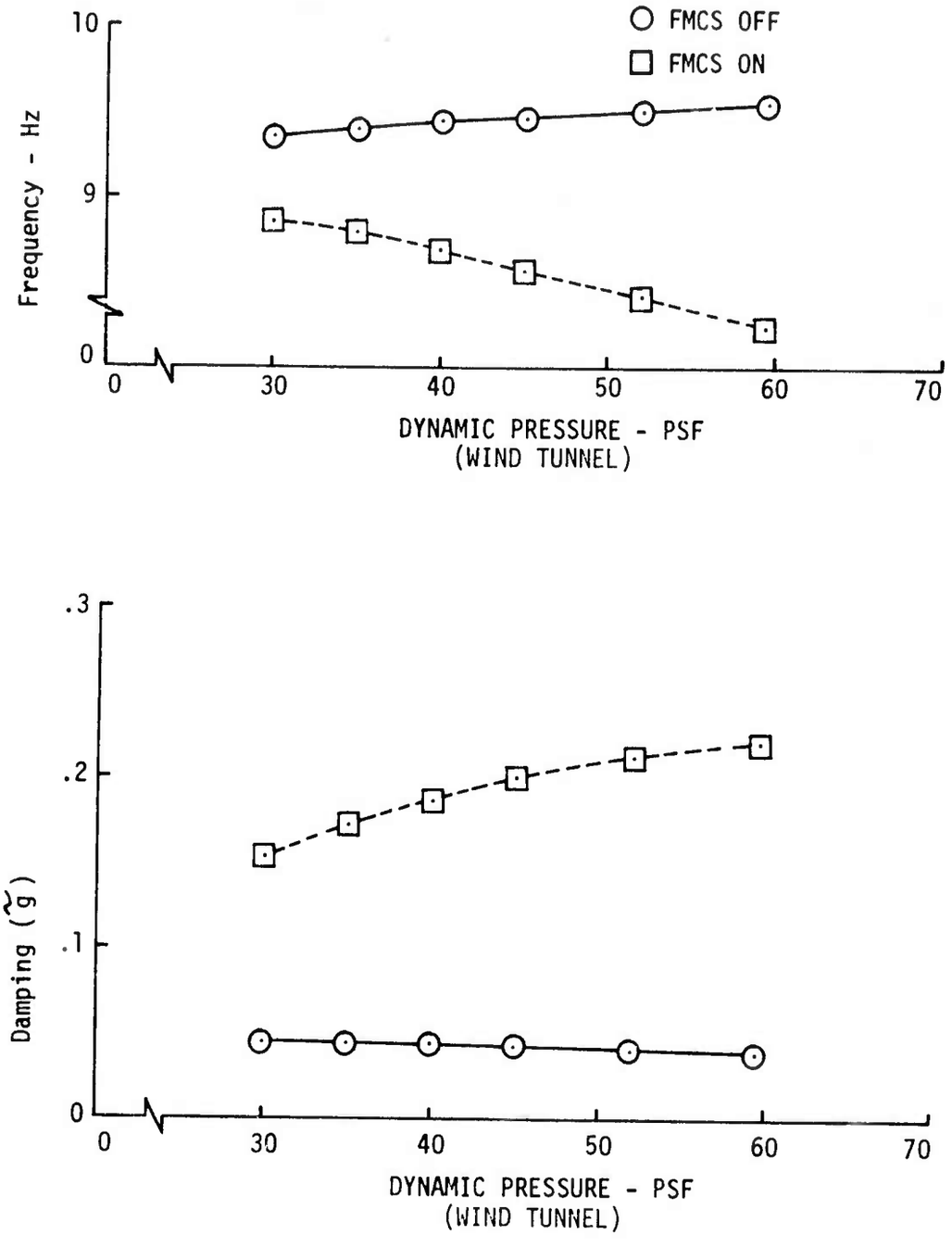

Figure 33. Second Elastic Mode Damping and Frequency - Theoretical Characteristic Equation Roots

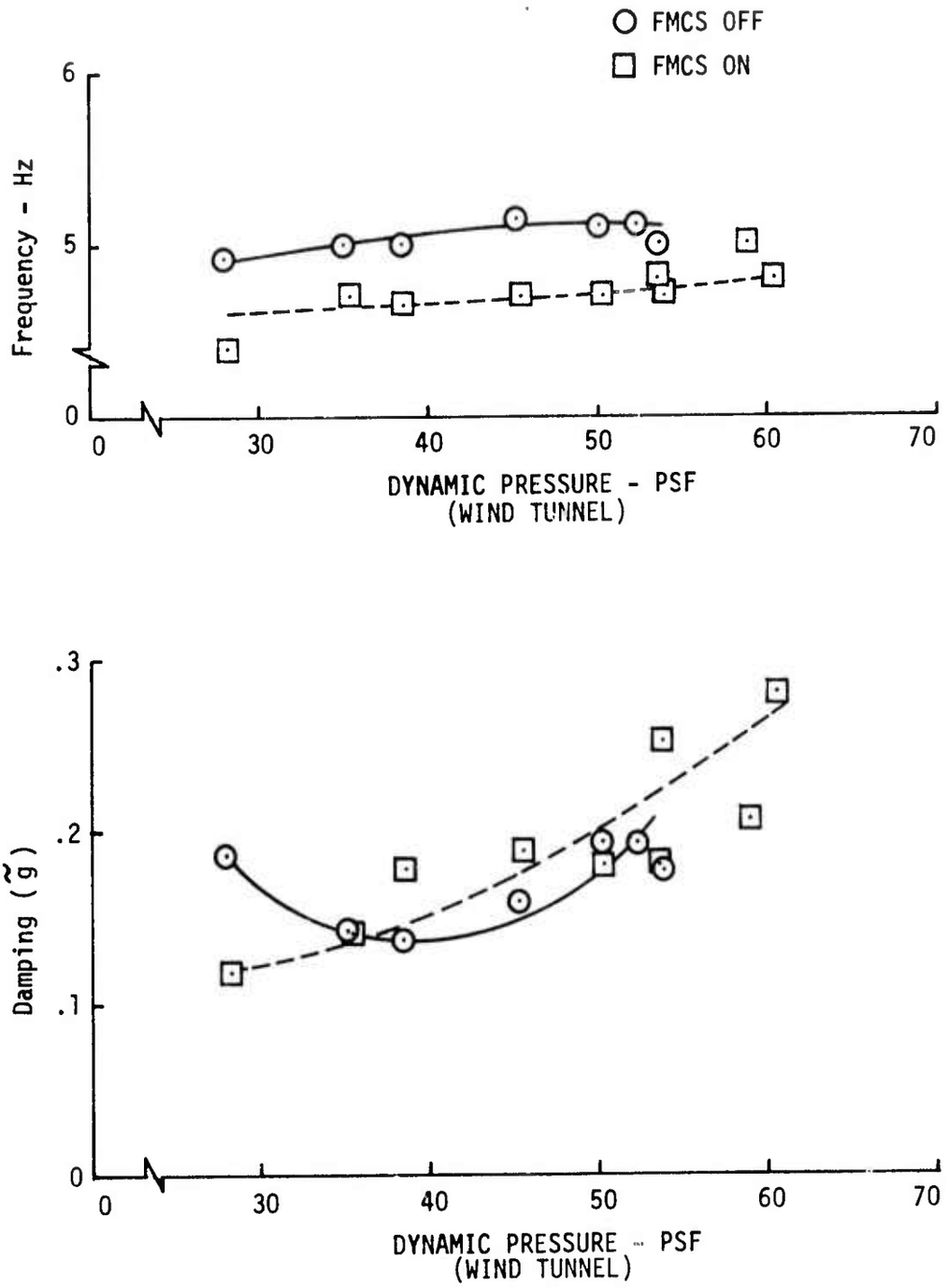

Figure 34. First Elastic Mode Damping and Frequency - Wind Tunnel Test Data

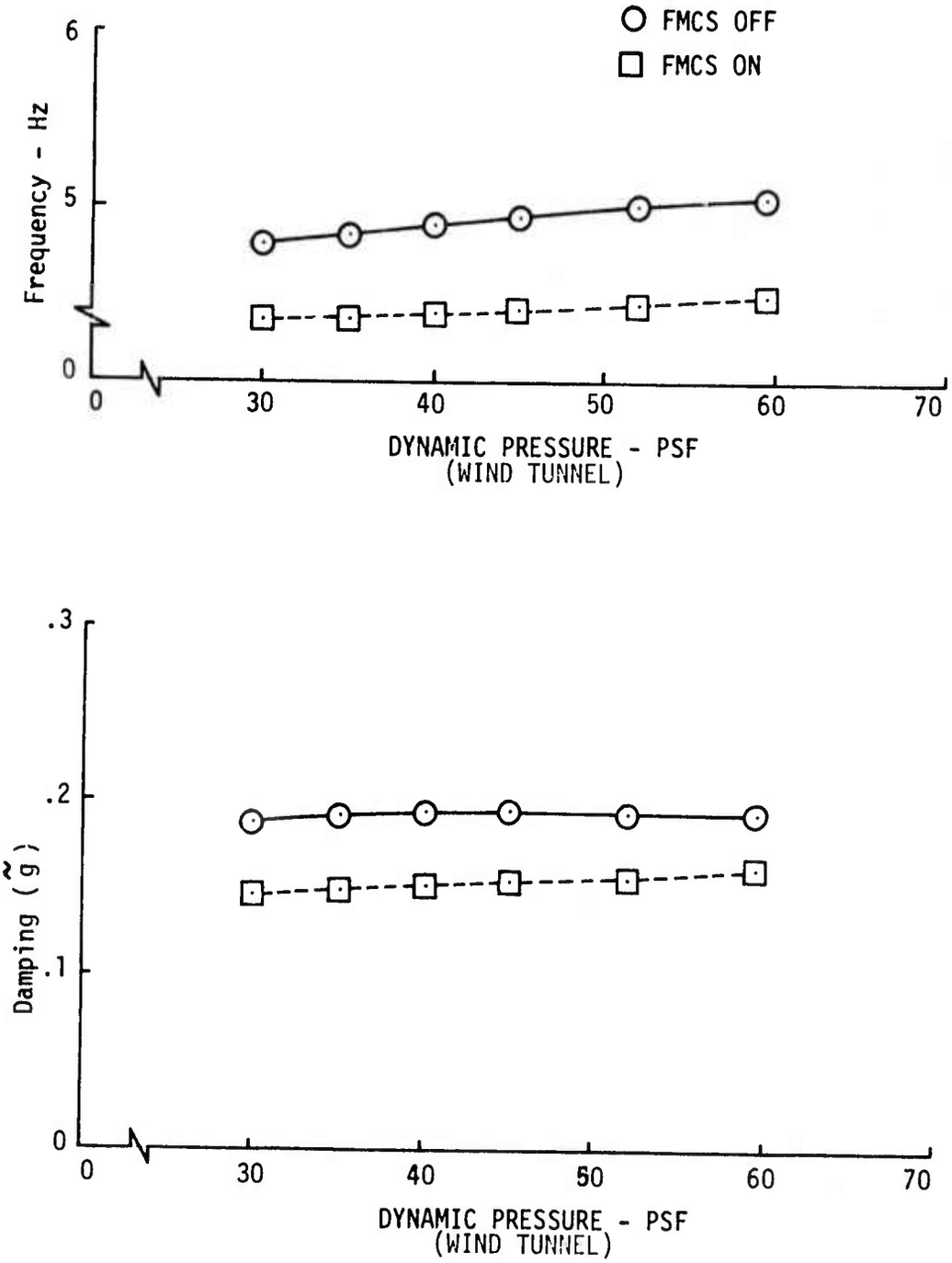

Figure 35. First Elastic Mode Damping and Frequency - Theoretical Characteristic Equation Roots

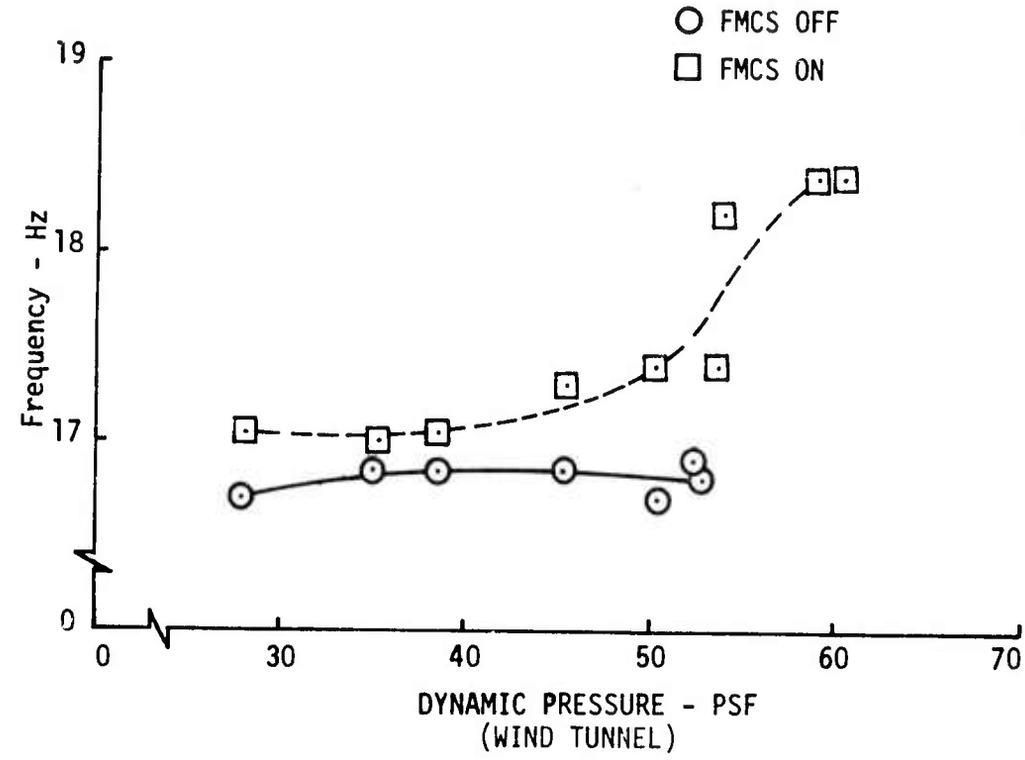

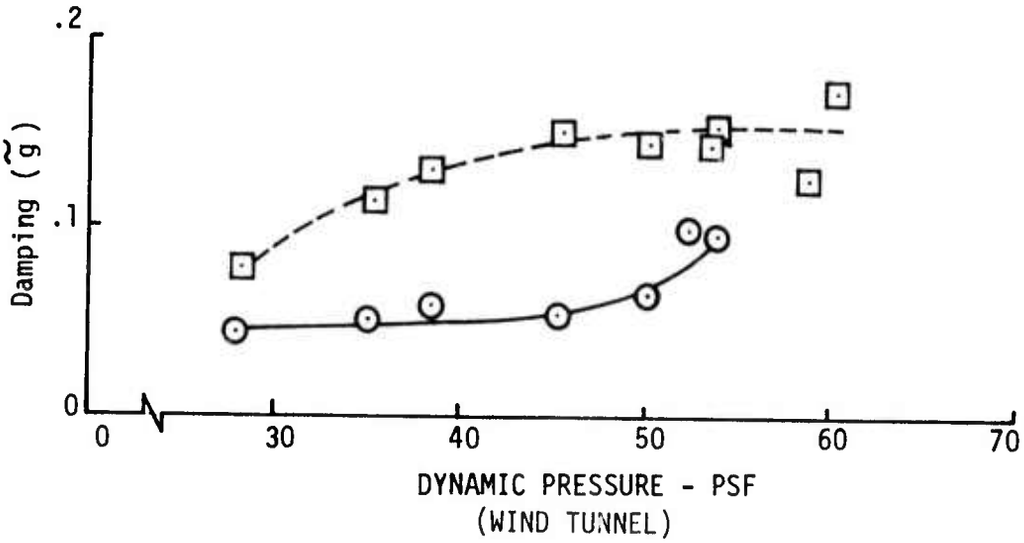

Figure 36. Eighth Elastic Mode Damping and Frequency - Wind Tunnel Test Data

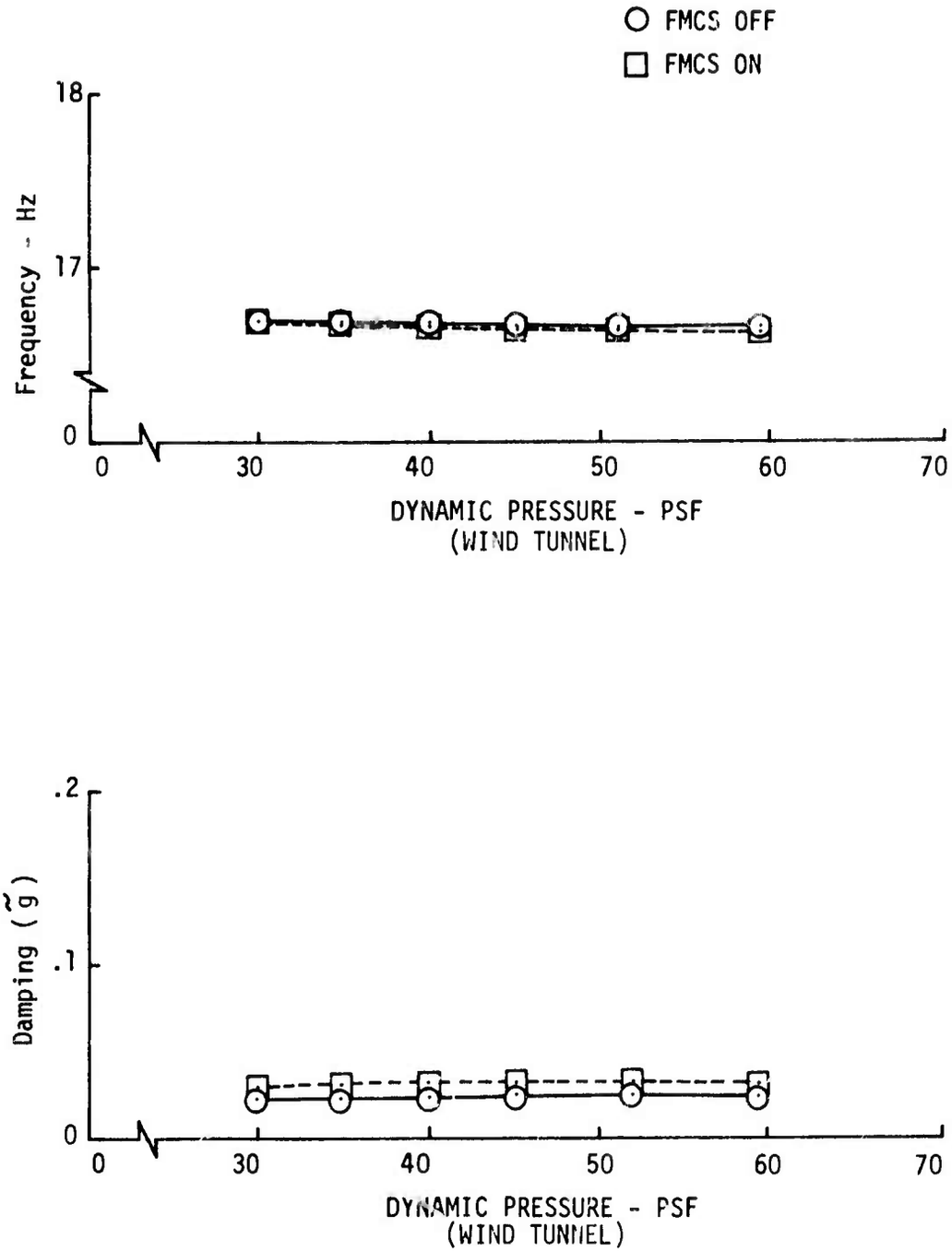

Figure 37. Eighth Elastic Mode Damping and Frequency - Theoretical Characteristic Equation Roots

The flutter mode damping values with the FMCS on obtained in the second wind tunnel entry are almost the same as attained during Phase I with the lower "nominal" gains. Feedback gains had been increased by a factor of two in the aileron channel and 1.25 in the flaperon channel for the Phase II tests to give FMCS performance similar to that predicted for the "nominal" gains used in Phase I. Thus, increasing the FMCS feedback gains appears to have had negligible effect on the FMCS performance. Note that when the gains were doubled during the Phase I testing, significantly better performance was attained (see Figure 24).

Some changes were made on the model and instrumentation between the two tunnel entries. Wing tip mass properties were corrected and all elevator actuation system components were installed so the elevator could be used to excite the model modes during the wind tunnel testing. The mass changes incurred through these two modifications were included in the Phase II analyses. Another model change involved correcting a slight misalignment of the aft fuselage main spar. The ground vibration test conducted in the tunnel before the second entry showed some differences in mode frequencies from the first entry, with the differences not as predicted. But, the cable tension was 10 pounds higher in the second entry than in the first, and this could account for some of the difference in the GVT results and the FMCS performance.

In the first entry, left and right wing accelerometers were wired inside the model to produce voltages proportional to average inboard and outboard vertical accelerations. The wiring was revised before the second entry to bring each accelerometer output out of the model separately, and the averages were formed on the analog computer for the FMC system. Some low frequency drift in the accelerometer outputs was observed, but the washouts in the aileron and flaperon channels of the FMCS prohibited any d.c. level from reaching the control surface actuation systems.

Control surface hysteresis was reduced between the two entries, which should have improved the FMCS performance as discussed in Section 4. The reduced performance of the system appears to be due to additional phase lag in either the model or the system itself at the flutter mode frequency. But, no known difference in the model or instrumentation could be identified as causing a significant phase difference.

6.1.3 Additional Discussion of Model Data

All model test damping and frequency values discussed so far were estimated from co-quad plots of right hand outboard wing vertical acceleration due to outboard aileron. The outboard flaperons and horizontal canards were also used to excite the model, and co-quad plots were obtained for both inboard and outboard wing vertical acceleration due to these surfaces. Flutter mode damping estimates were made from these plots, as well as through the Randomdec method discussed in Reference 8.

Figure 38 shows the flutter mode damping and frequency estimated from co-quad plots of inboard wing vertical acceleration due to outboard aileron frequency sweeps. In general, the subcritical damping values are lower than those shown in Figure 25 for the outboard sensor location. The same flutter point is predicted, and the damping estimates above 50 psf dynamic pressure are similar. The flutter mode frequency estimates are lower with both FMCS off and

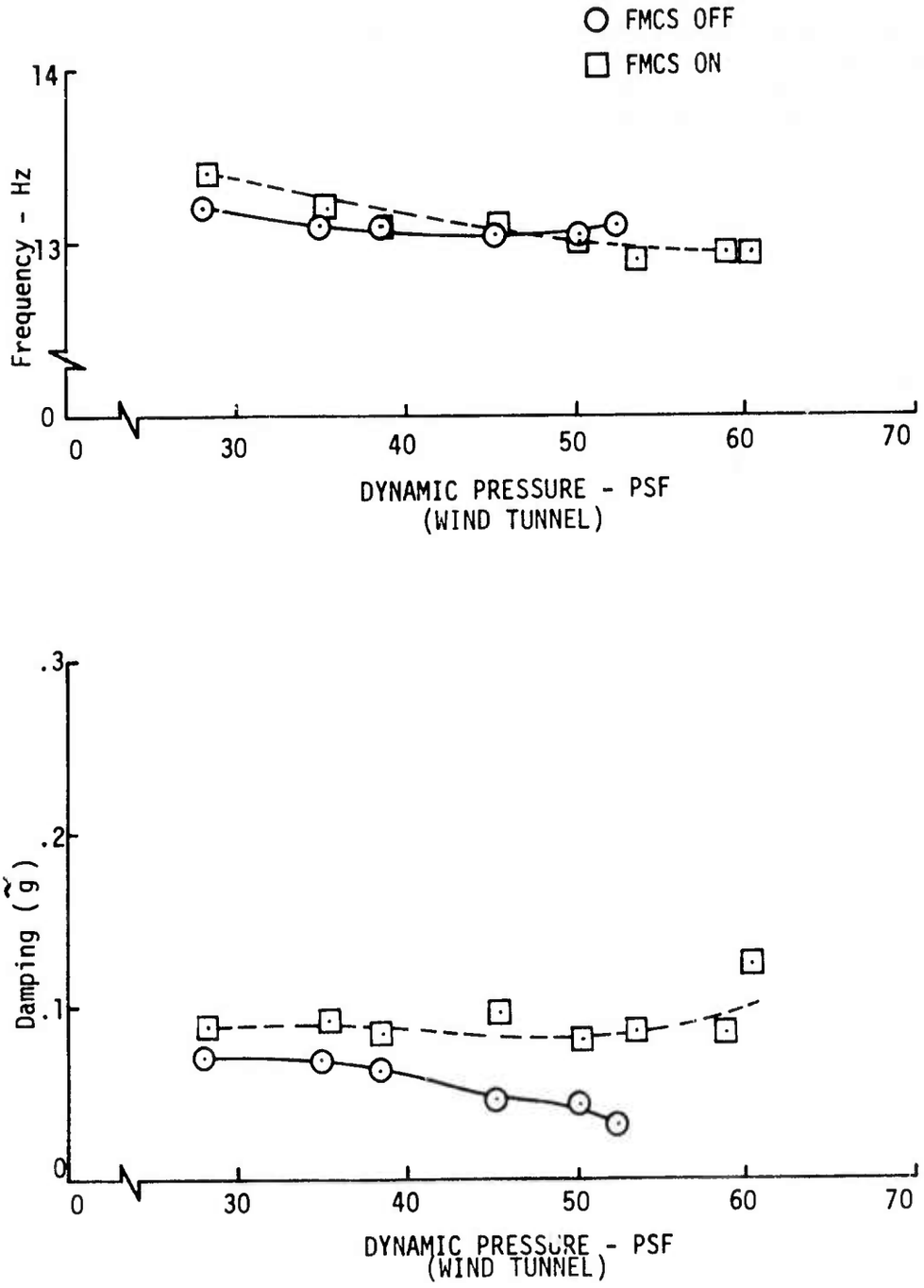

Figure 38. Flutter Mode Damping and Frequency Obtained From Co-Quad Plots of Inboard Wing Vertical Acceleration Due to Outboard Aileron

on, except at 28 psf dynamic pressure, but still higher than predicted. Either could be correct, but the outboard wing responses were used because damping and frequency estimates could be made for more modes from the co-quad plots.

A comparison of FMCS off flutter mode damping and frequency estimates made from outboard wing vertical acceleration responses to flaperon and aileron is shown in Figure 39, and Figure 40 offers the same comparison for inboard wing vertical acceleration responses. Figure 39 shows little difference in damping or frequency for the outboard wing responses to the two surfaces, but Figure 40 does show a significant difference in both damping and frequency. The results for aileron sweep were obtained during the same test run, as were the flaperon responses. The damping and frequency differences are due to differences in the inboard wing vertical acceleration responses to the two surfaces.

A limited number of conditions were tested using the horizontal canards to excite the model. Damping and frequency estimates for the flutter mode made from outboard and inboard wing vertical acceleration co-quad plots are shown in Figures 41 and 42, respectively. Neither plot shows any significant difference from the results shown in Figure 25.

Some definite conclusions can be drawn from this data. First, it points out that both damping and frequency estimates will vary depending on which sensor/surface combination is used. Secondly, as was discussed briefly in paragraph 6.1.1, some difficulty is encountered in estimating the mode frequencies required for damping estimates or for the undamped natural frequency. No two people working independently would obtain exactly the same damping and frequency estimates for all the modes on a given co-quad plot. This method is still the best, for this particular model, for estimating mode damping and frequency at subcritical conditions, but care must be exercised in applying the method.

The Q-$\tilde{g}$ and Q-f plots shown in Figure 43 offer the opportunity to evaluate the accuracy of the co-quad method for estimating modal damping and frequency. Data for these plots was taken from analytical co-quad plots, and the damping and frequency plots should agree with those shown in Figure 25 for predicted results. The damping and frequency for FMCS off agree very well, but with FMCS on the damping estimates are high and the frequency estimates are significantly higher (more than 1.0 Hz at 45 psf) than obtained from roots of the characteristic equation. This indicates that when modal damping is high and other modes close in frequency have similar or lower damping, accuracy of the method decreases.

Another method of estimating the flutter mode damping that required only the tunnel turbulence to excite the model was also used during the wind tunnel tests. This method, referred to as "randomdec", assumes the sensor output consists of components due to step, impulse and random disturbances (Reference 8). The sensor output is filtered and processed electronically, leaving only the step response from which damping estimates can be made using the logarithmic decrement technique. Figure 44 shows a Q-$\tilde{g}$ plot obtained from randomdec signatures. The results agree fairly well with those obtained using the co-quad method. This method works best for a very lightly damped mode, such as the flutter mode near flutter, and no external distrubance other than tunnel turbulence is required to excite the model.

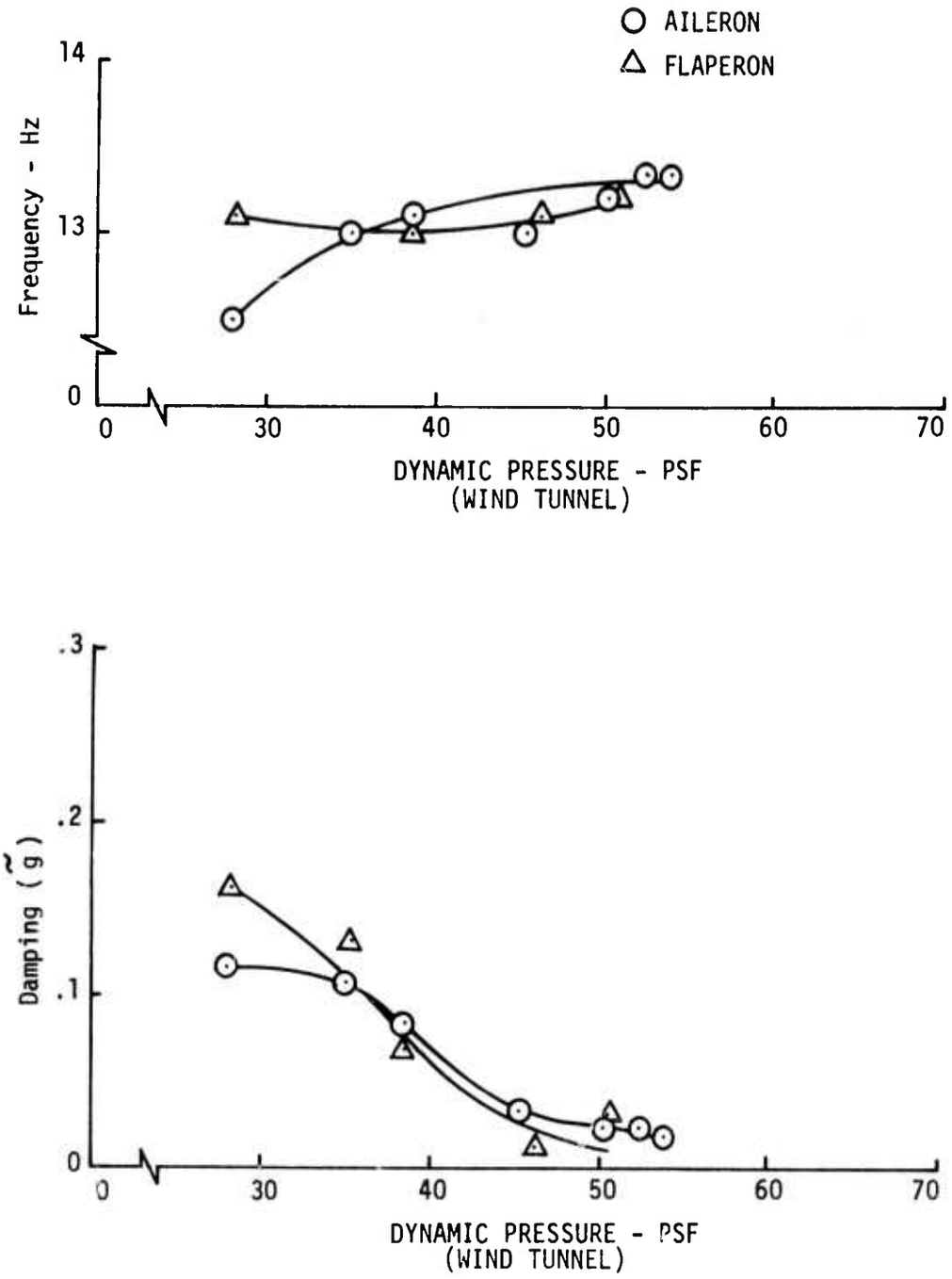

Figure 39. FMCS Off Flutter Mode Damping and Frequency - Comparison of Values Obtained from Co-Quad Plots of Outboard Wing Vertical Acceleration Due to Flaperon and Aileron

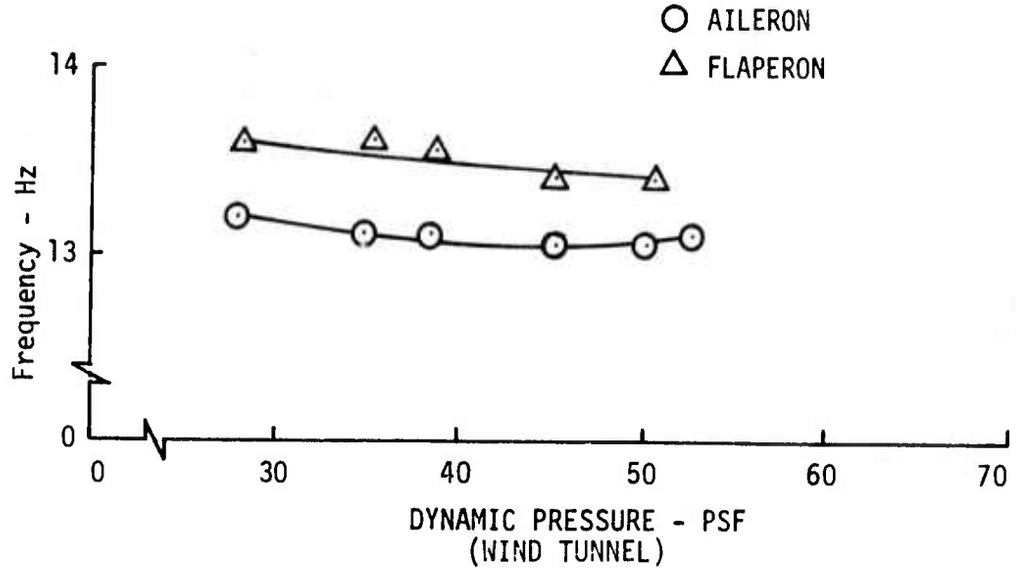

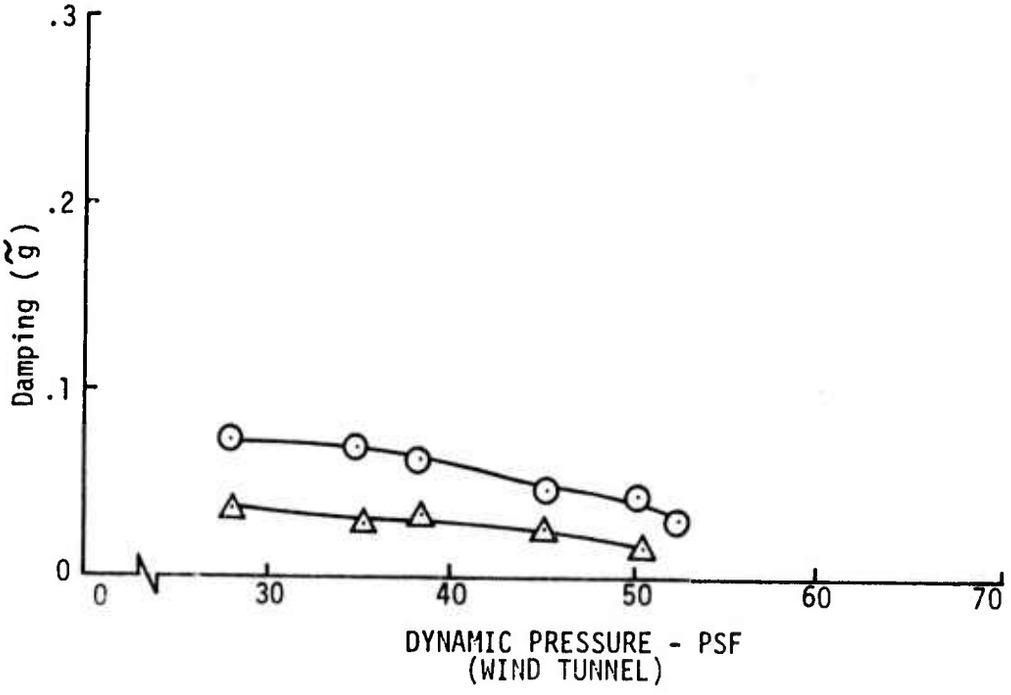

Figure 40. FMCS Off Flutter Mode Damping and Frequency - Comparison of Values Obtained from Co-Quad Plots of Inboard Wing Vertical Acceleration Due to Flaperon and Aileron

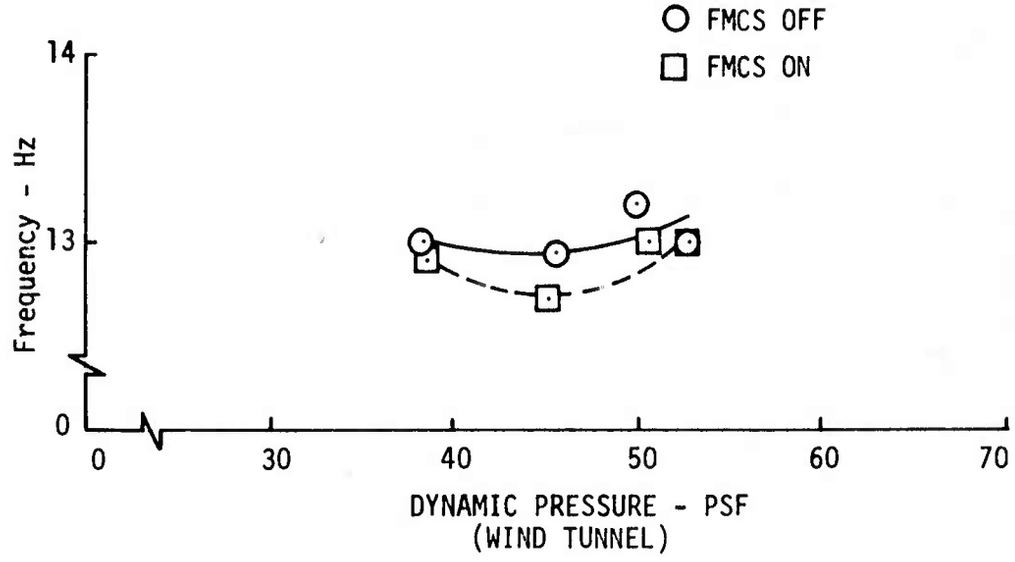

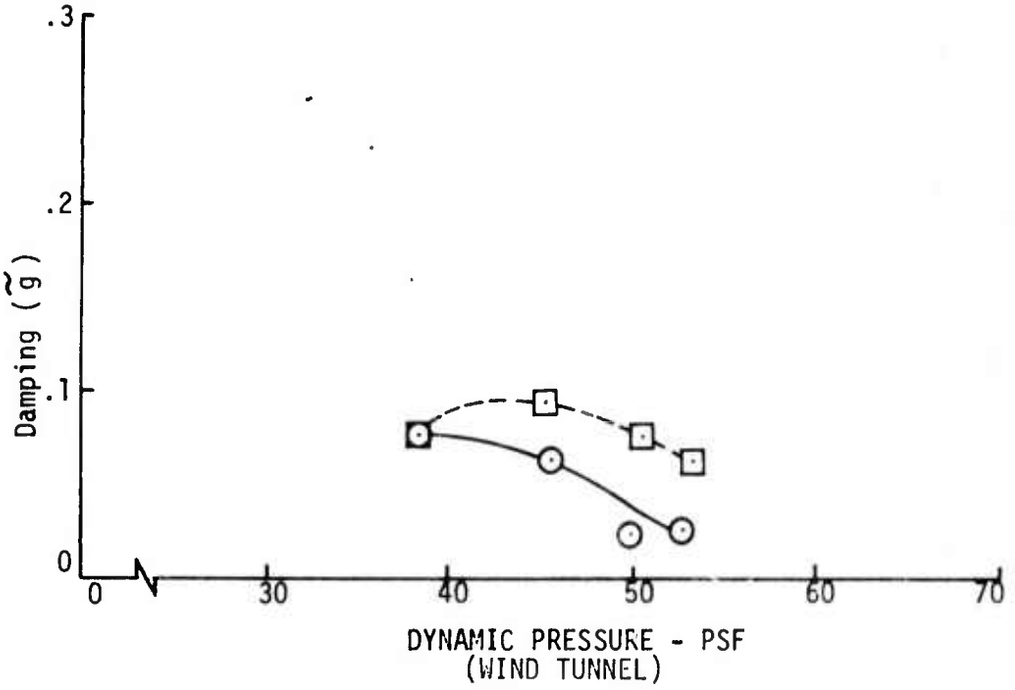

Figure 41. Flutter Mode Damping and Frequency Obtained From Co-Quad Plots of Outboard Wing Vertical Acceleration Due to Horizontal Canard

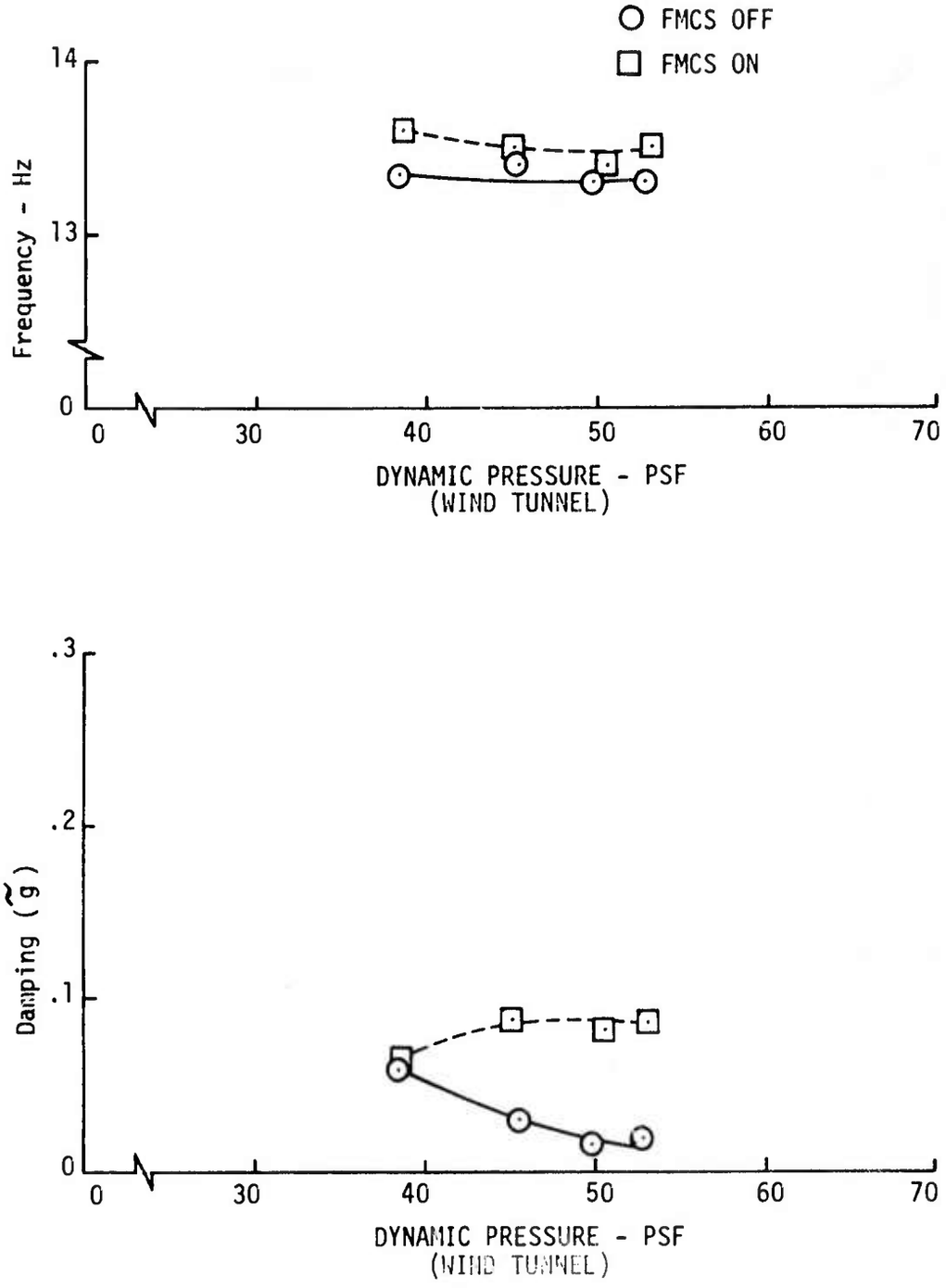

Figure 42. Flutter Mode Damping and Frequency Obtained From Co-Quad Plots of Inboard Wing Vertical Acceleration Due to Horizontal Canard

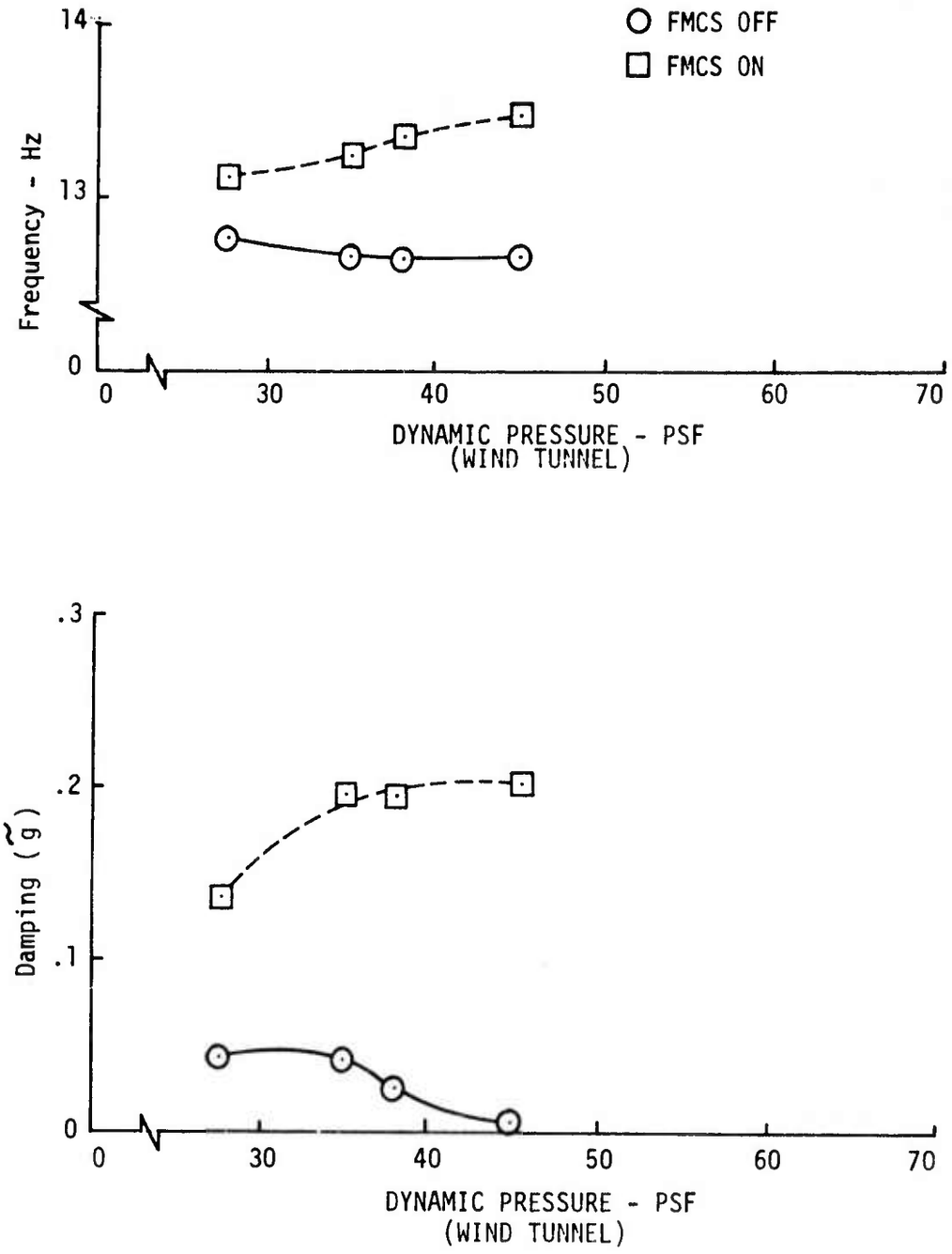

Figure 43. Flutter Mode Damping and Frequency Obtained From Analytical Co-Quad Plots of Outboard Wing Vertical Acceleration Due to Outboard Aileron

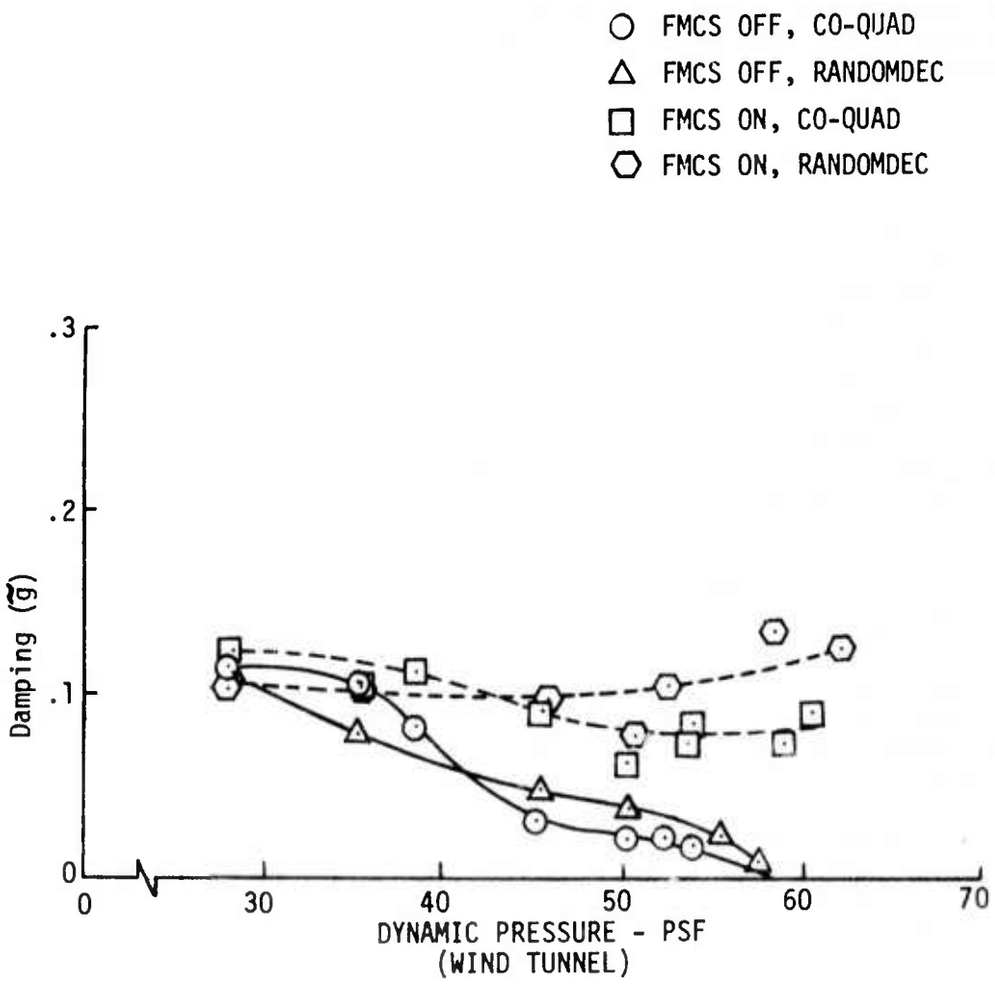

Figure 44. Flutter Mode Damping - Comparison of Randomdec and Co-Quad Values

6.2 Model and Airplane Test Data Comparison

The objective of correlation of model test data with the CCV program Fuel Configuration 3 flight test results is to determine how well the model predicts the airplane flutter characteristics. The correlation is accomplished primarily through comparison of model and airplane flutter mode V-$\tilde{g}$ and V-f plots. Aerodynamic hinge moments obtained during the wind tunnel and flight tests for the outboard segment flaperons are also compared. A discussion of airplane flight test results for the three CCV fuel configurations is included in Reference 9.

6.2.1 Comparison of Flutter Mode Characteristics

Model and airplane flutter characteristics, with the FMCS off and on, are summarized in the V-$\tilde{g}$ and V-f plots shown in Figure 45. Velocity in knots true airspeed is used to facilitate comparison of model data with airplane results. The model damping and frequency values are the same as those shown in Figure 25, but shown here in airplane velocity scale. The airplane damping and frequency values were taken from plots on pages 56 and 58 of Reference 10. These values were estimated from strip chart recordings of left hand wing tip chordwise acceleration response due to a one cycle sine wave elevator command. The responses were filtered electronically to approximately double integrate. Damping estimates were made using the logarithmic decrement method normally applied to transient responses.

The basic airplane flutter speed is 455.6 KTAS (339 KCAS), while the model fluttered at 492.3 KTAS (in airplane scale), only 8.1 percent higher than the airplane. The V-$\tilde{g}$ plots show that at lower airspeeds, the model flutter mode damping measured during the wind tunnel tests is nearly twice that measured for the airplane. As speed increases, the damping agrees better until the model plot flattens out around 450 KTAS. The model and airplane flutter mode frequencies agree very well for both FMCS off and on.

The model had been predicted to flutter at about 452.4 KTAS, 7.2 percent higher than the airplane predicted flutter velocity, 422.2 KTAS. Thus, the model and airplane flutter speeds compare about as was predicted analytically. The predicted FMCS off V-$\tilde{g}$ and V-f plots for model and airplane are shown in Figure 46.

As shown on Figure 45, the FMCS appears to be a little more effective on the model than on the airplane, but this may be due in part to the different methods used to estimate damping. The FMCS gains were the same for the model and airplane, and the shaping filters were scaled to model frequency scale for the wind tunnel tests. The model and airplane actuation system frequency responses were very similar in their respective frequency scales up to above the flutter mode frequencies. The two systems then were functionally identical. Note that airplane flutter mode damping estimates were made over a limited range of airspeeds for this configuration. In this range, the general shape of the two V-$\tilde{g}$ plots is similar in that both show a definite dip in flutter mode damping near the FMCS off flutter points.

Figure 47 shows V-$\tilde{g}$ and V-f plots obtained from airplane co-quad plots with FMCS off and on at four subcritical airspeeds. The open loop damping values estimated from the co-quad plots are higher than those in this region

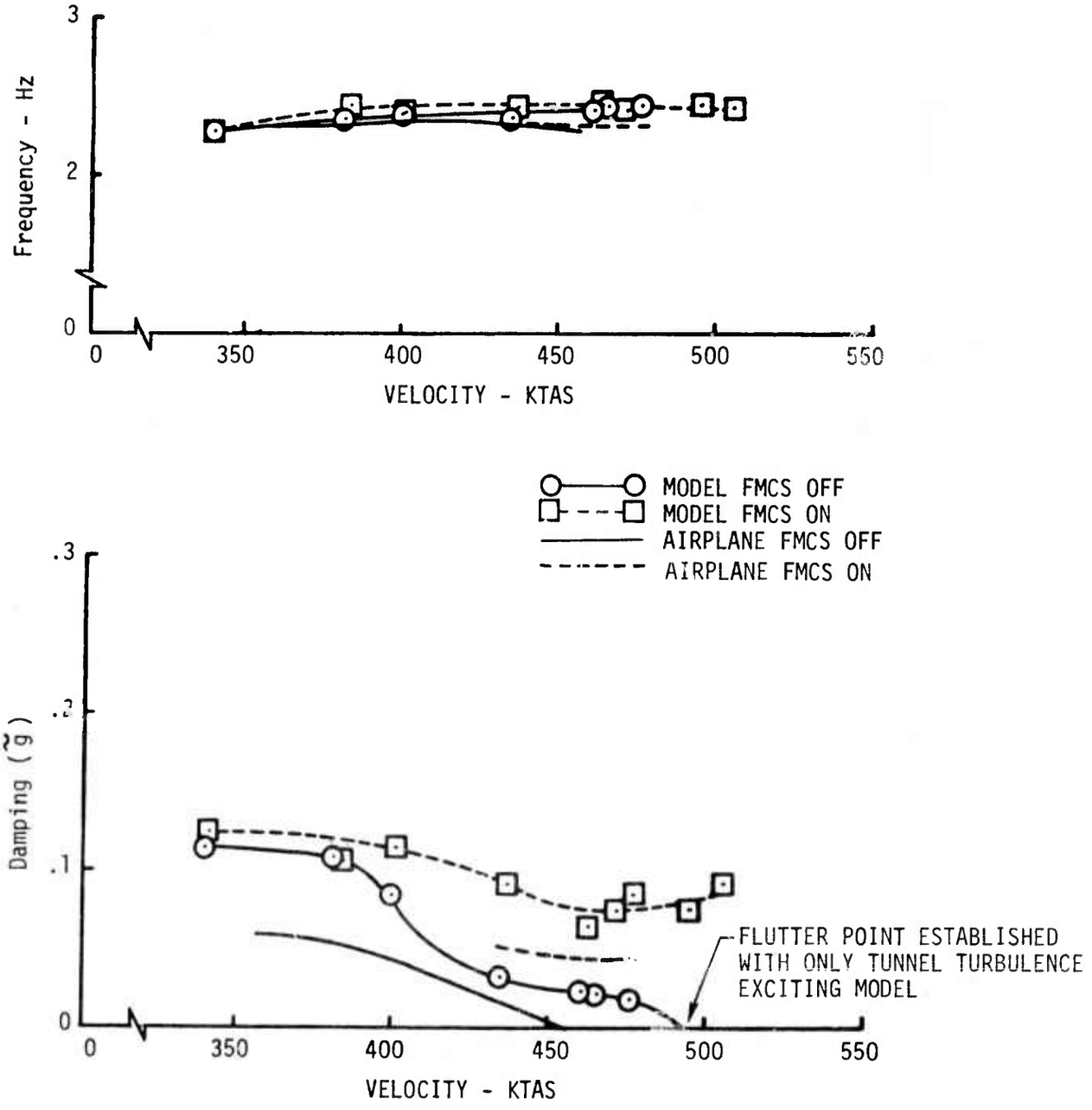

Figure 45. Flutter Mode Damping and Frequency - Model and Airplane Test Results Comparison

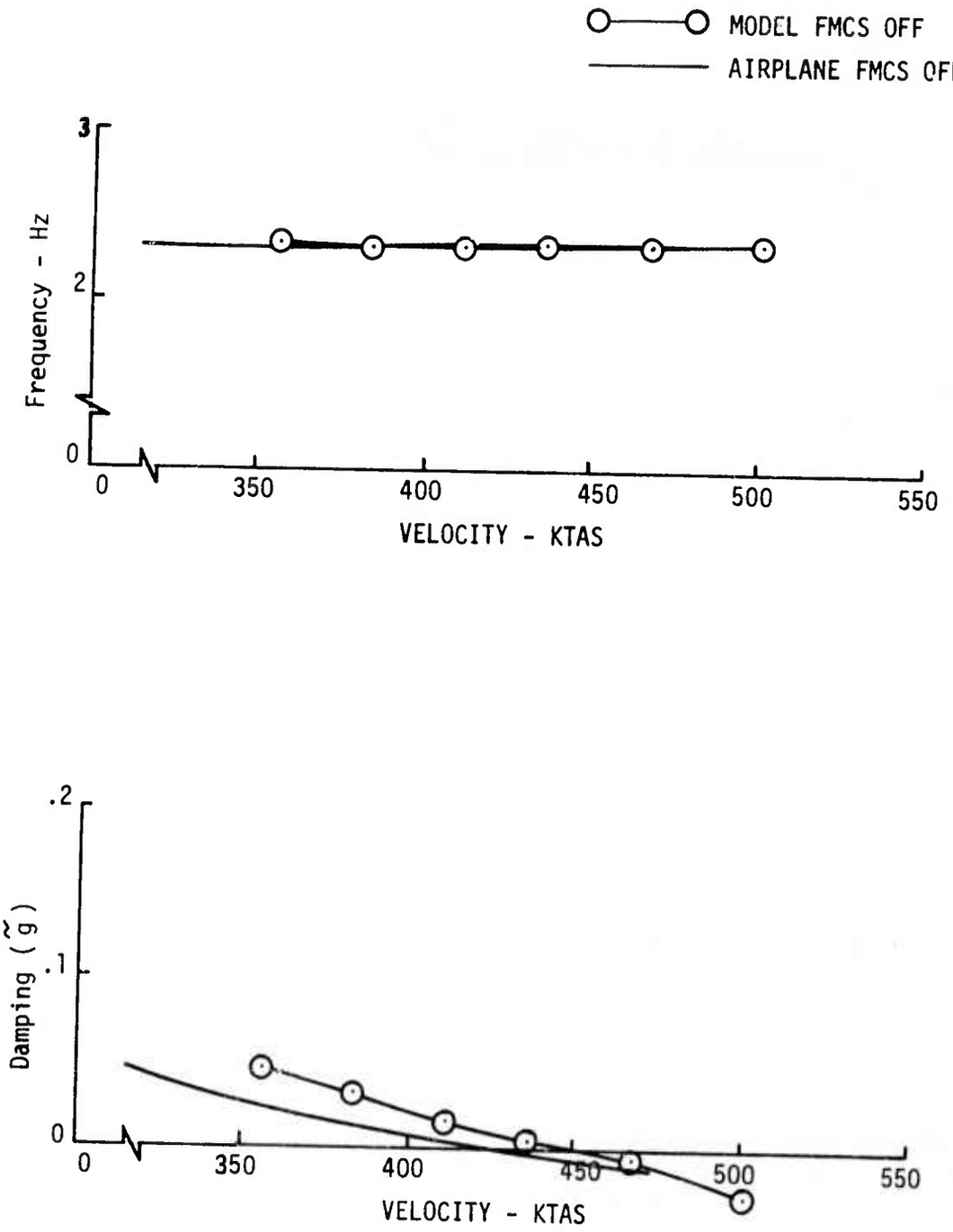

Figure 46. Analytical FMCS Off Flutter Mode Damping and Frequency Comparison

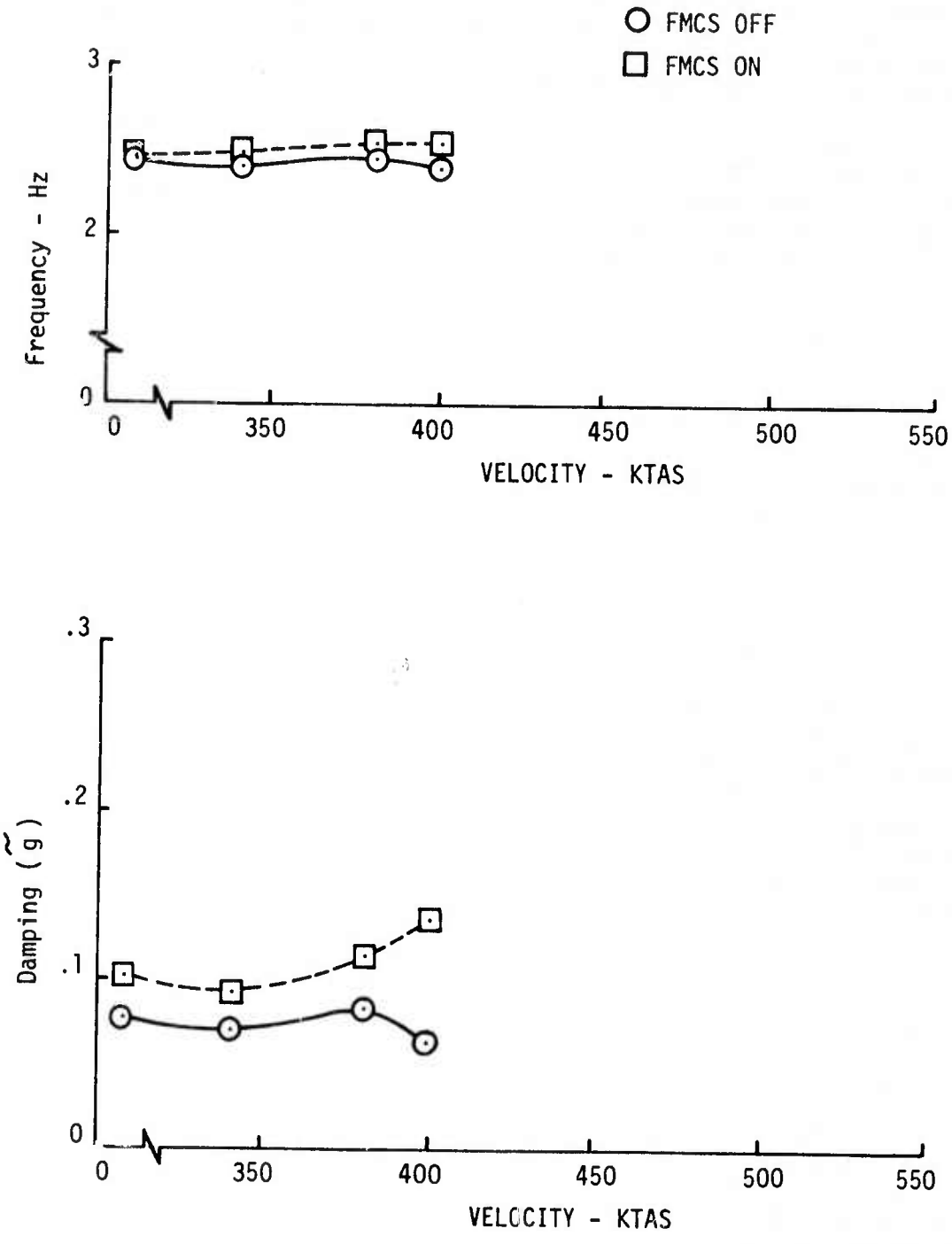

Figure 47. Airplane Flutter Mode Damping and Frequency Obtained from Outboard Wing Vertical Acceleration Due to Outboard Aileron Co-Quad Plots

obtained from transient responses, but the agreement is better as damping decreases. The FMCS on damping values are higher than the FMCS off values, and they appear inconsistent with the values estimated from the transient responses because damping is increasing with airspeed. Slightly higher frequency values were estimated from the co-quad plots also. This again points out that damping and frequency estimates vary with the method used.

Agreement between model and airplane flutter characteristics, and performance of the FMCS on the two vehicles is very good. Both vehicles fluttered at higher airspeeds than predicted, but at about the same percentage. Performance of the FMCS in increasing the flutter mode damping shows the same trend over the range flight test results were obtained.

6.2.2 Other Mode Comparisons

Co-quad plots for airplane outboard wing vertical acceleration due to 0.5 to 5.0 Hz outboard aileron sweeps are shown in Figure 48 for FMCS off and Figure 49 for FMCS on for a 381 KTAS (280 KCAS) condition. This condition is equivalent to the tunnel condition at which the model co-quad plots of Figures 26 and 27 were obtained (384.3 KTAS in airplane scale). Comparison of Figure 48 with Figure 26, and Figure 49 with Figure 27, shows the plots are similar, but some significant differences are apparent. Note that Figures 26 and 27 are in model frequency scale, which is 5.48 times airplane frequency. The general shape of the airplane co-quad plots looks very much like the model analytical plots shown in Figures 28 and 29.

One difference between the model and airplane co-quad plots is the mode at about 1.22 Hz on the airplane response. There should not be a symmetric elastic mode near this frequency, but this could be the first antisymmetric mode, predicted at 1.304 in the zero airspeed, free-free analysis. This frequency is 6.69 Hz in model scale, and Figure 26 does not show a mode near this frequency. The B-52 model was not scaled antisymmetrically. The antisymmetric mode encountered in the model GVT was at 8.6 Hz for this condition with FMCS off and is probably the second antisymmetric mode.

The airplane symmetric first elastic mode is at about .93 Hz with estimated .255 damping with FMCS off, and about .93 Hz and .245 damping with FMCS on. These values compare to .91 Hz and .141 damping for FMCS off and .86 Hz and .140 damping with FMCS on for the model at this condition. The effect of the FMCS on this mode is about the same for model and airplane.

The second elastic mode was predicted at 1.77 Hz with .067 damping at this condition with FMCS off. The out-of-phase component plot in Figure 48 indicates a well damped mode between 1.5 and 1.6 Hz. The next mode appears to be the third elastic mode, and the fourth mode can also be seen. The third mode appears to be similar to the 10.95 Hz mode shown in Figure 26, and the effect of the FMCS on the mode is similar.

The airplane flutter mode frequency and damping are estimated for this condition to be 2.44 Hz and .082 for FMCS off, and 2.54 Hz and .114 with FMCS on. The corresponding model values are 2.37 Hz and .108, and 2.45 Hz and .106 for FMCS off and on, respectively, in airplane scale. The seventh, eighth and ninth elastic modes are apparent in Figure 48, but only the eighth mode was discernible on the model plot.

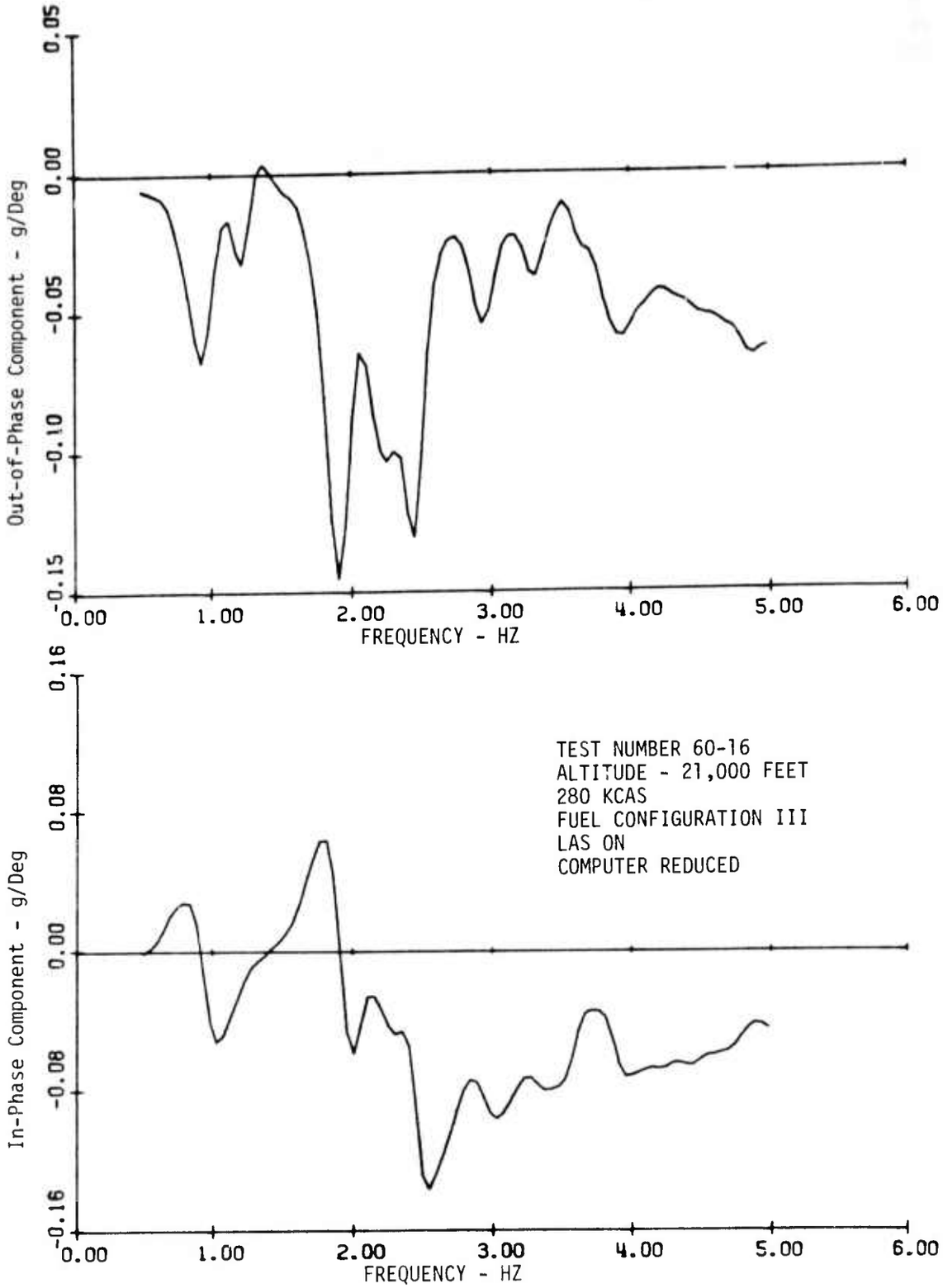

Figure 48. Airplane Outboard Wing Vertical Acceleration Due to Outboard Aileron Co-Quad Plot - FMCS Off

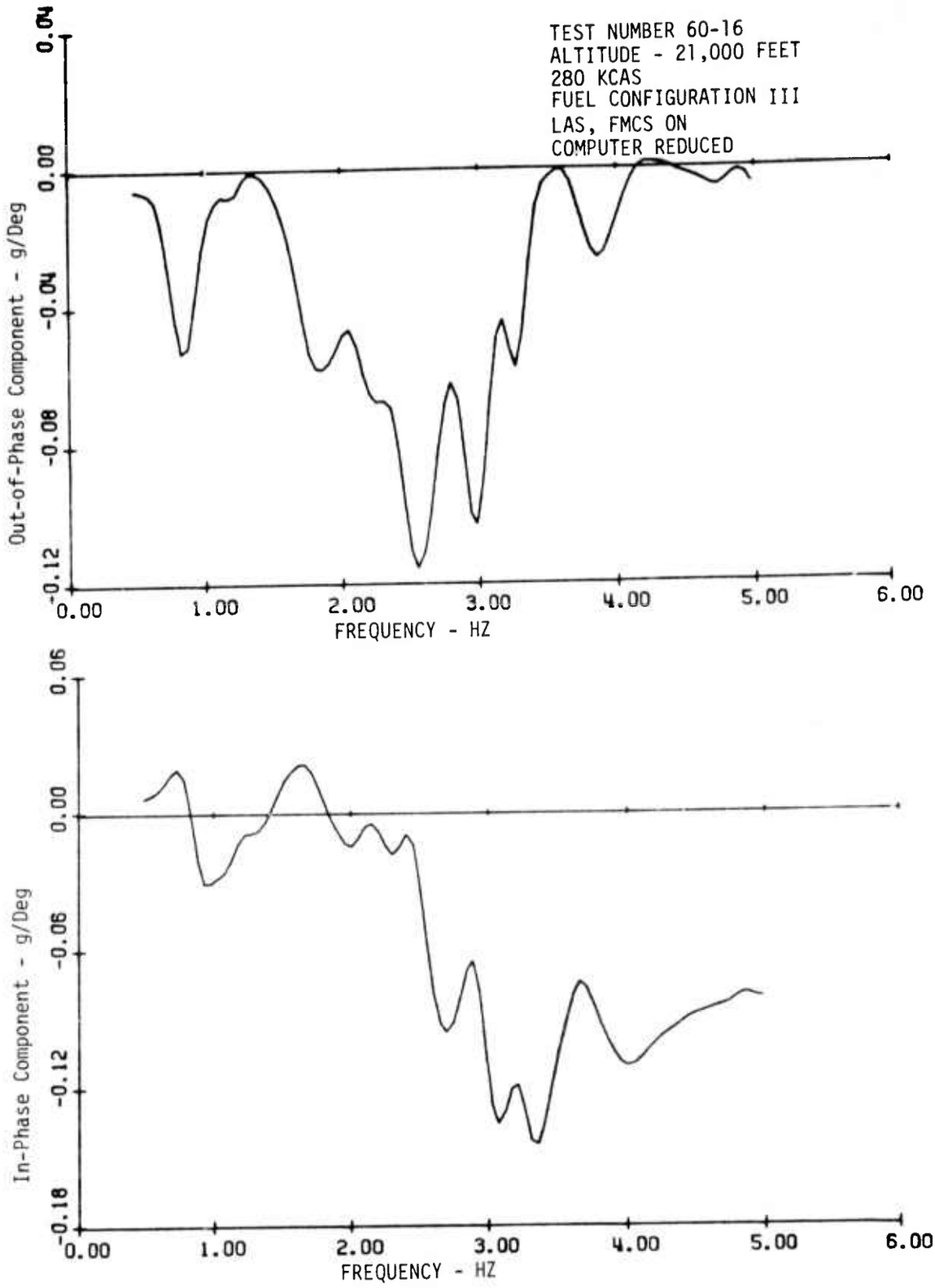

Figure 49. Airplane Outboard Wing Vertical Acceleration Due to Outboard Aileron Co-Quad Plot - FMCS On

Thus, the model provides a good representation of the airplane flutter characteristics, with good correlation of the first, third, sixth and eighth elastic modes. The model flutter velocity was higher than the airplane, as predicted. Performance trend of the FMCS on the model is similar to that demonstrated on the airplane. Both model and airplane test data with FMCS on exhibit a dip in flutter mode damping near the FMCS off flutter conditions.

6.2.3 Outboard Flaperon Segment Aerodynamic Hinge Moments

The model and airplane were both instrumented to measure total hinge moment of the outboard flaperon segment control surfaces during the wind tunnel and flight testing. On the airplane, the surface actuator ram had strain gages added and calibrated to read actuator force. A torsional link was installed in the model surface shaft, with strain gages calibrated to read moment about the surface shaft directly.

Total hinge moment data was recorded during the flight tests at the altitudes equivalent to the model test conditions, with .5 to 5.0 Hz linear sweep sine wave command to the surfaces. This data was plotted in frequency response form during the post test data reduction with amplitude and phase relative to the surface command plotted versus frequency. The 4.1 inch moment arm was taken into account to convert actuator force into moment about the surface hinge line. Actuator frequency responses for the four velocities (225, 250, 280 and 295 KCAS), presented in Reference 11, were used to convert the moment reference from surface command to surface displacement at discrete frequencies. The surface zero airspeed hinge moment, obtained previously, were then subtracted vectorially to give aerodynamic hinge moments relative to surface displacement.

Airplane aerodynamic hinge moment amplitude and phase for the four conditions are shown in Figures 50 and 51, respectively. The amplitude and phase are plotted versus reduced velocity with one-half of the airplane mean aerodynamic chord used as the reference length. The mean aerodynamic chord for the B-52 airplane is 275.5 inches.

Model hinge moments were recorded in co-quad form during the wind tunnel tests, with flaperon displacement used as reference. The zero airspeed hinge moment values were subtracted vectorially at discrete frequencies to give aerodynamic hinge moments at the five conditions tested. Plots of aerodynamic hinge moment amplitude and phase are shown in Figures 52 and 53, respectively, in airplane scale versus reduced velocity. One-half of the mean aerodynamic chord in model scale was used as the reference length.

Comparison of hinge moment amplitudes for airplane and model, Figures 50 and 52, indicate similar plots over the common range of reduced velocities. The airplane sweeps were conducted from 0.5 to 5.0 Hz, which would be 2.74 to 27.4 Hz in model scale. But, model sweeps were conducted only over the range 4 to 24 Hz. Thus, the first two points on the four airplane amplitude plots were not obtained during the model testing. Airplane data below 1.0 Hz was not used due to questionable phase data in the zero airspeed hinge moment data caused by extremely low voltage levels from the instrumentation to the transfer function analyzer. Thus, the highest reduced velocity points on Figure 50 corresponds to 1.0 Hz, and the lowest point corresponds to 5.0 Hz.

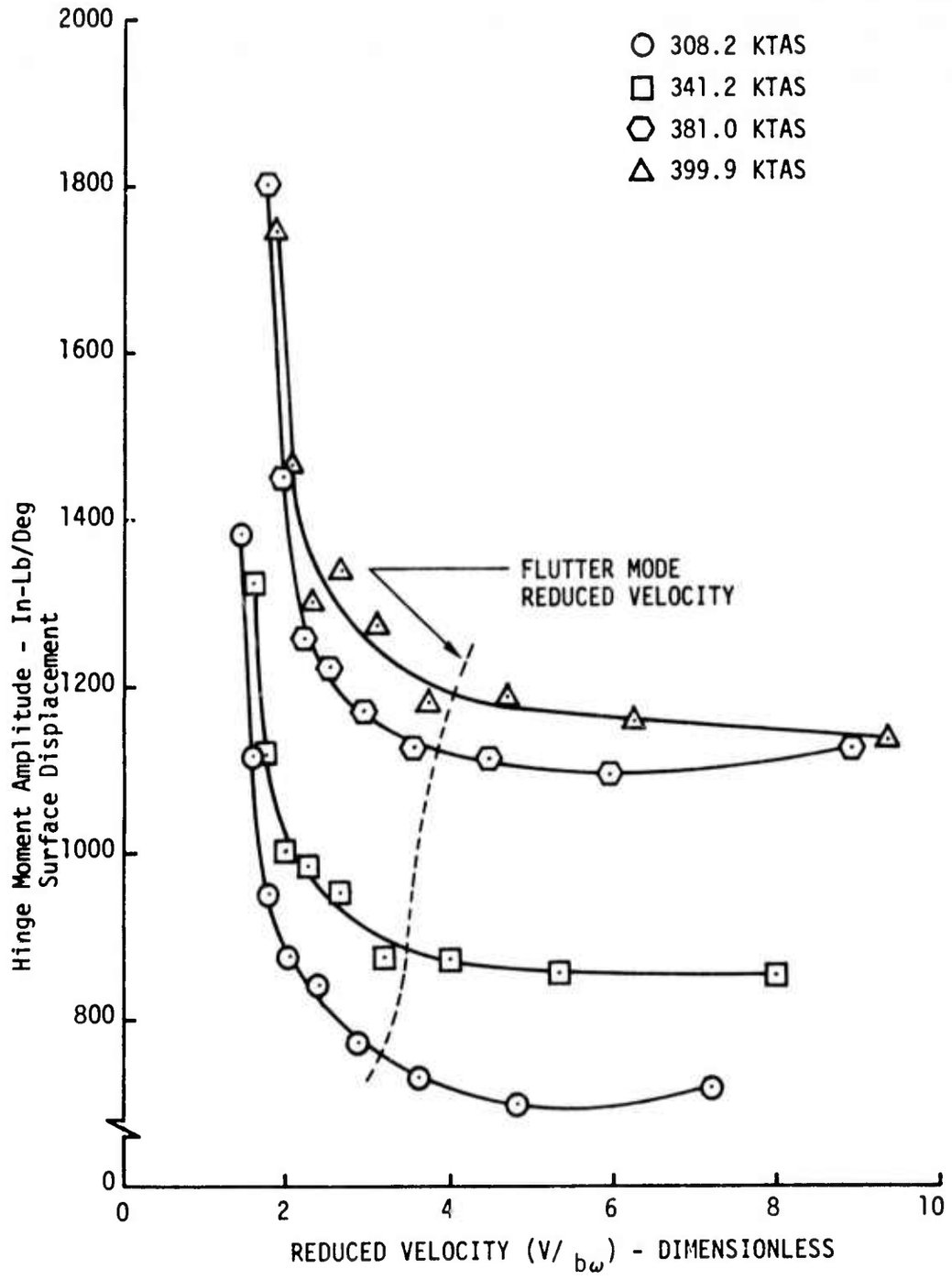

Figure 50. Airplane Outboard Flaperon Aerodynamic Hinge Moment Amplitude

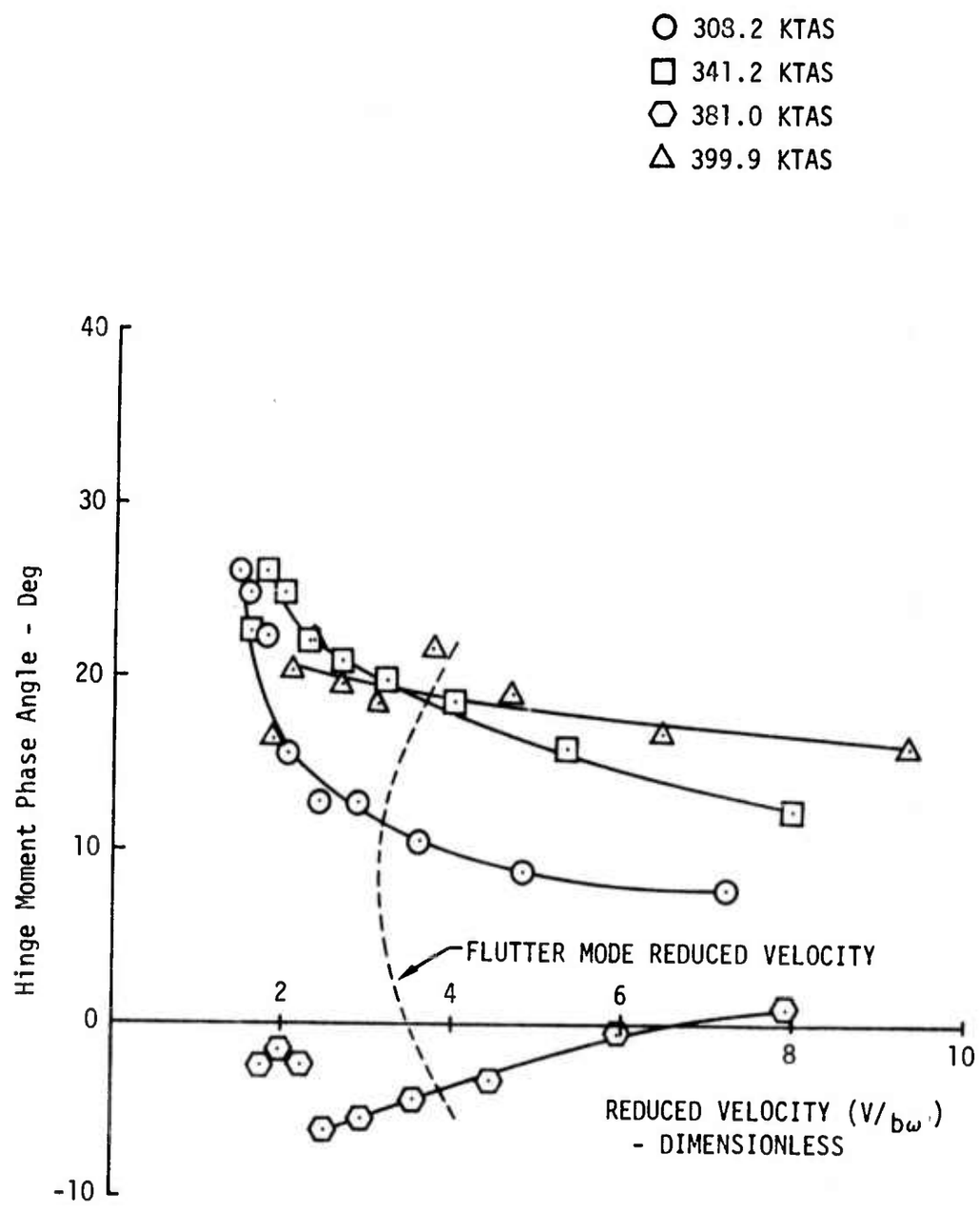

Figure 51. Airplane Outboard Flaperon Aerodynamic Hinge Moment Phase Angle Relative to Surface Displacement

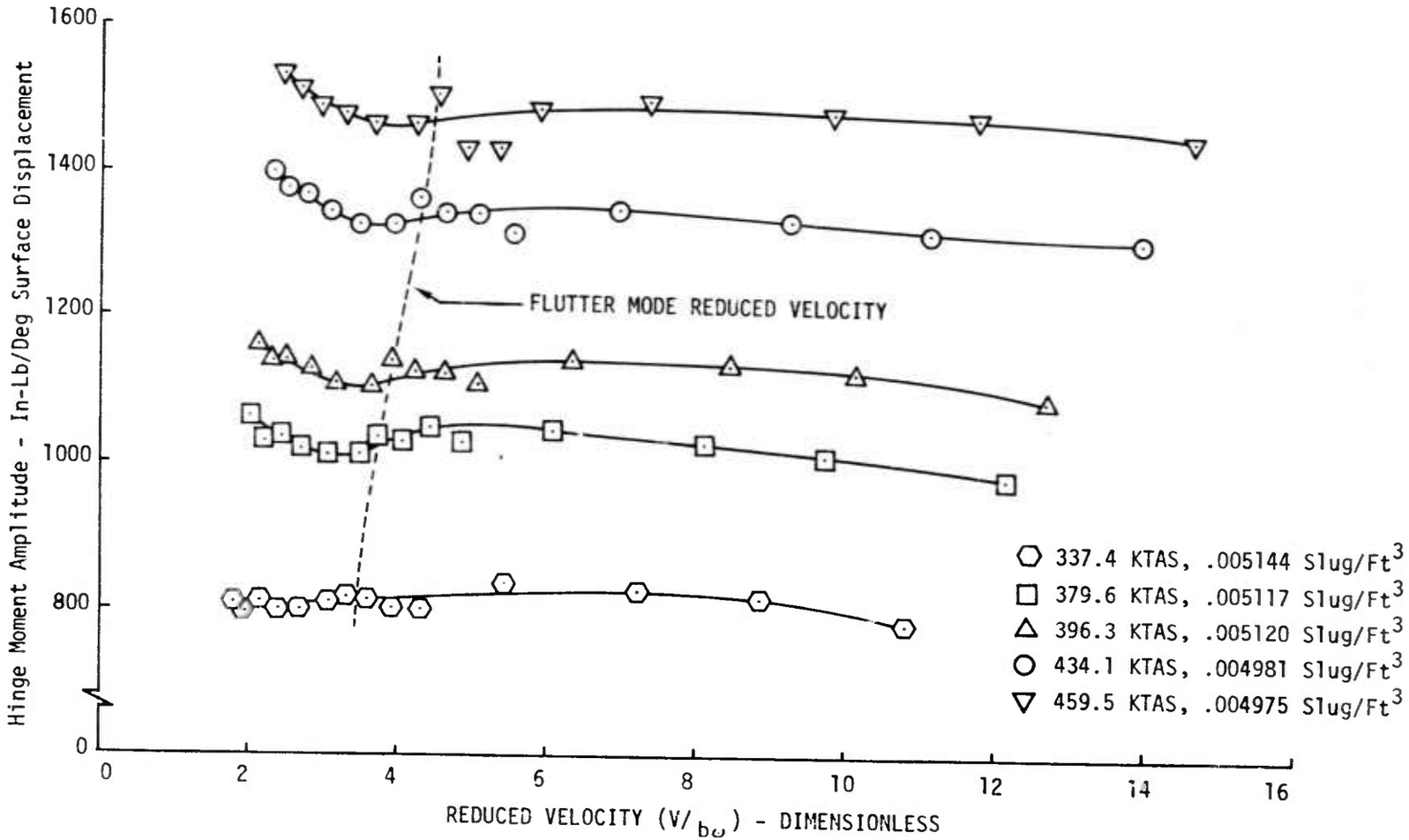

Figure 52. Model Outboard Flaperon Aerodynamic Hinge Moment Amplitude (Airplane Scale)

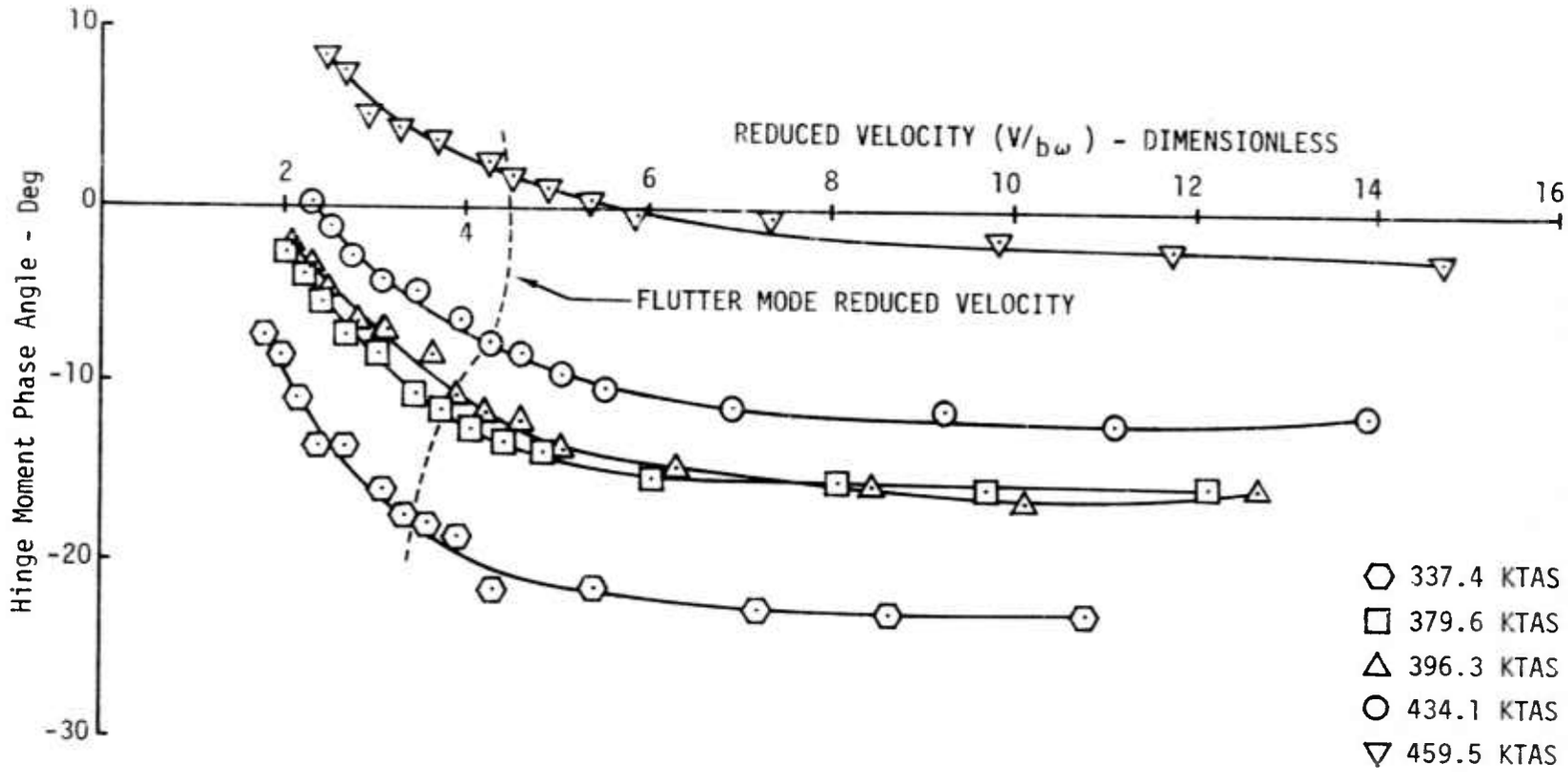

Figure 53. Model Outboard Flaperon Aerodynamic Hinge Moment Phase Angle Relative to Surface Displacement

The three lower model airspeed conditions correspond closely to the three higher airplane airspeed conditions. The airplane measurements were made at 21,000 feet altitude, and the corresponding tunnel density was .00499 slug/ft^3. The actual tunnel densities for these three conditions were slightly higher, indicating a lower equivalent airplane altitude condition.

Magnitude of the airplane aerodynamic hinge moment at 341.2 KTAS is about 5 percent higher than the model hinge moment at 337.4 KTAS for reduced velocities above 4.5. Similar agreement can be seen between the 396.3 KTAS model data and the 399.9 KTAS airplane results, with airplane values about 3.5 percent higher than the model values. The greatest difference occurs at the remaining common condition, with airplane values above 4.5 reduced velocity at 381.0 KTAS about 8.3 percent higher than model results at 379.6 KTAS.

Below 4.5 reduced velocity, the model amplitudes decrease slightly as the flutter mode frequency is approached, and then increase as frequency increases. This slight dip is not seen in the airplane hinge moment amplitudes, but the increase is evident, more pronounced than on the model results.

The model and airplane hinge moment phase angles relative to surface deflection show the same trends, except for the 381.0 KTAS airplane test condition. Reason for the phase angles being different at this condition is unknown, but it appears on the total hinge moment frequency response plot. The model phase angles appear to be biased 25-30 degrees lag from the airplane results. Theoretically, the phase angle should asymptotically approach zero as reduced velocity approaches infinity (zero frequency).

6.3 System Parameter Variations and Gust Responses

Performance of the flutter mode control system was evaluated with variations in the flaperon and aileron loop gains and filter time constants to demonstrate the insensitivity of the system to system changes. Effects of saturation in the system shaping filters were also evaluated. These tests were conducted at the nominal 21,000 foot equivalent airplane condition. The system was also tested at a 9,300 foot equivalent altitude to demonstrate insensitivity to changing test condition.

Model responses with the flutter mode control system off and on to the transonic dynamics tunnel gust vanes were obtained to demonstrate the capability of the system to function in a gust environment.

6.3.1 System Parameter Variations

Capability of the flaperon and aileron channels to control the flutter mode while operating alone at nominal gain is shown in Figure 54. The flaperon system operating alone is not as effective as the aileron system, and neither gives the performance attained with both operating simultaneously. With the flaperon system operating alone, flutter mode damping appears to be approaching zero with increasing dynamic pressure, but the trend established at the three subcritical points tested is not conclusive.

Figure 55 illustrates the effects of gain changes in the two channels. The nominal Phase II gains are K_A = 42.4 deg/g and K_F = 52.5 deg/g. A

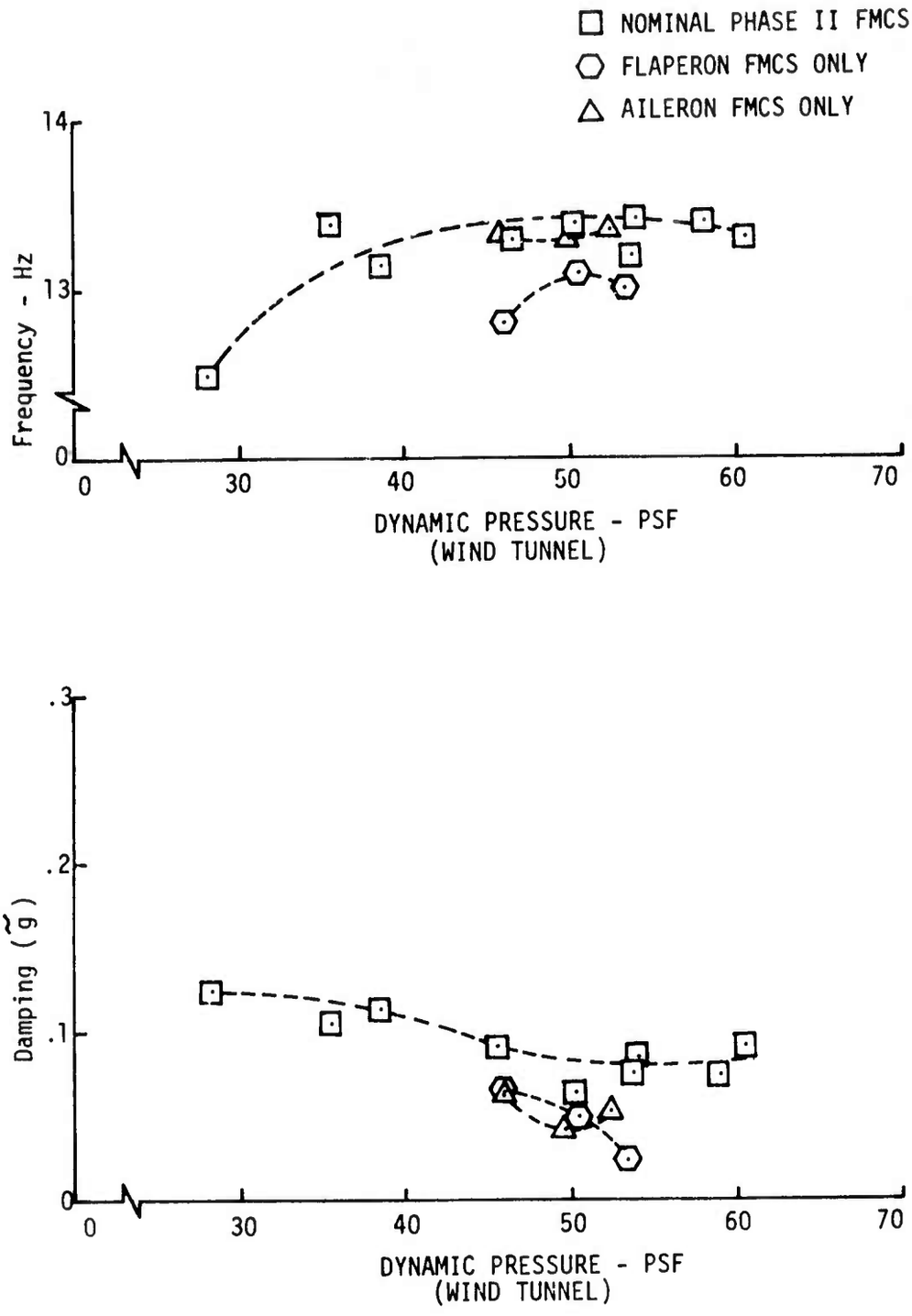

Figure 54. Flutter Mode Damping and Frequency - Flaperon and Aileron FMCS Performance (Wind Tunnel Test Results)

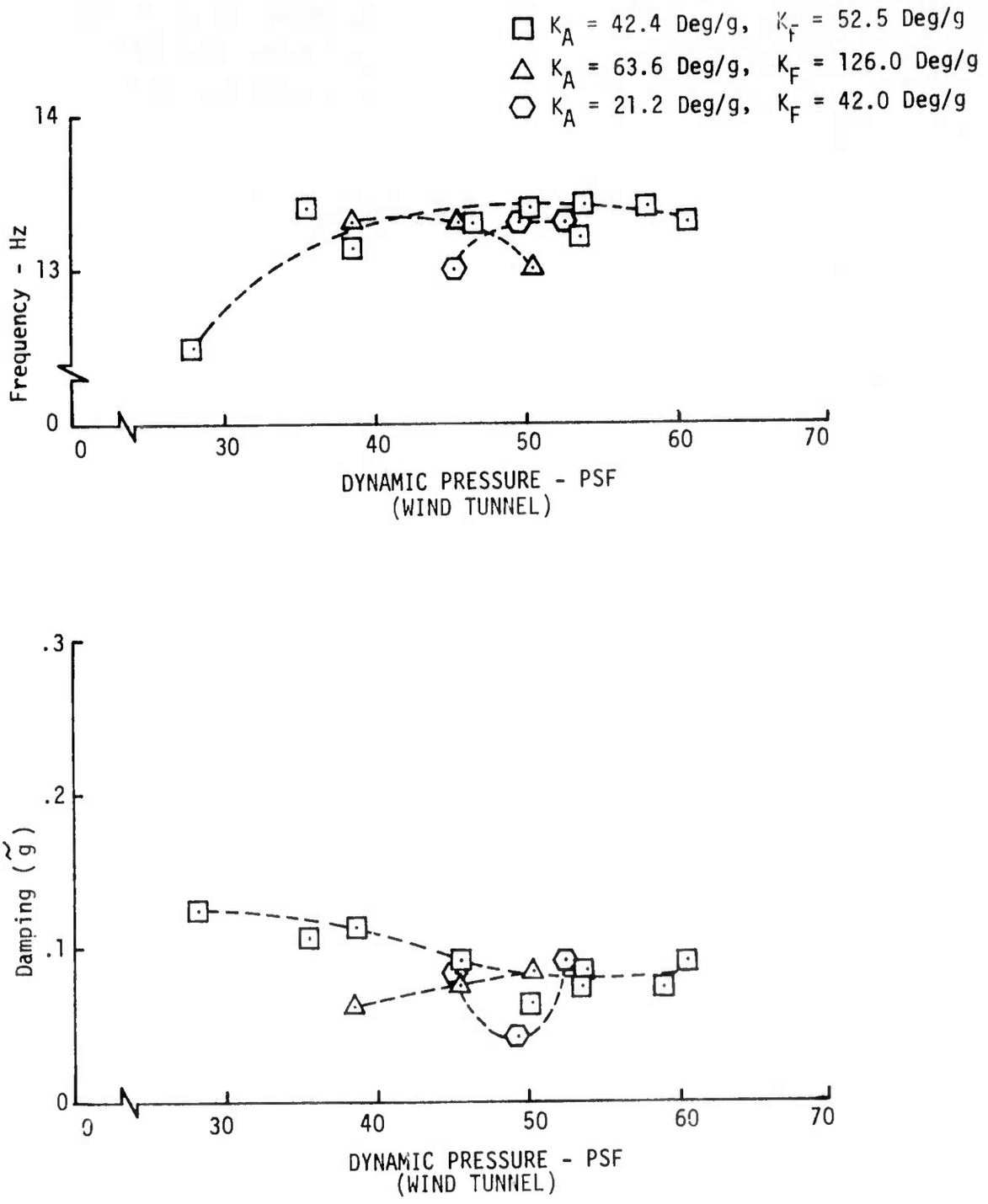

Figure 55. Flutter Mode Damping and Frequency - FMCS Gain Variations (Phase II Wind Tunnel Test Results)

definite dip in the flutter mode damping is evident around 50 psf dynamic pressure with K_A = 21.2 deg/g and K_F = 42.0 deg/g. Damping value measured with K_A = 63.6 deg/g and K_F = 126.0 deg/g appears lower than attained with K_A = 42.4 deg/g and K_F = 52.5 deg/g at 38 psf dynamic pressure, but about the same values were estimated at 45 and 50 psf.

Figure 56 shows the effects on the FMCS performance of varying the aileron and flaperon filter break frequencies. Changing the break frequencies from the nominal 82.2 rad/sec to 61.65 rad/sec introduces 24.4 degrees lag and about 19 percent gain reduction in the flaperon channel, and 32.6 degrees lag and 31 percent gain reduction in the aileron channel, at the flutter mode frequency relative to the nominal system. This combination of phase lag and gain reduction degrades effectiveness of the system. The 100 rad/sec break frequency introduces 16.7 degrees lead and about 7 percent gain increase in the flaperon channel, and 22.3 degrees lead and 17 percent gain increase in the aileron channel, at the flutter mode frequency relative to the nominal system. The phase lead and increased gain has little effect on the FMCS performance.

Saturation of the flutter mode control system commands to the aileron and flaperon actuation systems was mechanized using bridge limiters on the analog computer. Figure 57 shows some degradation in the system performance with ±1.0 degree limits on both system commands. The limit was more severe in the aileron system as the command to the actuation system reached about 2.5 degrees at the flutter mode frequency during the aileron sweeps at these conditions without saturation. The flaperon system command peaked at about 1.5 degrees for the same condition.

Performance of the nominal Phase II FMCS at about 9,300 feet equivalent airplane altitude is shown in Figure 58. This figure demonstrates that the ability of the system to increase flutter mode damping at lower altitude is about the same as the performance attained at 21,000 feet equivalent altitude.

The test results shown that the aileron system is more effective than the flaperon system in controlling the flutter mode. System performance is not affected significantly by gain variations or altitude change, but saturation and phase lag in the system shaping filters cause significant degradation in system performance.

6.3.2 Model Gust Response

Model responses were obtained with a sinusoidal gust, generated by symmetric gust vanes upstream of the tunnel test section, exciting the model. This testing was accomplished to demonstrate the capability of the FMCS to function in a gust environment.

A co-quad plot of outboard wing vertical acceleration normalized to gust vane displacement angle is shown in Figure 59 for FMCS off at 50.67 psf dynamic pressure. This response was obtained with gust vane frequency increased linearily from about 2 to 16 Hz. The co-quad plot shown in Figure 60 for a similar condition with the FMCS on shows the flutter mode significantly better damped than with the system off. With the FMCS off, the flutter mode damping, estimated from Figure 59, is .023. The damping estimated from Figure 60 with FMCS on is .077. Damping of the first elastic mode is also increased by the FMCS. Other modes can be seen in the responses, but with amplitudes too low to make accurate damping comparisons.

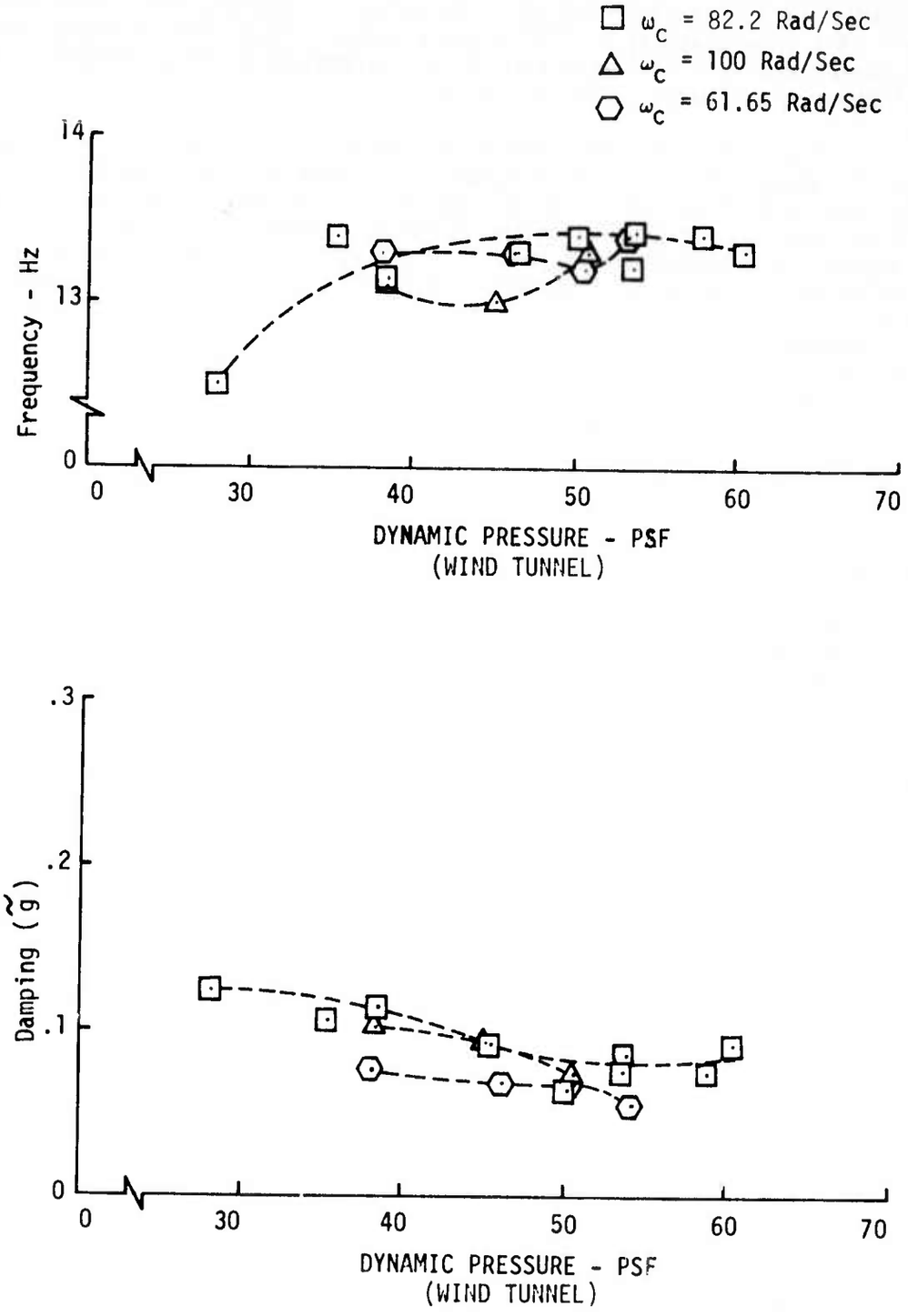

Figure 56. Flutter Mode Damping and Frequency - FMCS Filter Time Constant Variations (Phase II Wind Tunnel Test Results)

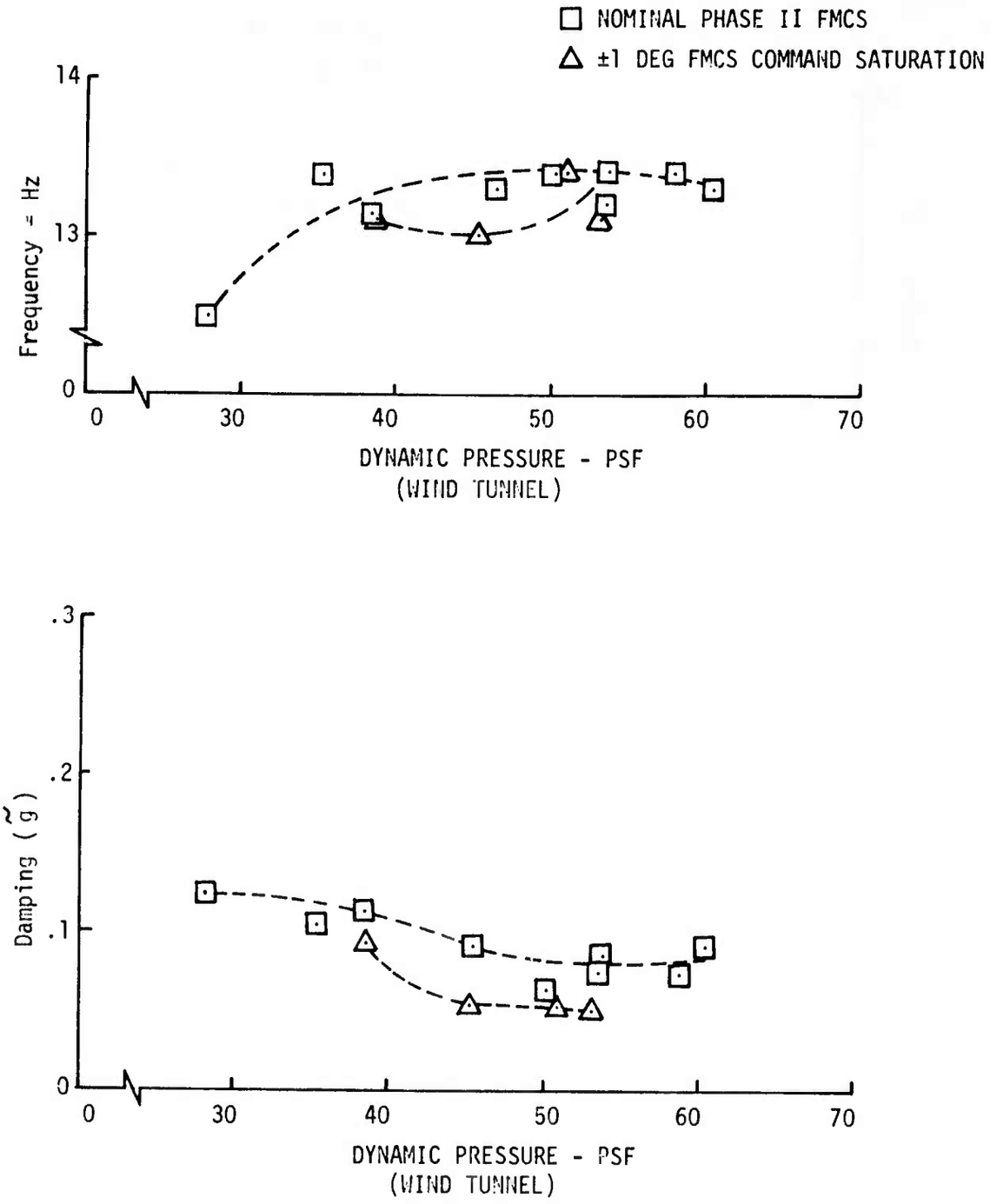

Figure 57. Flutter Mode Damping and Frequency - FMCS Command Saturation

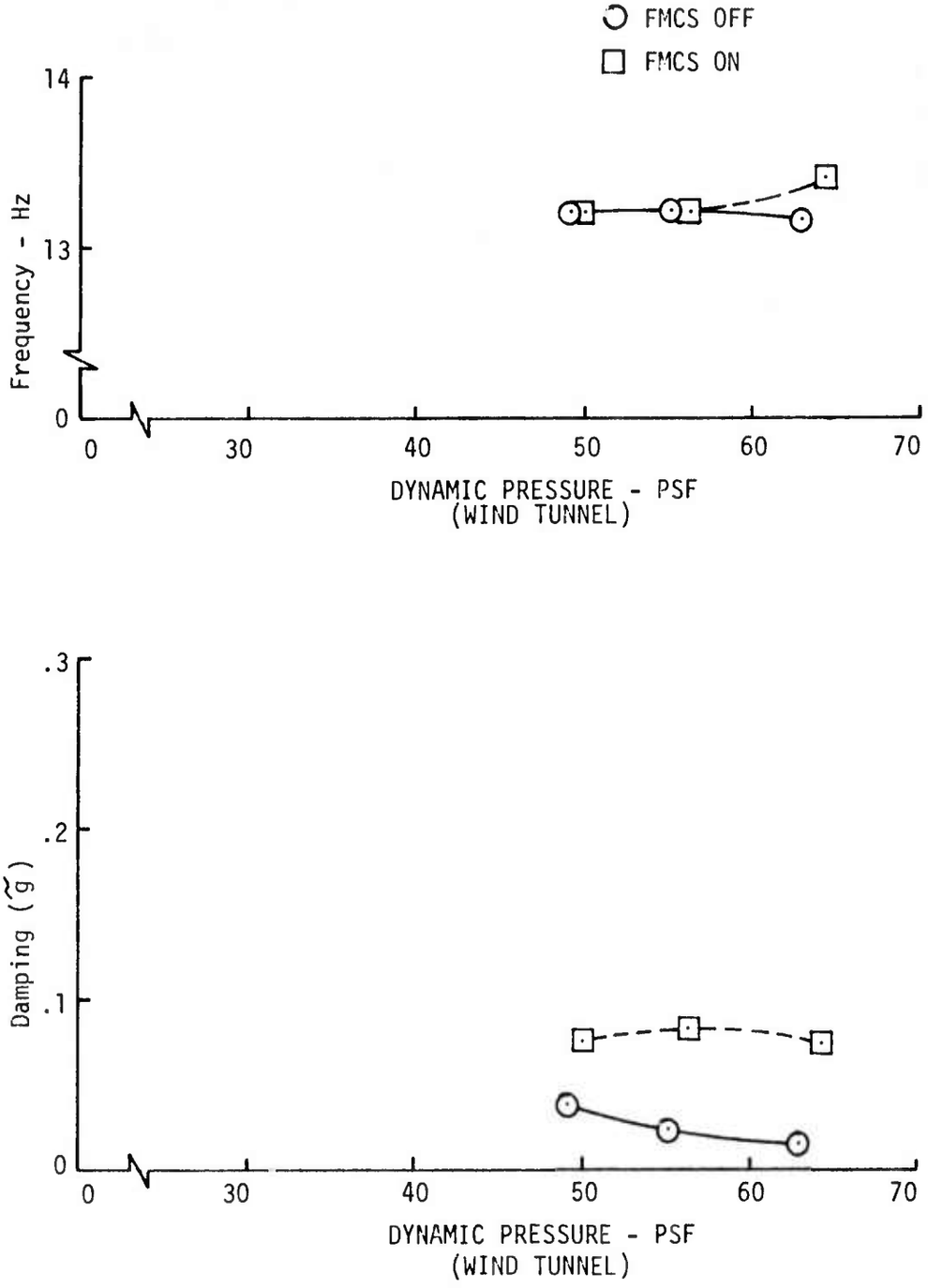

Figure 58. Flutter Mode Damping and Frequency - FMCS Performance at .0073 Slug/Ft^3 Tunnel Density (9300 Feet Equivalent Airplane Altitude)

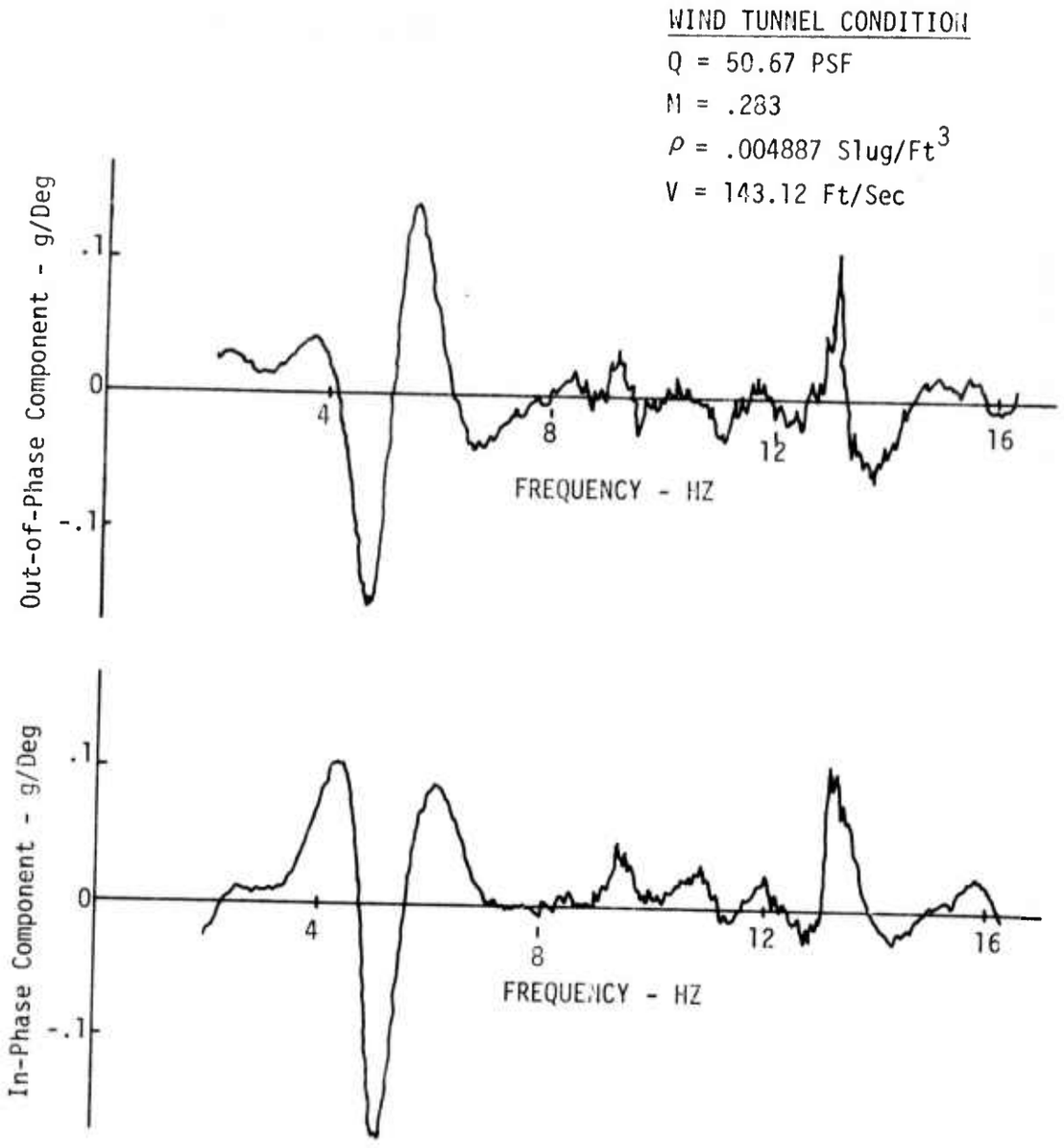

Figure 59. Outboard Wing Vertical Acceleration Due To Gust Vane Displacement Co-Quad Plot - FMCS Off

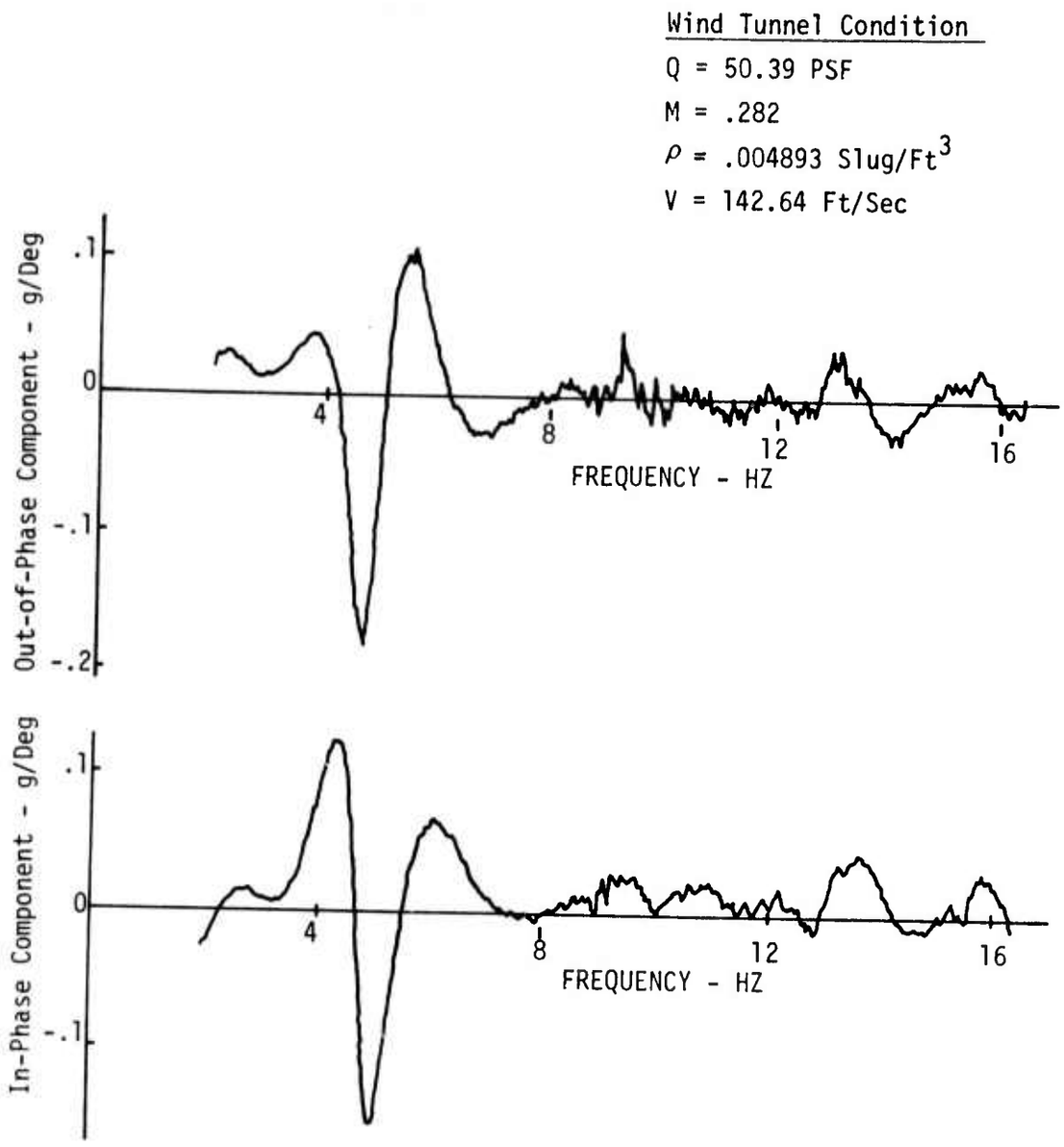

Figure 60. Outboard Wing Vertical Acceleration Due To Gust Vane Displacement Co-Quad Plot - FMCS On

Amplitude of the vertical gust at the test section decreases dramatically with increase in frequency of the gust vanes. Figure 61 shows a co-quad plot of the alpha gust (vertical gust divided by airstream velocity) normalized to vane displacement measured with a gust probe in the test section. It is apparent that the gust amplitude decreases significantly with increasing gust vane frequency.

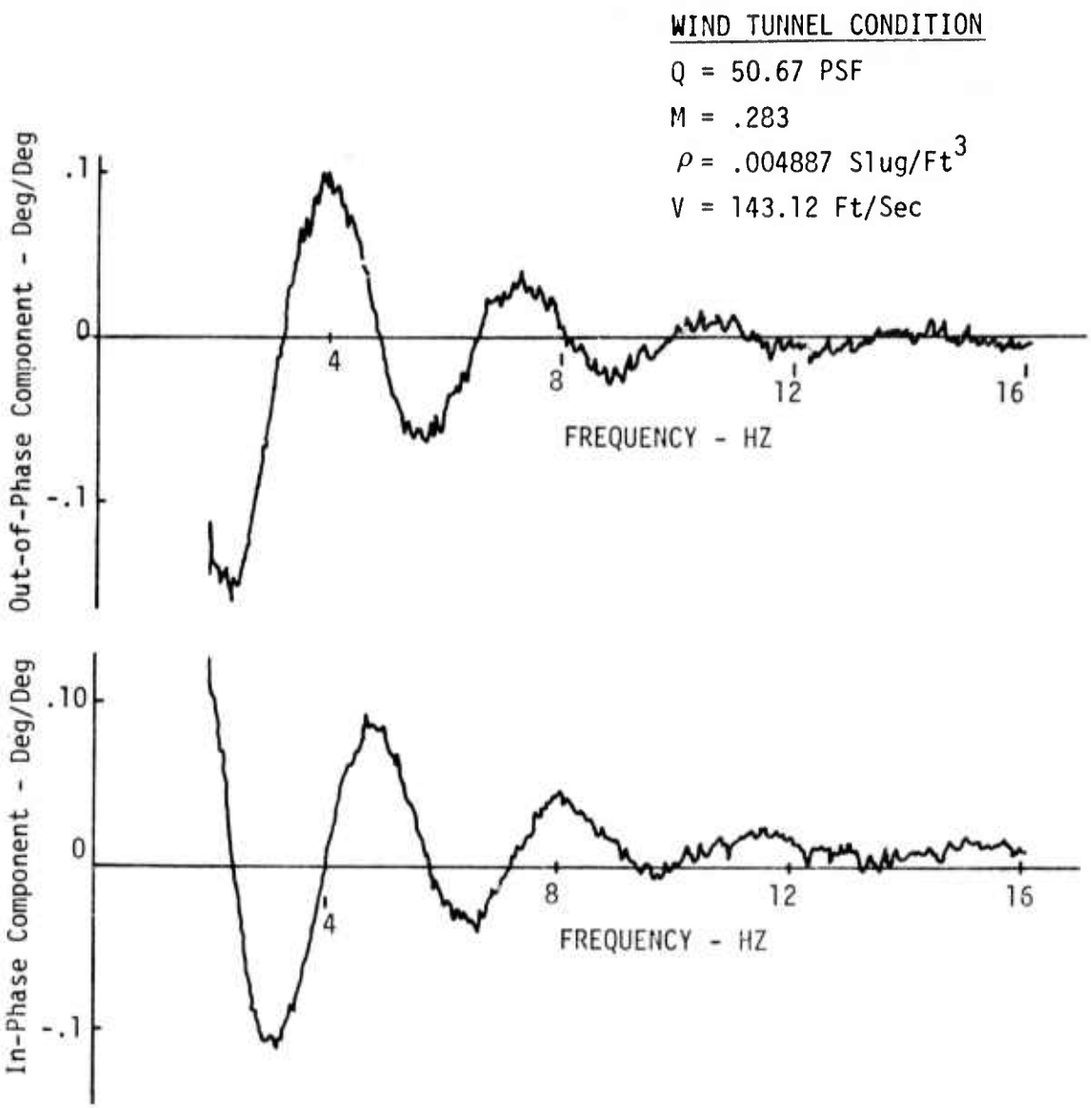

Figure 61. Alpha Gust Due to Gust Vane Displacement Co-Quad Plot

7.0 CONCLUSIONS AND RECOMMENDATIONS

Wind tunnel test data has been obtained on a dynamically scaled model of the B-52E CCV flight test vehicle in a 375,000 pound gross weight, 21,000 foot altitude condition. Model testing was accomplished to determine the basic model flutter characteristics and to evaluate the CCV program flutter mode control system. Results of the wind tunnel testing have been compared with model analytical and CCV program flight test results obtained at the equivalent condition. The following paragraphs discuss the degree of correlation attained and areas requiring additional research effort to improve the technique of evaluating airplane stability augmentation systems on dynamically scaled wind tunnel test models.

7.1 Conclusions

Under this program, equivalent flutter conditions for the B-52 aeroelastic model and the CCV program flight test airplane have been determined through structural analyses to provide suitable vehicles for wind tunnel and flight test data correlation. The model and airplane were predicted to have similar flutter characteristics, with the model flutter speed, in airplane scale, only 7.2 percent higher than the airplane flutter speed. Ground vibration tests verified that the model, after modification to the flutter configuration, possessed good representation of all symmetric elastic modes except the seventh, and to a lesser extent, the third and fourth, but the flutter mode representation was good.

The CCV airplane FMC system was scaled to model frequencies, and evaluated on model equations of motion. Results showed performance of the system on the model would be similar to the performance predicted for the airplane.

The NASA one-thirtieth scale model was modified from a 419,000 pound configuration with scaled B-52E ailerons and elevators active to the 375,000 pound, ballasted external wing tank flutter configuration with the CCV airplane outboard flaperon segments and outboard ailerons active. The model control surface actuation systems were mechanized using d.c. torque motors with position and rate feedback to produce actuator dynamic performance similar to the airplane actuators up to above the flutter mode frequency.

The model was then tested in the NASA Langley Transonic Dynamics Tunnel following test plans prepared to obtain tunnel test data using flight flutter test techniques. The model was tested in two entries, the first to verify the model's representation of the airplane flutter characteristics, and the second to obtain data for correlation with CCV airplane flight test results obtained in the equivalent airplane configuration and flight condition. Tests were conducted in both the model and airplane tests to compare the unaugmented vehicle flutter characteristics and performance of the flutter mode control system. Both vehicles were tested with the FMC system on up to about 10 knots (airplane scale) above the open loop flutter speed. Damping of the flutter mode was increasing with airspeed at this point in both tests, demonstrating that the desired 30 percent increase in airplane flutter placard airspeed had been exceeded.

Wind tunnel test data was then compared with analytical results. The comparison showed good correlation with the predicted model flutter characteristics and FMC system performance. The unaugmented model fluttered at 58.4 psf dynamic pressure, only 8.8 percent higher in velocity than predicted. The model flutter point extrapolated from subcritical testing during the first entry was 9.8 percent higher than the predicted flutter velocity for the model configuration tested, but the extrapolated flutter point was 55 psf. The model was modified slightly between the two entries, as evidenced by the different flutter points. The flutter mode control system performance was similar to that predicted, but not as effective in increasing the flutter mode damping.

The airplane flutter speed, with gross weight and altitude equivalent to the model, was established through flight testing at 455.6 KTAS. The model flutter point, established in the second series of wind tunnel tests, was only 8.1 percent higher, 492.3 KTAS in airplane scale. The difference between the model and airplane flutter speeds (in airplane scale) was within 1.0 percent of the difference predicted analytically.

Performance of the FMC system on the airplane was similar to the performance demonstrated on the model. The trends of flutter mode damping with increasing velocity with the system on are almost identical, with both model and airplane test results showing a dip in damping around 450-460 KTAS and then increasing. The FMC system was more effective in increasing flutter mode damping on the model than on the airplane, but the difference may be due to estimating damping from steady state sinusoidal responses on the model and from transient responses on the airplane.

The correlation of model wind tunnel test data with flight test results shows that a dynamically scaled aeroelastic model can predict the airplane flutter velocity, for an equivalent gross weight and altitude condition, within 8.1 percent. The model and airplane flutter speeds agreed better than the model test and analytical flutter speeds. Performance of the FMCS on the model also agreed better with the performance attained on the airplane than was predicted for the model. Model and airplane equations of motion were conservative in predicting lower flutter speeds and better performance with the FMCS than was obtained during the wind tunnel and flight tests.

The agreement between model and airplane test results demonstrates that dynamically scaled models can be used to verify design of active flutter mode control systems. Such modeling technology will play an important role in the future development and design of flutter suppression systems and other CCV concepts.

Wind tunnel testing of dynamically scaled models to verify predicted flutter speeds has proved successful and economically justifiable. This program has demonstrated that a flutter mode control system can be mechanized on such models using miniature sensors and control surface actuation system components and tested successfully in the wind tunnel. For a relatively small increase in cost, the flutter mode control system can be tested to give increased confidence in its design, and the model flutter testing can be conducted with greater model safety with the system to fall back on should hard flutter occur. Although the other CCV systems were not tested in this program, it is logical that they be incorporated in the wind tunnel model of an aircraft relying upon such systems.

7.2 Recommendations

During the course of this program, several areas requiring additional work to improve the technology of testing active control systems on wind tunnel models were encountered, and other areas were recognized as logical extensions of this work. This program has proved that such testing can be accomplished successfully, but additional work is required to extend the testing to other control configured vehicles systems. The following paragraphs discuss the most significant of these items.

Of the problems encountered in mechanizing the flutter mode control system on the B-52 model, probably the most difficult to overcome was to attain satisfactory performance from the outboard aileron electromechanical actuation system. The d.c. torque motor was, of necessity, located in the model fuselage with torque transmitted some 38 inches from the motor shaft out each wing to the control surfaces. Although the lowest frequency shaft mode was above 60 Hz, the friction arising from the bearings and crank-pushrod linkages resulted in significant hysteresis, more than was measured on the airplane actuation systems. The effects of hysteresis on the FMC system performance was demonstrated in the hybrid computer simulation studies. Hysteresis more nearly equivalent to the airplane actuator could have been attained with hydraulic actuators located near the control surfaces. Development of a miniature hydraulic power supply tailored to model space and weight limitations would improve the model's representation of the airplane actuators, not only in terms of hysteresis but in dynamic performance as well. Hydraulic pressure and return lines could be brought into the model from a tunnel sting, but the dynamic effects on a cable-mounted model would be significant.

The B-52 model was tested in the study on the NASA Langley Transonic Dynamics Tunnel two-cable mount system. Structural analyses showed the mount system affected primarily the model short period and the second, third and fourth elastic modes, but did not materially affect the model flutter characteristics. However, in testing control systems requiring accurate representation of these modes, either a modified mount system will have to be developed or analytical methods developed to "back out" effects of the mount system on these modes. The CCV program augmented stability, maneuver load control and forward body ride control systems involve the short period mode and the ability of the model systems to function similar to the airplane depends upon accurate simulation of this mode.

The model must be designed and constructed to accurately represent all significant rigid body and elastic modes. The B-52 aeroelastic model was designed to have scaled dimensions, stiffness properties, inertia properties (in roll, pitch and yaw freedoms), aerodynamic properties, and center of gravity location of the airplane. It was dynamically scaled over the frequency range 0 to 25 Hz, model scale, to match the airplane symmetric modes in frequency and mode shape. Model ground vibration and wind tunnel tests showed the design criteria was met except for the seventh elastic mode, and to a certain extent, the third and fourth modes. But, the significant mode (the sixth) was represented accurately, as evidenced by its good correlation with theoretical predictions and the mode on the airplane.

Another area requiring work is in model testing and data reduction techniques. For the B-52 model, steady state frequency response methods provided the best subcritical data, primarily because tunnel turbulence masked

transient responses to the point damping estimates could not be made. The main shortcoming of the frequency response methods is that the damping and frequency estimates are made assuming a single degree of freedom system, and accuracy improves when the flutter mode is lightly damped. Testing to verify analytical results requires considerable testing below the critical flutter condition, and methods need to be developed to improve modal damping and frequency estimates for such well damped modes from measurable model responses.

The wind tunnel testing accomplished in this program opens the door to many tests to be conducted in the future. With the current interest in self adaptive, digital control systems, a flutter mode control system mechanized on a digital mini-computer employing possible redundancy required for the airplane would be a logical high priority program. The system could be configured to suppress flutter over a wide range of weight/altitude conditions, or perhaps a wing store flutter control system adaptable to a wide range of external stores. Eventually such systems will be employed on military aircraft, and wind tunnel testing of the systems will be required to increase confidence in analysis results.

A flutter mode control system using a leading edge control surface, alone or in combination with a trailing edge surface, is another concept that could be evaluated on a wind tunnel model. The FMCS tested on the B-52 model in this study used an inboard wing vertical accelerometer driving an inboard wing surface (flaperon outboard segment) and an outboard wing vertical accelerometer driving an outboard wing surface (outboard aileron), with either system operating alone increasing flutter mode damping over the unaugmented vehicle. It may be possible to develop an FMC system with similar capability using leading edge surfaces with the trailing edge outboard aileron surfaces. A brief study, discussed in Appendix III, was conducted on the model to evaluate a leading edge aileron surface, forward of the outboard aileron, in a system to control the flutter mode. The analysis showed that vertical acceleration from the accelerometer at WBL 925 fed through the CCV aileron system shaping filter to the leading edge surface would increase the flutter mode damping. The surface worked to suppress flutter through controlling wing vertical bending as did the trailing edge surface system. This indicates that a system using the leading and trailing edge surfaces could be developed to provide the same measure of redundancy attained with the outboard aileron/flaperon system tested on the model and CCV airplane.

Other flutter mode control areas that are definite candidates for future model testing are multiple flutter modes and violent flutter. The weight savings achievable with flutter mode control systems are probably dependent on the airplane configuration and on the type of flutter (mode, gradient, severity, etc.). Studies of various types of flutter should be conducted to determine if certain classes of flutter are more practical to control using passive or active flutter suppression techniques. To fully assess the benefits of flutter suppression CCV technology, a new airplane configuration that requires flutter suppression because of minimum structural design needs to be developed and evaluated using active and passive flutter techniques. Models of these configurations could be fabricated with a fully redundant flutter mode control system and tested to demonstrate that predicted savings in weight are realizable.

APPENDIX I

ANALYTICAL FORMULATION OF AEROELASTIC EQUATIONS

Analytical techniques used to formulate airplane and model equations of motion are described in this appendix. The details associated with selecting a suitable model configuration and generating airplane and model aeroelastic equations for evaluating the flutter suppression system are discussed in Section 3 of the text.

1.0 STRUCTURAL IDEALIZATION

Elastic and inertia characteristics of airplane and model structure were represented with a lumped parameter idealization. An isometric sketch of the idealization is shown in Figure 62. Mass properties (mass, static moments, moments of inertia) were lumped at the structural nodes as applicable. Section stiffness properties were defined at the end nodes and center of each elastic axis beam connecting a given pair of nodes. The vibration analysis computer program generates a tapered beam stiffness representation from the specified section stiffness properties.

Symmetric or antisymmetric cantilevered vibration modes were computed for each component using the lumped parameter idealization. Components included a cable mount (simulation of wind tunnel cable support system), forward body, aft body, wing, inboard nacelle, outboard nacelle, horizontal tail, and vertical tail. Stiffness properties for the model cable mount component were generated from installation geometry and estimated cable tension and drag parameters supplied by NASA.

Coupled vibration modes for either the free-free or restrained analyses were determined using a sufficient number of cantilever modes to adequately represent the desired coupled mode frequency content. All flutter analyses and aeroelastic equation formulations were based on the number of modes shown in Table XI.

TABLE XI

NUMBER OF MODES INCLUDED IN FLUTTER ANALYSES

	FREE-FREE		CABLE RESTRAINTS	
	Symmetric	Antisym	Symmetric	Antisym
Center of Gravity or Cable Modes	3	3	2	3
Elastic Modes	27	27	25	24

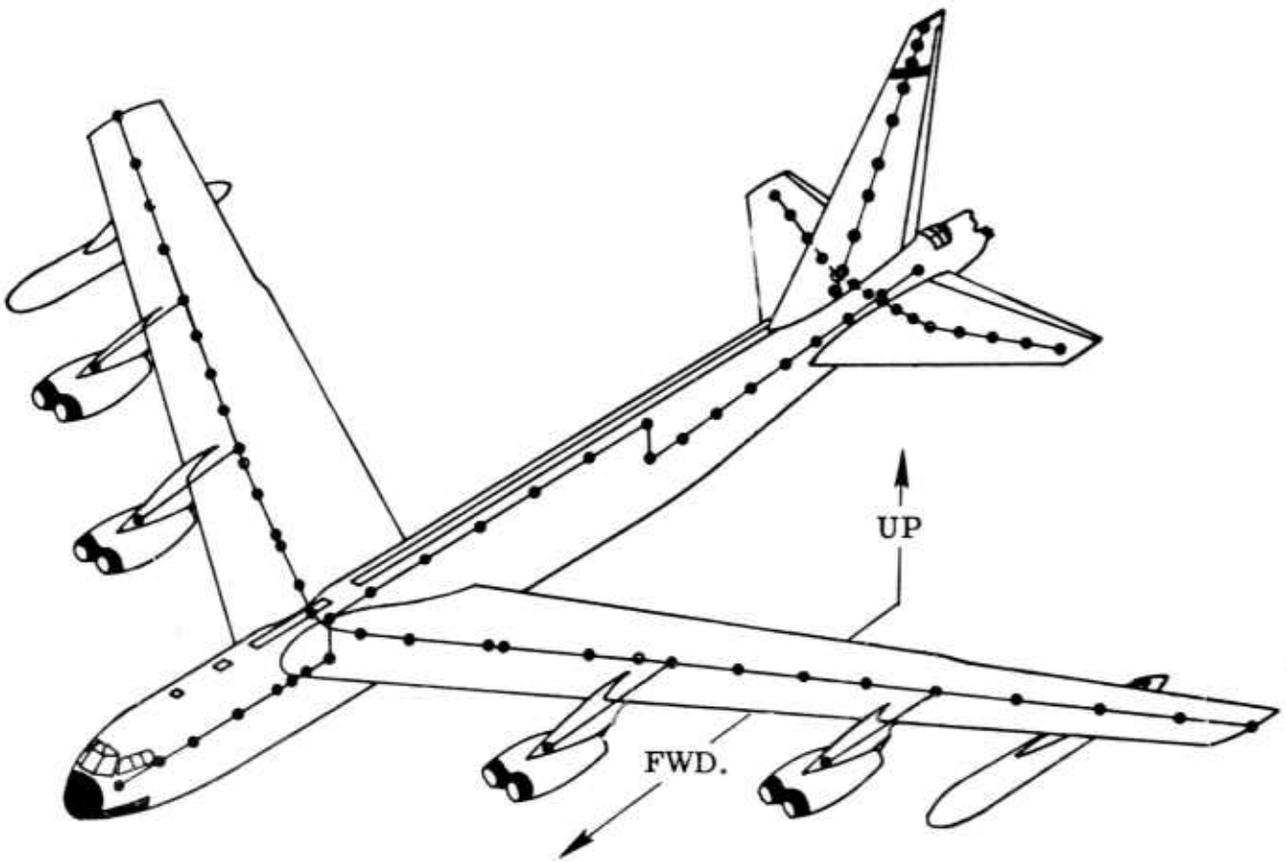

FIGURE 62
B-52 LUMPED PARAMETER STRUCTURAL IDEALIZATION

2.0 AERODYNAMIC LOADING

Airloads were based on a doublet lattice method that included aerodynamic coupling and interference effects between wing, nacelles, fuselage, tail surfaces and control surfaces. Primary surfaces and control surfaces were idealized with a lattice of doublets lying in the plane of the lifting surface. The nacelles were represented with doublets placed in horizontal and vertical planes passing through the centerline of the structural component. The fuselage vertical panels passed through the fuselage centerline and the horizontal panels were in the plane of the wing. The complete aerodynamic patch representation is shown in the isometric sketch of Figure 63. Control surfaces defined for synthesis studies include horizontal canards, CCV vehicle outboard flaperon segment, outboard aileron and elevator. With the exception of the horizontal canards, all control surfaces were represented with aerodynamic patches. A quasi-steady aerodynamic representation (not coupled with the doublet lattice formulation) was included for the horizontal canards.

3.0 EQUATIONS OF MOTION

Flutter analyses were accomplished using complex oscillatory aerodynamic coefficients generated for specific values of the reduced frequency parameter, ω/U_o. However, equations of motion were formulated in terms of real matrices through introduction of an "interpolating" or "approximating" function.

The original equations were the standard form:

$$\left(-(j\omega)^2\,[\text{MASS}] + (j\omega)\,[\text{DAMPING}] + [\text{STIFFNESS}]\right)\left\{q(j\omega)\right\}$$

$$+ \rho U_o^2 \left[A\left(\frac{j\omega}{U_o}\right)\right]\left(\left[C_\theta\right]\left\{q(j\omega)\right\} + \frac{j\omega}{U_o}\left[C_Z\right]\left\{q(j\omega)\right\}\right.$$

$$\left. + \frac{1}{U_o}\left[C_W\right]\left\{\begin{matrix} W_g(j\omega) \\ - \quad - \\ V_g(j\omega) \end{matrix}\right\}\right) = 0$$

where "q" is the generalized coordinate and "A" is an aerodynamic influence matrix which can be evaluated for specific values of ω/U_o. The matrices C_θ, C_Z and C_W prescribe the usual linearized boundary conditions.

If one of the elements of the matrix "A" is plotted, as ω takes on selected values from zero to 40 radians/second, the plot appears as the "X's" in Figure 64.

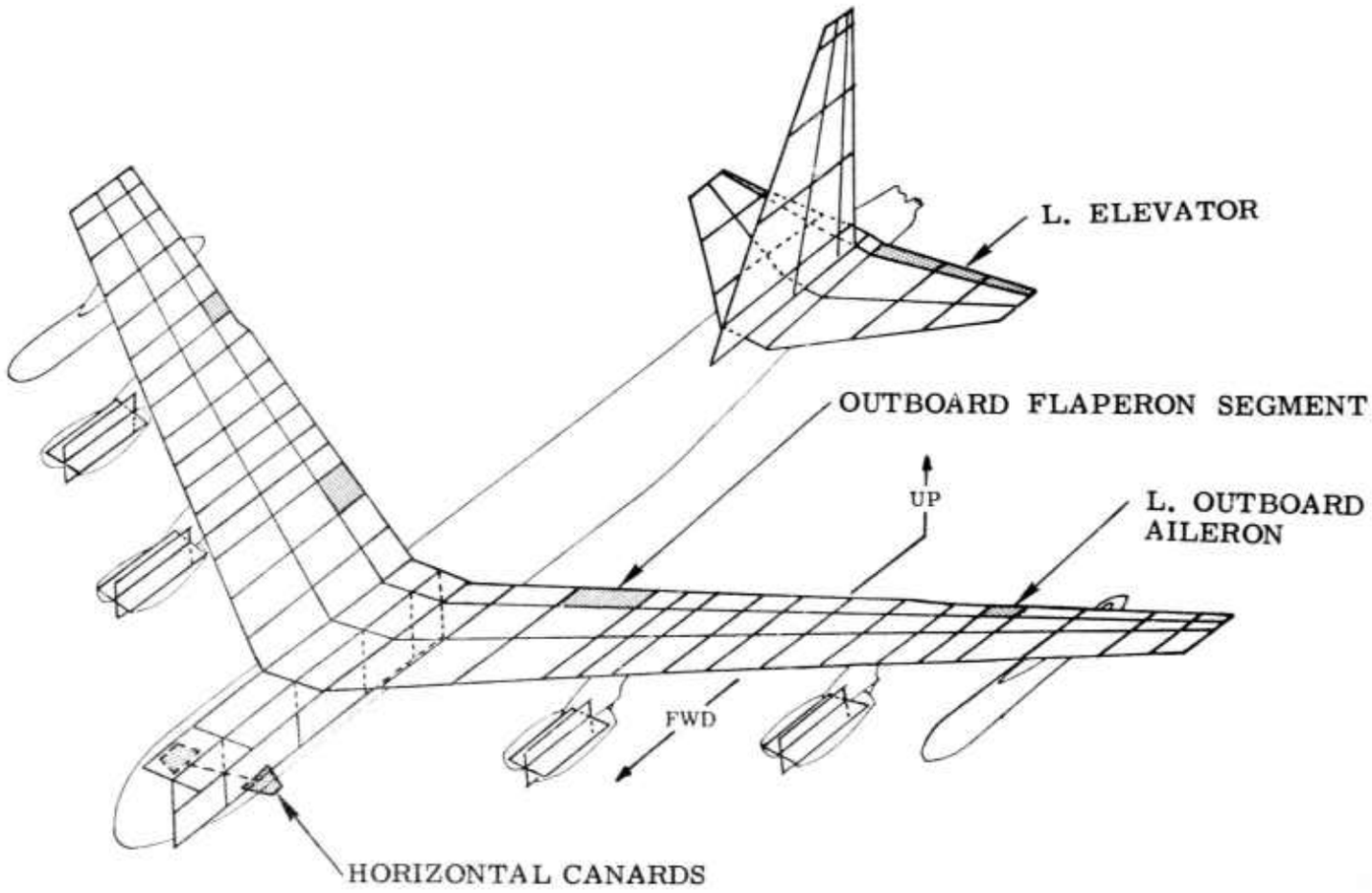

FIGURE 63
B-52 DOUBLET LATTICE AIR FORCE PANELIZATION

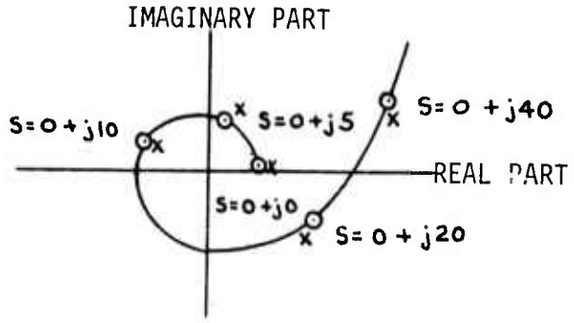

Figure 64. Typical Complex Aerodynamic Coefficient Vs. ω

The solid line of Figure 64 is an approximating function, chosen as a rational polynominal function of the complex variable "S". The "O's" are values of the approximating function at values of "S" for which the "X's" are plotted. The approximating function was chosen to permit accurate approximation of the time delays inherent in the unsteady aerodynamics subject to the following restrictions:

- It must have complex conjugate symmetry
- It must have denominator roots in the left half-plane
- It must approximate the value of the complex coefficient when $S = 0 + j\omega$, for those values of ω analyzed.

The approximating function for each element in the aerodynamic coefficient was determined after analysis at 8 to 12 discrete frequencies. When the approximating functions are substituted in the equations of motion for the complex aerodynamic coefficients, a new set of equations results, whose coefficients are coefficients of the approximating function. After rearrangement, the final form of the equations of motion with variable density "ρ" and velocity "U_o" is:

$$\left(S^2 \left[\text{MASS}\right] + S \left[\text{DAMPING}\right] + \left[\text{STIFFNESS}\right]\right)\left\{\bar{q}(s)\right\}$$

$$+ \left(S^2 \rho \left[C_1\right] + S\rho U_o \left[C_2\right] + \rho U_o{}^2 \left[C_3\right] + \rho U_o{}^2 \sum_{i=1}^{4} \left[D_i\right] \frac{S}{S + U_o d_i}\right)\left\{\bar{q}(s)\right\}$$

$$+ \left(\rho U_o \left[R_o\right] + \rho U_o \sum_{i=1}^{4} \left[R_i\right] \frac{S}{S + U_o \beta_i}\right) \begin{Bmatrix} \bar{w}_g \\ \dot{\bar{w}}_g \end{Bmatrix}(s) = 0$$

where:

items in first line of this equation are structural coefficients;
items in second line are aerodynamic coefficients; and
items in third line are gust force coefficients.

Because of the continuity of the aerodynamic coefficients as ω varies (no finite aerodynamic poles or zeros in the vicinity of the imaginary axis) these equations are good approximations of the Laplace transformed equations. They should not be depended upon for values of S too remote from imaginary axis (greater than 6 radians per second) or above the highest frequency analyzed (greater than 60 radians per second). All analyses (model and airplane) were accomplished in airplane scale; therefore, these frequencies are in airplane scale. Frequency limitation of the model equations would be scaled up appropriately by the frequency scale factor, 5.48. Model equations of motion were subsequently scaled by this factor up to model frequency scale.

APPENDIX II

PHASE II WIND TUNNEL TEST PLAN

1.0 INTRODUCTION

A program entitled "Development of Active Flutter Suppression Wind Tunnel Testing Technology" has been initiated by the Air Force Flight Dynamics Laboratory under Contract No. F33615-72-C-1913. The objectives of this program are to analyze and wind tunnel test the CCV program flutter mode control (FMC) system on the NASA one-thirtieth scale B-52E aeroelastic model.

A model flutter mode control system was analyzed and the necessary model modifications were accomplished. Preliminary (Phase I) wind tunnel tests were conducted in the transonic dynamic wind tunnel at Langley Research Center in June and July 1973. The objectives of the Phase I wind tunnel tests were to establish the model open loop flutter dynamic pressure and to evaluate the FMC system.

Phase I wind tunnel test results indicate that the open loop estimated flutter dynamic pressure is 55 psf, compared to predicted analytical open loop flutter condition of 45.6 psf. Effectiveness of the FMC system was also demonstrated during the Phase I tests.

Phase II wind tunnel tests will be conducted at Langley Research Center beginning in December 1973 to evaluate the FMC system above the open loop flutter dynamic pressure and to conduct FMC parametric variations, as well as to provide data for correlation with CCV program Fuel Configuration 3 flight test results. This plan describes tests to evaluate:

- Flutter characteristics of the unaugmented model and performance of the FMC system
- Effects of FMC system gain and filter cut-off frequency variations
- FMC channel failure effects
- Wind tunnel density variation effects (μ-effects)
- Outboard flaperon hinge moment frequency response
- Model and FMCS response characteristics to gust
- Control surface displacement saturation effects.

The model configuration required for this series of tests is the same as tested during Phase I, but with the elevator system operative to permit its use similar to the planned flight testing.

2.0 TEST SET-UP AND INSTRUMENTATION

2.1 Test Set-Up

The model FMC system block diagram is shown in Figure 65. The FMC system compensation filter and feedback gains will be mechanized on an analog computer located in the tunnel control room. The FMC system aileron loop gain is twice the gain used in the Phase I testing, and the flaperon loop gain is increased by 25 percent. Control surface actuation system position and rate feedback loops will be mechanized on separate operational amplifiers mounted in instrumentation racks if available, or on the analog computer. Umbilical cables will provide electrical signal transmission between the model and equipment located outside the tunnel test section.

Oscillating gust vanes located upstream of the test section will be used to generate sinusoidal vertical gust.

2.2 Instrumentation

Model instrumentation will provide the following data:

a. Vertical acceleration at Wing Buttock Line 925 (left and right wing)

b. Vertical acceleration at Wing Buttock Line 565 (left and right wing)

c. Outboard aileron actuator position

d. Left wing flaperon actuator position

e. Right wing flaperon actuator position

f. Outboard aileron actuator rate

g. Left wing flaperon actuator rate

h. Right wing flaperon actuator rate

i. Right wing root vertical bending moment

j. Right wing root torsion moment

k. Right wing outboard flaperon hinge moments

3.0 TEST CONDITIONS

Model subcritical test conditions have been selected which are compatible with the additional heavy weight airplane flutter tests in the CCV program. The airplane and model test parameters which will be constant during testing are presented below.

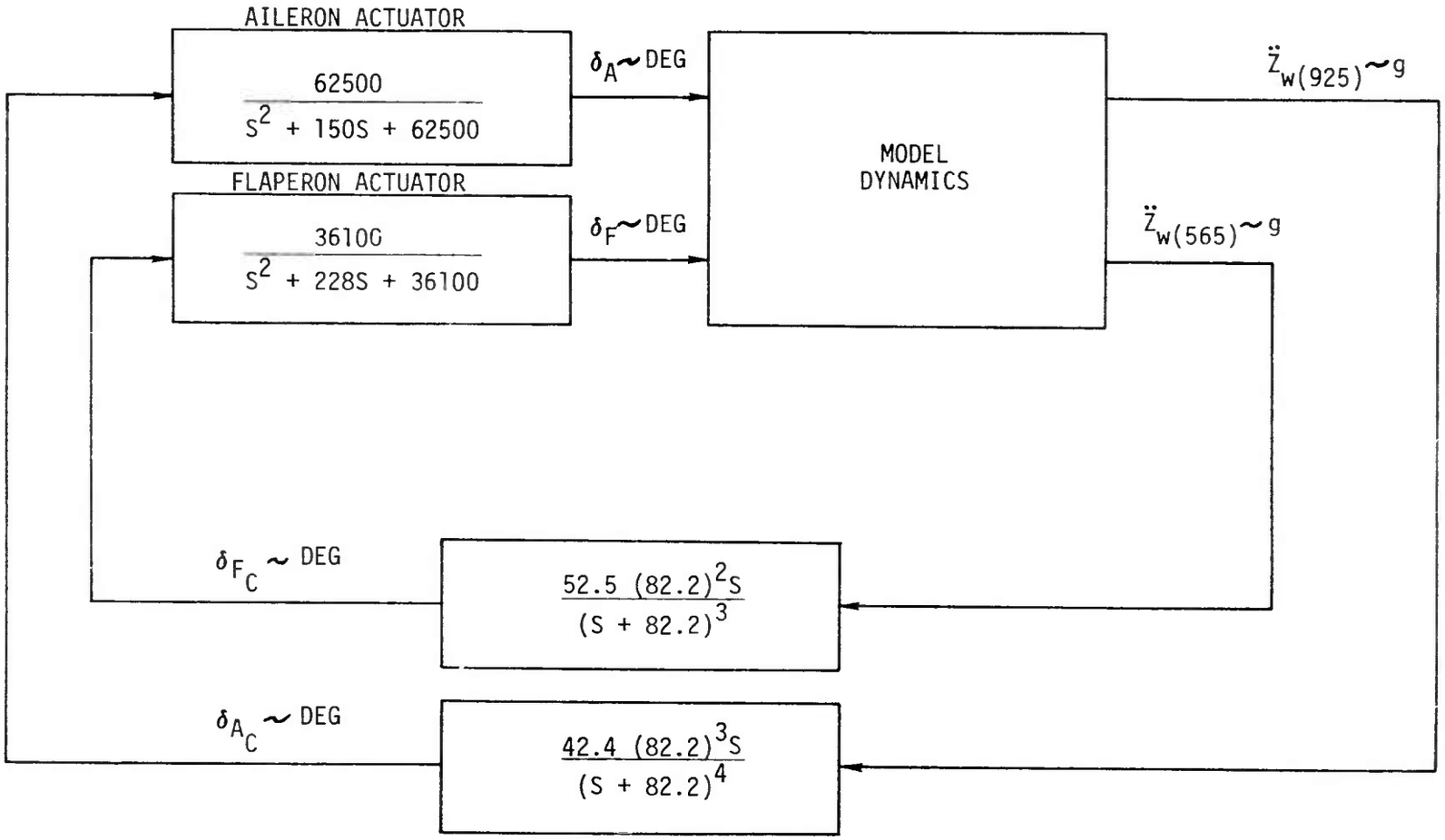

Figure 65. B-52 Aeroelastic Model Flutter Mode Control System

Parameter	Units	Airplane	Model
Altitude	Ft.	21,000	--
Weight	Lbs.	345,000 - 375,000	56.59
Density	Slugs/Ft^3	.0012249	.00499
Flight Environment	--	Air	95% Freon -12

However, the altitude and density parameters will be changed as shown below for the μ effects study.

Parameter	Units	Airplane	Model
Altitude	Ft.	5,400	--
Density	Slugs/Ft^3	.002024	.0080

From the Phase I wind tunnel test data, the model open loop flutter condition was estimated at 55 psf. Therefore, subcritical test conditions ranging from 27.75 to 52.5 psf have been selected for open and closed loop testing. Tests above 52.5 psf will be conducted only with the FMC system on.

4.0 WIND TUNNEL TESTS

This section describes the significant wind tunnel tests required to meet program objectives listed in Section 1.0. The wind tunnel test conditions are selected considering:

a. heavy gross weight (Fuel Configuration 3) airplane flight test condition, and

b. basic model flutter condition of 55 psf estimated from Phase I wind tunnel test results.

A summary of Phase II wind tunnel tests is given in Table XII, which also shows the equivalent airplane flight test condition for comparison. The standard atmosphere is assumed for the airplane conditions, with speed of sound 1032.8 ft/sec at 21,000 feet and 1095.5 ft/sec at 5400 feet. The model conditions assume 530°R tunnel temperature with 95% freon, 5% air in the tunnel. For these conditions, the speed of sound at .00499 slug/ft^3 is 502.9 ft/sec and for .0080 slug/ft^3, it is 500.7 ft/sec.

4.1 Model Excitation

The elevators and outboard ailerons will be the primary control surfaces for exciting the model. The outboard flaperons will be used to obtain the control surface hinge moment data and frequency response data will be obtained using the horizontal canards. Electrical command signals will be generated on the analog computer or an external function generator. The following three types of control surface command signals will excite the model:

TABLE XII: PHASE II WIND TUNNEL TEST SUMMARY

TEST NO.	EXCITATION	TYPE OF INPUT	WIND TUNNEL TEST CONDITION			EQUIVALENT A/P FLIGHT TEST CONDITION			SYSTEM	REMARKS
			DYN. PRESS PSF	KTAS	MACH	KCAS	KTAS	MACH		
1.	Elevator	Pulse	37.91	73.0	.245	295.0	399.9	.654	• FMCS Off • FMCS On	• Tunnel density .00499 Slug/Ft^3 • Equivalent A/P Condition 21,000 Ft.
			45.00	79.5	.267	323.5	435.7	.713		
			50.00	83.8	.282	342.0	459.4	.751		
			52.50	85.9	.289	351.0	470.8	.770		
			55.00	87.9	.295	260.0	481.8	.788	• FMCS on only	
			57.50	89.9	.302	368.2	492.5	.805		
			60.00	91.8	.308	377.0	503.2	.823		
2.	Outboard Aileron Outboard Flaperon Segment Horizontal Canard	4 - 24 Hz Frequency Sweep	27.59	62.3	.209	250.0	341.2	.558	• FMCS Off • FMCS On • FMCS Variations at Q = 37.91, 45, 50, 52.5 psf	• Flaperon Tests with FMCS Off only at Q = 27.59, 35, 37.91, 45, 50 psf • Canard tests at Q = 37.91, 45, 52.5 psf • Tunnel Density .00499 Slug/Ft^3 • Equivalent A/P Condition 21,000 Ft.
			35.0	70.1	.235	283.0	384.2	.628		
			37.91	73.0	.245	295.0	399.9	.654		
			45.00	79.5	.267	323.5	435.7	.713		
			50.00	83.8	.282	342.0	459.4	.751		
			52.50	85.9	.289	351.0	470.8	.770		
			55.00	87.9	.295	360.0	481.8	.788	• FMCS On only	
			57.50	89.9	.302	368.2	492.5	.805		
			60.00	91.8	.308	377.0	503.2	.823		
3.	Outboard Aileron Outboard Flaperon Segment	Dwell at Resonant Frequencies	27.59	62.3	.209	250.0	341.2	.558	• FMCS Off • FMCS On	• Tunnel Density .00499 Slug/Ft^3 • Equivalent A/P Condition 21,000 Ft. • Flaperon Tests with FMCS Off only
			35.00	70.1	.235	283.0	384.2	.628		
			37.91	73.0	.245	295.0	399.9	.654		
			45.00	79.5	.267	323.5	435.7	.713		
			50.00	83.8	.282	342.0	459.4	.751		

TABLE XII: PHASE II WIND TUNNEL TEST SUMMARY

TEST NO.	EXCITATION	TYPE OF INPUT	WIND TUNNEL TEST CONDITION			EQUIVALENT A/P FLIGHT TEST CONDITION			SYSTEM	REMARKS
			DYN. PRESS PSF	KTAS	MACH	KCAS	KTAS	MACH		
4.	Outboard Aileron	4 - 24 Hz Frequency Sweep	34.71	55.2	.186	280.0	302.3	.466	• FMCS Off • FMCS On	• Tunnel Density .0080 Slug/Ft^3 • Equivalent A/P Condition 5,400 Ft.
			48.00	64.9	.219	330.0	355.4	.548		
			54.89	69.4	.234	353.0	380.1	.586		
			63.75	74.7	.252	381.0	409.6	.632		
			70.00	78.3	.264	399.5	429.2	.662		
5.	Gust Vanes	2 - 16 Hz Frequency Sweep	37.91	73.0	.245	295.0	399.9	.654	• FMCS Off • FMCS On	• Tunnel Density .00499 Slug/Ft^3 • Equivalent A/P Condition 21,000 Ft.
			45.00	79.5	.267	323.5	435.7	.713		
			50.00	83.8	.282	342.0	459.4	.751		
			52.50	85.9	.289	351.0	470.8	.770	• FMCS On only	

Pulse Input: The pulse will be one cycle sine wave at the flutter mode frequency.

Frequency Sweep Input: A 4 - 24 Hz frequency sweep signal of constant command amplitude will be used with a sweep time of 8 minutes using a logarithmic frequency increment.

Sinusoidal Input: This signal will be obtained by dwelling the sweep oscillator at significant structural mode frequencies.

In addition to the above control surface inputs, the model will also be excited by sinusoidal gusts generated by gust vanes. The sinusoidal gust frequencies will be swept linearily from 2 to 16 Hz. Maximum gust amplitudes are frequency dependent and are limited by the gust vane capability.

Amplitudes of the control surface and gust inputs will be selected to ensure that the model structural load limits are not exceeded and that proper signal to noise ratios are maintained throughout the frequency range. Wing loads will be closely monitored during the high density testing to prevent damage to the model.

4.2 Test Procedure

In general, the test procedure will follow the schedule of tests presented in Table XIII. Deviations from this schedule may occur during the testing at the discretion of the NASA test director. The FMC system gain and filter time constant variations, and changes in system displacement command limits, will require placing the analog computer in the "POT SET" mode. If the control surface actuation system feedback loops are mechanized on the computer, the surfaces will "float" while the computer is in the "POT SET" mode. This can be accomplished without difficulty with the tunnel running.

The following paragraphs describe tests to be conducted with different excitations and significant data to be acquired. Detailed tests for all inputs are defined in Table XIII.

4.2.1 Pulse Input

A pulse input to the elevators will be used to measure damping and frequency of the most lightly damped mode. The pulse will be a one cycle sine wave at the flutter mode frequency. Figure 66 shows a typical input and a typical time history of vertical acceleration at the wing tip ($\ddot{Z}_{925}$). The response shown assumes negligible tunnel turbulence effects. The Phase I testing showed the tunnel turbulence affected transient responses significantly.

The one cycle sine wave pulse inputs will be used with the FMCS off and on at the conditions defined by Test No. 1 in Table XII. The nominal FMCS gains are the same as the revised nominal gains of the heavy gross weight CCV airplane system. Thus, the nominal system will provide direct correlation with the airplane flight test. The nominal system gains and filter cut-off frequencies are shown in the block diagram of Figure 65.

TABLE XIII: PHASE II WIND TUNNEL TEST PROCEDURE

TEST NO.	TEST PARAMETERS: DYNAMIC PRESS.- PSF	TEST PARAMETERS: V_T FT/SEC	TEST PARAMETERS: MACH NO.	CONTROL SURFACE INPUT: SURFACE	CONTROL SURFACE INPUT: PULSE	CONTROL SURFACE INPUT: FREQ. SWEEP	CONTROL SURFACE INPUT: FREQ. DWELL	FLUTTER MODE CONTROL SYSTEM (FMCS): SYS. ON	FLUTTER MODE CONTROL SYSTEM (FMCS): SYS. OFF	FLUTTER MODE CONTROL SYSTEM (FMCS): AILERON LOOP GAIN	FLUTTER MODE CONTROL SYSTEM (FMCS): FLAPERON LOOP GAIN	FLUTTER MODE CONTROL SYSTEM (FMCS): FILTER CUTOFF FREQ. RAD/SEC	TYPE OF OUTPUT DATA: TIME HISTORY	TYPE OF OUTPUT DATA: FREQ. RESPONSE	NOTES
2.	27.59	105.2	.209	Aileron		X			X					X	• Tunnel density $= .00499$ Slug/Ft^3
↕	27.59	105.2	.209	↕		↕		X		NOM	NOM	NOM		X	
	35.00	118.4	.235						X					X	
	35.00	118.4	.235					X		NOM	NOM	NOM		X	• Nominal FMCS:
	37.91	123.3	.245						X					X	$K_A = 42.4$ Deg/g
	37.91	123.3	.245					X		NOM	NOM	NOM		X	$K_F = 52.5$ Deg/g
	45.00	134.3	.267						X					X	$\omega_c = 82.2$ Rad/Sec
	45.00	134.3	.267					X		NOM	NOM	NOM		X	
	50.00	141.6	.282						X					X	
	50.00	141.6	.282					X		NOM	NOM	NOM		X	
	52.50	145.1	.289						X					X	
↕	52.50	145.1	.289	↕		↕		X		NOM	NOM	NOM		X	
2.	55.00	148.5	.295	Aileron		X		X		↕	↕	↕		X	
1.	55.00	148.5	.295	Elevator	X			X					X		
2.	57.50	151.8	.302	Aileron		X		X						X	
1.	57.50	151.8	.302	Elevator	X			X					X		
2.	60.00	155.1	.308	Aileron		X		X						X	
1.	60.00	155.1	.308	Elevator	X			X		NOM	NOM	NOM	X		
3.	27.59	105.2	.209	Aileron			X		X				X		• Tunnel density $= .00499$ Slug/Ft^3
3.	↕	↕	↕	Aileron			X	X		NOM	NOM	NOM	X		
2.				Flaperon		X			X					X	} Hinge moments
3.	27.59	105.2	.209	Flaperon			X		X				X		
3.	35.00	118.4	.235	Aileron			X		X				X		• Tunnel density $= .00499$ Slug/Ft^3
3.	↕	↕	↕	Aileron			X	X		NOM	NOM	NOM	X		
2.				Flaperon		X			X					X	} Hinge moments
3.	35.00	118.4	.235	Flaperon			X		X				X		

TABLE XIII: PHASE II WIND TUNNEL TEST PROCEDURE

TEST NO.	TEST PARAMETERS: DYNAMIC PRESS.-PSF	TEST PARAMETERS: V_T FT/SEC	TEST PARAMETERS: MACH NO.	CONTROL SURFACE INPUT: SURFACE	CONTROL SURFACE INPUT: PULSE	CONTROL SURFACE INPUT: FREQ. SWEEP	CONTROL SURFACE INPUT: FREQ. DWELL	FMCS: SYS. ON	FMCS: SYS. OFF	FMCS: AILERON LOOP GAIN	FMCS: FLAPERON LOOP GAIN	FMCS: FILTER CUTOFF FREQ. RAD/SEC	TYPE OF OUTPUT DATA: TIME HISTORY	TYPE OF OUTPUT DATA: FREQ. RESPONSE	NOTES
1.	37.91	123.3	.245	Elevator	X				X				X		● Tunnel density .00499 Slug/Ft^3
1.				Elevator	X			X		NOM	NOM	NOM	X		
3.				Aileron			X		X				X		
3.				Aileron			X	X		NOM	NOM	NOM	X		
2.				Flaperon		X			X					X	} Hinge moments
3.				Flaperon			X		X				X		
2.				Canard		X			X					X	
2.				Canard		X		X		NOM	NOM	NOM		X	
2.				Aileron		X		X		NOM	0	NOM		X	
2.						X		X		0	NOM	NOM		X	
2.						X		X		21.2	0	NOM		X	
2,						X		X		0	42.0	NOM		X	
2.						X		X		21.2	42.0	NOM		X	
2.						X		X		63.6	126.0	NOM		X	
2.						X		X		NOM	NOM	61.65		X	
2						X		X		NOM	NOM	102.75		X	
2	37.91	123.3	.245	Aileron		X		X		NOM	NOM	NOM		X	Saturation effects

TABLE XIII: PHASE II WIND TUNNEL TEST PROCEDURE

TEST NO.	TEST PARAMETERS: DYNAMIC PRESS.- PSF	TEST PARAMETERS: V_T FT/SEC	TEST PARAMETERS: MACH NO.	CONTROL SURFACE INPUT: SURFACE	CONTROL SURFACE INPUT: PULSE	CONTROL SURFACE INPUT: FREQ. SWEEP	CONTROL SURFACE INPUT: FREQ. DWELL	FLUTTER MODE CONTROL SYSTEM (FMCS): SYS. ON	FLUTTER MODE CONTROL SYSTEM (FMCS): SYS. OFF	FLUTTER MODE CONTROL SYSTEM (FMCS): AILERON LOOP GAIN	FLUTTER MODE CONTROL SYSTEM (FMCS): FLAPERON LOOP GAIN	FLUTTER MODE CONTROL SYSTEM (FMCS): FILTER CUTOFF FREQ. RAD/SEC	TYPE OF OUTPUT DATA: TIME HISTORY	TYPE OF OUTPUT DATA: FREQ. RESPONSE	NOTES
1.	45.00	134.3	.267	Elevator	X				X				X		• Tunnel density $= .00499$ Slug/Ft^3
1.	↕	↕	↕	Elevator	X			X		NOM	NOM	NOM	X		
3.				Aileron			X		X				X		
3.				Aileron			X	X		NOM	NOM	NOM	X		
2.				Flaperon		X			X					X	} Hinge moments
3.				Flaperon			X		X				X		
2.				Canard		X			X					X	
2.				Canard		X		X		NOM	NOM	NOM		X	
2.				Aileron		X		X		NOM	0	NOM		X	
2.				↕		X		X		0	NOM	NOM		X	
2.						X		X		21.2	0	NOM		X	
2.						X		X		0	42.0	NOM		X	
2.						X		X		21.2	42.0	NOM		X	
2.						X		X		63.6	126.0	NOM		X	
2.						X		X		NOM	NOM	61.65		X	
2.	45.00	134.3	.267	Aileron		X		X		NOM	NOM	102.75		X	
												NOM		X	Saturation effects
1.	50.00	141.6	.282	Elevator	X				X				X		• Tunnel density $= .00499$ Slug/Ft^3
1	↕	↕	↕	Elevator	X			X		NOM	NOM	NOM	X		
3.				Aileron			X		X				X		
3.				Aileron			X	X		NOM	NOM	NOM	X		
2.				Flaperon		X			X					X	} Hinge moments
3.				Flaperon			X		X				X		
2				Aileron		X		X		NOM	0	NOM		X	
2.	50.0	141.6	.282	Aileron		X		X		0	NOM	NOM		X	

TABLE XIII: PHASE II WIND TUNNEL TEST PROCEDURE

TEST NO.	TEST PARAMETERS: DYNAMIC PRESS.- PSF	TEST PARAMETERS: V_T FT/SEC	TEST PARAMETERS: MACH NO.	CONTROL SURFACE INPUT: SURFACE	CONTROL SURFACE INPUT: PULSE	CONTROL SURFACE INPUT: FREQ. SWEEP	CONTROL SURFACE INPUT: FREQ. DWELL	FLUTTER MODE CONTROL SYSTEM (FMCS): SYS. ON	FLUTTER MODE CONTROL SYSTEM (FMCS): SYS. OFF	FLUTTER MODE CONTROL SYSTEM (FMCS): AILERON LOOP GAIN	FLUTTER MODE CONTROL SYSTEM (FMCS): FLAPERON LOOP GAIN	FLUTTER MODE CONTROL SYSTEM (FMCS): FILTER CUTOFF FREQ. RAD/SEC	TYPE OF OUTPUT DATA: TIME HISTORY	TYPE OF OUTPUT DATA: FREQ. RESPONSE	NOTES
2.	50.00	141.6	.282	Aileron		X		X		21.2	0	NOM		X	• Tunnel density $.00499\ Slug/Ft^3$
2	↕	↕	↕	↕		X		X		0	42.0	NOM		X	
2.						X		X		21.2	42.0	NOM		X	
2.						X		X		63.6	126.0	NOM		X	
2.						X		X		NOM	NOM	61.65		X	
2.						X		X		NOM	NOM	102.75		X	
2.	50.00	141.6	.282	Aileron		X		X		NOM	NOM	NOM		X	Saturation effects
1.	52.50	145.1	.289	Elevator	X				X				X		• Tunnel density $.00499\ Slug/Ft^3$
1.	↕	↕	↕	Elevator	X			X		NOM	NOM	NOM	X		
2.				Canard		X			X					X	
2.				Canard		X		X		NOM	NOM	NOM		X	
2.				Aileron		X		X		NOM	0	NOM		X	
2.				↕		X		X		0	NOM	NOM		X	
2.						X		X		21.2	0	NOM		X	
2.						X		X		0	42.0	NOM		X	
2.						X		X		21.2	42.0	NOM		X	
2.						X		X		63.6	126.0	NOM		X	
2.						X		X		NOM	NOM	61.65		X	
2.						X		X		NOM	NOM	102.75		X	
2.	52.50	145.1	.289	Aileron		X		X		NOM	NOM	NOM		X	Saturation effects

TABLE XIII: PHASE II WIND TUNNEL TEST PROCEDURE

TEST NO.	TEST PARAMETERS			CONTROL SURFACE INPUT				FLUTTER MODE CONTROL SYSTEM (FMCS)					TYPE OF OUTPUT DATA		NOTES
	DYNAMIC PRESS.- PSF	V_T FT/SEC	MACH NO.	SURFACE	PULSE	FREQ. SWEEP	FREQ. DWELL	SYS. ON	SYS. OFF	AILERON LOOP GAIN	FLAPERON LOOP GAIN	FILTER CUTOFF FREQ. RAD/SEC	TIME HISTORY	FREQ. RESPONSE	
4.	34.71	93.2	.186	Aileron		X			X					X	• Tunnel density .0080 Slug/Ft^3
↑	34.71	93.2	.186	↑		↑		X		NOM	NOM	NOM		X	
↕	48.00	109.5	.219	↕		↕			X					X	
↕	48.00	109.5	.219	↕		↕		X		NOM	NOM	NOM		X	• μ Effect tests
↕	54.89	117.1	.234	↕		↕			X					X	
↕	54.89	117.1	.234	↕		↕		X		NOM	NOM	NOM		X	
↕	63.75	126.2	.252	↕		↕			X					X	
↕	63.75	126.2	.252	↕		↕		X		NOM	NOM	NOM		X	
↓	70.00	132.3	.264	↓		↓			X					X	
4.	70.00	132.3	.264	Aileron		X		X		NOM	NOM	NOM		X	
5.	37.91	123.3	.245	None					X					X	• Tunnel density .00499 Slug/Ft^3
↑	37.91	123.3	.245	↑		↑		X		NOM	NOM	NOM		X	
↕	45.00	134.3	.267	↕		↕			X					X	• Gust response test
↕	45.00	134.3	.267	↕		↕		X		NOM	NOM	NOM		X	• 6 and 12 Deg vane amplitudes
↕	50.00	141.6	.282	↕		↕			X					X	
↓	50.00	141.6	.282	↓		↓		X		NOM	NOM	NOM		X	
5.	52.5	145.1	.289	None				X		NOM	NOM	NOM		X	

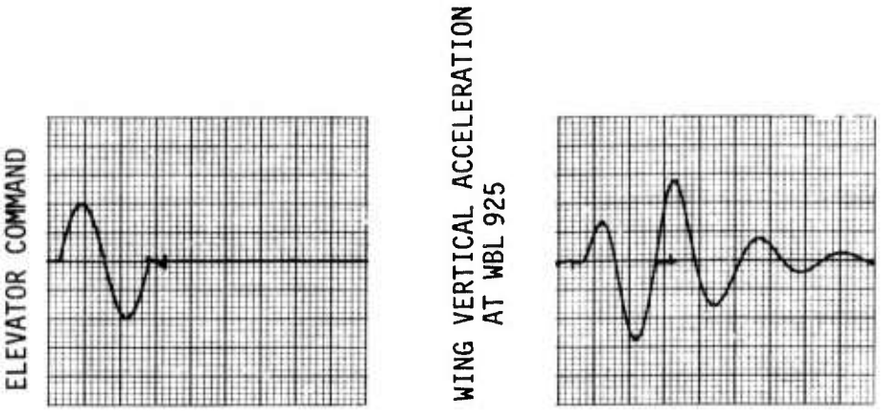

(a) Pulse Input (b) Wing Tip Vertical Acceleration

FIGURE 66. TYPICAL PULSE INPUT AND RESPONSE

The Randomdec equipment will be used in data reduction to enhance the pulse response data. The responses obtained during the Phase I testing due to aileron commands did not show a clean decay. The Randomdec equipment did enhance the responses by averaging out the random components due to the tunnel turbulence.

Pulse response data will be obtained at the following test conditions:

1) FMCS off and FMCS on

   Q = 37.91, 45.00, 50.00, and 52.50 psf

2) FMCS on only

   Q = 55.00, 57.50, and 60.00 psf.

4.2.2 Frequency Response Tests

Continuous frequency response tests will be conducted using the 4 - 24 Hz frequency sweep signals to the control surfaces.

4.2.2.1 Outboard Aileron Commands

Frequency responses due to outboard ailerons will be used primarily to determine frequency and damping of the significant modes. Vertical acceleration responses at WBL925 and WBL565 will be recorded. Reduced data will be presented in magnitude and phase and colinear and quadrature amplitudes versus frequency plots.

Outboard aileron frequency sweeps will be conducted with the FMCS off and on with the nominal FMC system and with FMCS gain and filter cut-off frequency variations, as defined by Test No. 2 in Table XII. The aileron

frequency sweeps will also be used for the μ-effects testing, Test No. 4 in Table XII.

Outboard aileron frequency responses will be conducted at the following test conditions:

1) FMCS off and FMCS on

   Q = 27.59, 35.00, 37.91, 45.00, 50.00, and 52.5 psf

2) FMCS Variations

   Q = 37.91, 45.00, 50.00, and 52.5 psf

3) FMCS on only

   Q = 55.00, 57.5 and 60.00 psf

4) μ- Effects Evaluation

   Q = 34.71, 48.00, 54.89, 63.75, and 70.00 psf

4.2.2.2 Outboard Flaperon Responses

These tests will be conducted to obtain outboard flaperon hinge moment frequency responses. Strain gages mounted on the surface shaft will be calibrated for hinge moments (in-oz). Data will be reduced to give frequency response and co-quad plots of hinge moments versus frequency.

These tests will be conducted at Q = 27.59, 35.00, 37.91, 45.00, and 50.00 psf with FMCS off only.

4.2.2.3 Horizontal Canards

$\ddot{Z}_{565}$ and $\ddot{Z}_{925}$ frequency responses to the horizontal canards are required for data correlation with airplane flight test data. These tests will be conducted at Q = 37.91, 45.00, and 52.5 psf with FMCS off and on.

4.2.3 Sinusoidal Dwell and Clamp Surface Inputs

Significant model frequencies will be estimated from analytical data and frequency response test results. A sinusoidal command at constant amplitude will be applied to the control surface until the model response reaches steady state. Then, the command will be removed as it passes through zero.

4.2.3.1 Outboard Ailerons

Sinusoidal excitation to the outboard aileron will be removed abruptly to provide a response decay envelope from which the damping ratio of the flutter mode can be estimated. Figure 67 shows a typical decay envelope, assuming negligible tunnel turbulence effects on the response and mode frequencies widely separated.

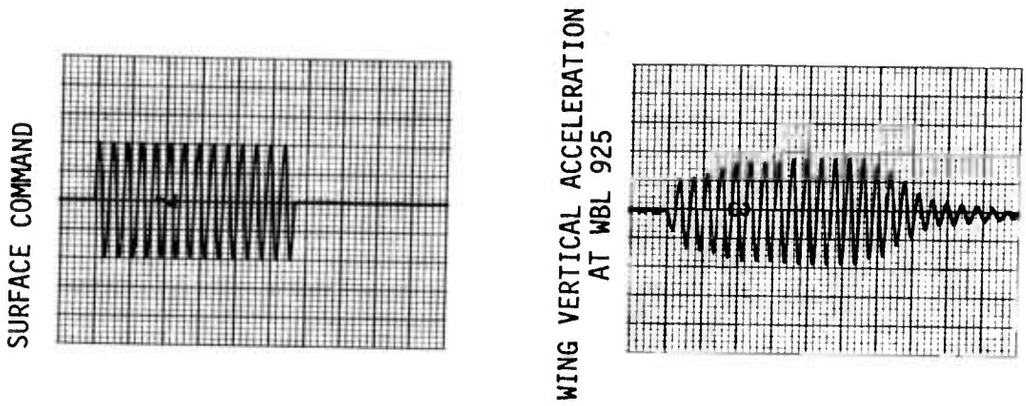

FIGURE 67. TYPICAL DECAY ENVELOPES

These tests will be conducted with FMCS off and on at Q = 27.59, 35.00, 37.91, 45.00, and 50.00 psf test conditions.

4.2.3.2 Outboard Flaperons

Surface hinge moments will be recorded for sinusoidal outboard flaperon excitation at resonant and antiresonant frequencies. These tests will be conducted with FMCS off at Q = 27.59, 35.00, 37.91, 45.00, and 50.00 psf test conditions.

4.2.4 Sinusoidal Gust Excitation

These tests will be conducted with slow frequency sweeps from 2 - 16 Hz on the gust vanes. Gust vane amplitudes will be set to provide good model response without endangering the model. Data from these tests will be recorded in co-quad form. Test conditions are at Q = 37.91, 45.00, 50.00, and 52.5 psf.

4.3 FMC System Variations and μ-Effects Evaluation

Tests will be conducted to determine effects of gain and filter cut-off frequency variations and system saturation on the FMC system performance. Performance of the FMC system will also be evaluated at higher test fluid density.

4.3.1 FMC System Variations

These tests will be conducted with gain and filter cut-off frequency variations from the nominal system made on the analog computer mechanization of the system. The variations are:

1) Outboard aileron loop only

   a. Nominal gain (K_A)

b. 0.5 nominal gain (0.5 K_A)

2) Outboard flaperon loop only

a. Nominal gain (K_F)

b. 0.8 nominal gain (0.8 K_F)

3) Aileron and flaperon loops

a. 0.5 aileron loop nominal gain and 0.8 flaperon loop nominal gain (0.5 K_A and 0.8 K_F)

b. 1.5 K_A and 2.4 K_F

c. 0.75 x nominal filter cut-off frequency

d. 1.25 x nominal filter cut-off frequency

The FMCS variations will also include control surface saturation effects on system performance. Only surface displacement saturation will be implemented because a practical method for mechanizing surface rate limits is not available. The displacement saturation will be mechanized by applying limits to the FMCS surface commands on the analog computer. Nominal FMCS gain and filter cut-off frequencies will be used for these tests. FMCS command limits will be set at approximately 75 percent lower than the surface displacement required for normal FMCS operation.

4.3.2 μ-Effects Evaluation

Wind tunnel density will be changed to .0080 slug/ft^3, which is equivalent to .002024 slug/ft^3 at 5400 feet altitude for the airplane flight test. Frequency responses will be used to determine critical mode damping ratio and frequency. These tests will be conducted at the following test conditions:

FMCS off and on: Q = 34.71, 48.00, 54.89, 63.75, and 70.00 psf.

Wing loads will be closely monitored for these tests, especially at high dynamic pressures.

5.0 DATA REDUCTION

Available test data will also include flutter mode control feedback signals and command signals on the analog computer in addition to the model instrumentation data listed in Section 2.0.

Data will be recorded on magnetic tape for future off-line data reduction. On-line frequency response data analyses accomplished by NASA will provide preliminary test evaluation results. In addition, strip chart recorders will provide real time data to assist in preliminary qualitative test evaluations and in early identification of possible model instabilities or problems.

APPENDIX III

LEADING EDGE SURFACE FMCS FEASIBILITY STUDY

A brief study was conducted after the wind tunnel tests were completed to investigate the feasibility of using leading edge control surfaces in an active flutter mode control system on the B-52 model. Model equations of motion were revised for this study to include wing leading edge control surfaces of the same size as the outboard aileron and located streamwise directly forward of the outboard ailerons. The model equations were written in airplane scale, and all analyses were conducted in airplane scale.

The study was conducted at one condition, 331 psf dynamic pressure (45 psf in model scale) at 21,000 feet altitude. At this condition, the sixth elastic mode was marginally stable with a damping ratio of only .00298.

A root locus analysis was conducted using wing vertical accelerations at WBL 720, WBL 822 and WBL 925 individually with the leading edge surface. The model outboard aileron actuation system transfer function was used to represent the leading edge surface actuation system dynamic behavior. The root locus analysis was conducted using the CCV FMCS outboard aileron loop shaping filter, with sign reversed to produce negative feedback. Figure 68 shows the root locus obtained using vertical acceleration at WBL 925. Damping of the flutter mode (sixth elastic mode) is increased to .0120 with the shaping filter used with feedback gain of 84.8 deg/g. A shaping filter developed specifically for the leading edge surface and vertical acceleration at WBL 925 would provide even greater increase in the flutter mode damping.

Results of this brief study show that an FMC system using a wing leading edge control surface is feasible. Additional effort would be required to develop a practical system, using the leading edge surface alone or in conjunction with a wing trailing edge surface such as the CCV outboard aileron.

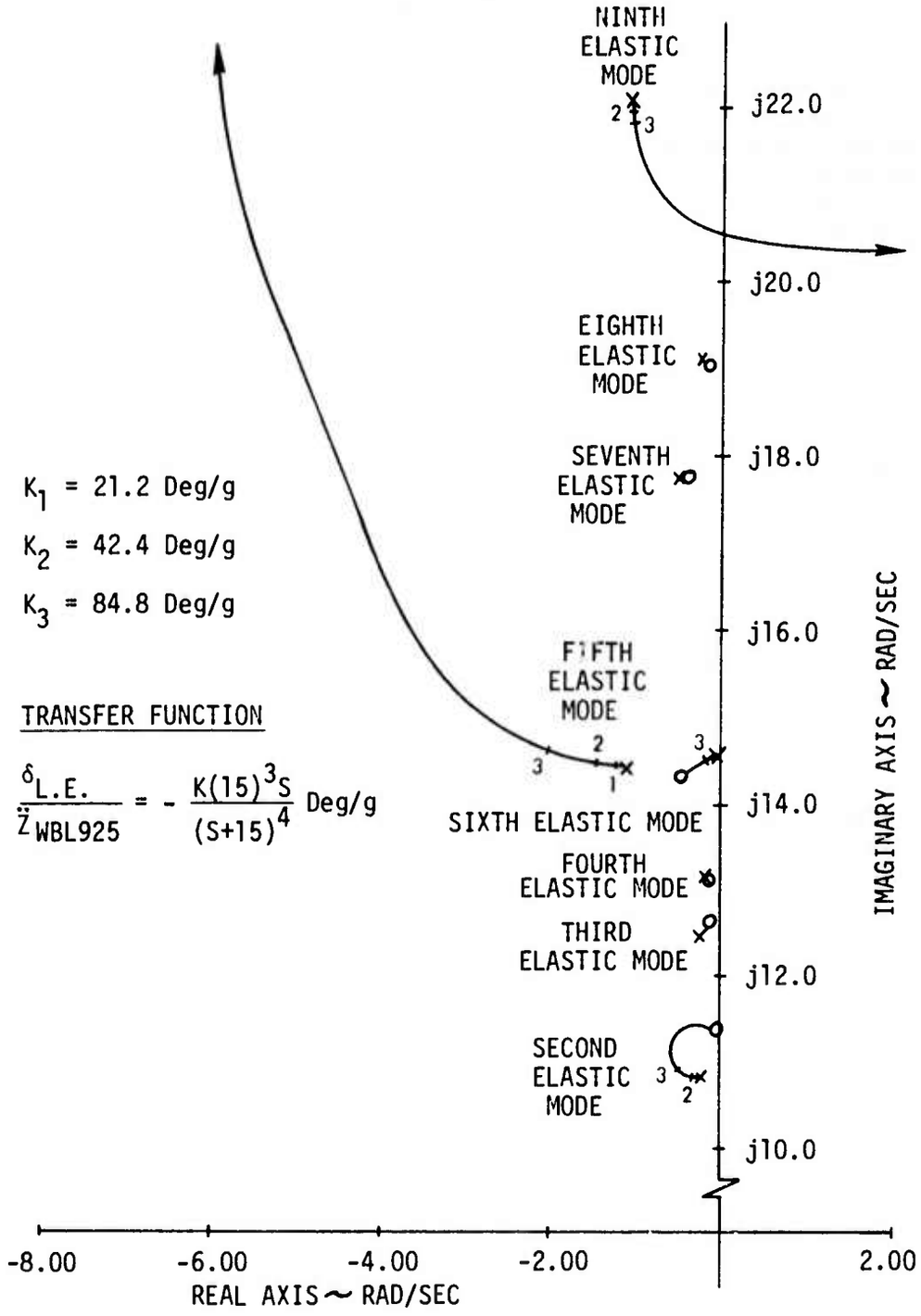

Figure 68. Leading Edge Surface FMCS Root Locus

REFERENCES

1. "B-52 Control Configured Vehicles Program Summary," AFFDL-TR-74-92, Vol. I, Air Force Flight Dynamics Laboratory, Wright-Patterson AFB, Ohio, (to be published).

2. "B-52 CCV Control System Synthesis," AFFDL-TR-74-92, Vol. II, Air Force Flight Dynamics Laboratory, Wright Patterson AFB, Ohio, (to be published).

3. "Design Control Specification for a One-Thirtieth Scale B-52E Flexible Model," Boeing Document D3-7387-1, June 15, 1967.

4. "Development of Active Flutter Suppression Wind Tunnel Testing Technology - Interim Report," Boeing Document D3-9224, December 17, 1973.

5. "Analysis and Testing of Aeroelastic Model Stability Augmentation Systems - Final Report," Boeing Document D3-9245, October 15, 1973 (also available as NASA CR-132345).

6. "B-52 Aeroelastic Model Dynamic Response Wind Tunnel Test Data," Boeing Document D3-9557, October 23, 1974 (to be released to DDC).

7. Anton C. Keller, "Vector Component Techniques: A Modern Way to Measure Modes," Sound & Vibration, Vol. 3, No. 3, March 1969.

8. Henry A. Cole, Jr., "On-Line Failure Detection and Damping Measurement of Aerospace Structures by Random Decrement Signatures," NASA CR-2205, March 1973.

9. "B-52 CCV Control System Flight Test Validation," AFFDL-TR-74-92, Vol. V, Air Force Flight Dynamics Laboratory, Wright-Patterson AFB, Ohio (to be published).

10. "B-52 CCV Flutter Flight Test Data," Boeing Document D3-9350-1, March 1974.

11. "B-52 CCV Dynamic Response Flight Test Data," Boeing Document D3-9350-2, March 1974.

UNCLASSIFIED

SECURITY CLASSIFICATION OF THIS PAGE *(When Data Entered)*

REPORT DOCUMENTATION PAGE		READ INSTRUCTIONS BEFORE COMPLETING FORM
1. REPORT NUMBER AFFDL-TR-74-126	2. GOVT ACCESSION NO.	3. RECIPIENT'S CATALOG NUMBER
4. TITLE *(and Subtitle)* DEVELOPMENT OF ACTIVE FLUTTER SUPPRESSION WIND TUNNEL TESTING TECHNOLOGY		5. TYPE OF REPORT & PERIOD COVERED Final Report June 1972 - September 1974
		6. PERFORMING ORG. REPORT NUMBER D3-9556
7. AUTHOR(s) The Boeing Company Wichita Division		8. CONTRACT OR GRANT NUMBER(s) F33615-72-C-1913
9. PERFORMING ORGANIZATION NAME AND ADDRESS The Boeing Company, Wichita Division 3801 S. Oliver Wichita, Kansas 67210		10. PROGRAM ELEMENT, PROJECT, TASK AREA & WORK UNIT NUMBERS Project 1370 Task 137001
11. CONTROLLING OFFICE NAME AND ADDRESS Air Force Flight Dynamics Laboratory AFFDL/FYS Wright-Patterson AFB, Ohio 45433		12. REPORT DATE January 1975
		13. NUMBER OF PAGES 133
14. MONITORING AGENCY NAME & ADDRESS *(if different from Controlling Office)*		15. SECURITY CLASS. *(of this report)* Unclassified
		15a. DECLASSIFICATION/DOWNGRADING SCHEDULE

16. DISTRIBUTION STATEMENT *(of this Report)*

Distribution limited to U.S. Government Agencies only; test and evaluation; statement applied 1 November 1974. Other requests for this document must be referred to the Air Force Flight Dynamics Laboratory (FYS).

17. DISTRIBUTION STATEMENT *(of the abstract entered in Block 20, if different from Report)*

18. SUPPLEMENTARY NOTES

19. KEY WORDS *(Continue on reverse side if necessary and identify by block number)*

Aeroelastic Models, Active Control, Flutter Mode Control Systems, Wind Tunnel Testing, Control Configured Vehicles (CCV)

20. ABSTRACT *(Continue on reverse side if necessary and identify by block number)*

A research study was conducted to develop active flutter suppression wind tunnel testing technology. A one-thirtieth scale B-52 aeroelastic model was modified to represent the Control Configured Vehicles (CCV) B-52 flight test airplane with an active flutter mode control system (FMCS). The system was mechanized on the model using electromechanical actuation systems for the scaled CCV airplane outboard aileron and flaperon outboard segment control surfaces. The model was tested in the NASA-Langley Transonic Dynamics Tunnel

DD FORM 1 JAN 73 1473 EDITION OF 1 NOV 65 IS OBSOLETE

UNCLASSIFIED

SECURITY CLASSIFICATION OF THIS PAGE *(When Data Entered)*

20. Continued

to evaluate the unaugmented model flutter characteristics and performance of the flutter mode control system. Test results were compared with model analytical results and CCV program flight test results for equivalent weight and altitude conditions. The model flutter speed, in airplane scale, is 8.1 percenter higher than the airplane flutter speed, less than 1.0 percent higher than the predicted difference. Flutter mode damping with the FMCS engaged is higher on the model than on the airplane, but the damping trends with increasing airspeed are similar. The good agreement attained between model and airplane test results demonstrates that dynamically scaled models can be used to verify analytical methods used to design active flutter mode control systems.

☆U.S.Government Printing Office: 1975 — 657-019/453